Organic and Biological Molecular Layers on Functionalised Sensor Surfaces Studies with Atomic Force Microscopy

Holmberg, Maria

Publication date:
2004

Document Version
Publisher's PDF, also known as Version of record

Organic and Biological Molecular Layers on Functionalised Sensor Surfaces Studied with Atomic Force Microscopy

Ph.D. Thesis

Maria Holmberg
Danish Fundamental Metrology[1] and MIC[2]

December 2003

[1]Danish Fundamental Metrology (DFM), Matematiktorvet 307, DK-2800 Kgs. Lyngby, Denmark
[2]MIC - Department of Micro and Nanotechnology, Technical University of Denmark (DTU), Building 345east, DK-2800 Kgs. Lyngby, Denmark

Preface

This thesis has been written as a partial fulfillment of the requirements for obtaining the Ph.D.-degree at the Technical University of Denmark (DTU) and the Industrial Ph.D.-degree from the Danish Academy of Technical Sciences (ATV). The Ph.D.-project has been conducted at Danish Fundamental Metrology (DFM) and MIC, Department of Micro and Nanotechnology at DTU. Radiometer Medical A/S has been third-part in the Industrial Ph.D.-project. The work has been performed in the period from December 2000 to December 2003.

The work has been financed by ATV and DFM, and has been carried out under the supervision of:
Anders Kühle and **Jørgen Garnæs**
Danish Fundamental Metrolgy
Anja Boisen and **Erik V. Thomsen**
MIC, Department of Micro and Nanotechnology
Christian Strange
Radiometer Medical A/S

Acknowledgments

A special thanks to Michael Svendsmark Hansen for scientific discussions and his personal support.

I would like to thank the members of the staff at DFM, who have made my three years at DFM inspiring, interesting and challenging. I would also like to thank the members of the BioProbe project at MIC, especially Peter Rasmussen and Zachary Davis for interesting discussions, and Rodolphe Marie for introducing me to the experimental work at MIC. Furthermore, a thanks goes to Knud A. Mørch at the Department of Physics at DTU for the fruitful collaboration during the work with nanobubbles.

Kgs. Lyngby, December 2003

Maria Holmberg

Abstract

Biological and organic molecular layers related to two specific sensor surfaces have been studied with Atomic Force Microscopy (AFM). Besides AFM imaging, scratching experiments, where parts of a molecular layer are physically removed by the AFM tip have been performed. The AFM measurements have been supplemented by electrochemistry, fluorescence- and radioactive-labelling experiments. The two sensors are a cantilever-based sensor developed in the BioProbe project at MIC, and a blood-gas sensor developed at Radiometer Medical A/S.

In the cantilever-based sensor system short, single stranded DNA (ssDNA) molecules have been immobilized on ultra-flat gold surfaces, whereafter mercaptohexanol (MCH) and the complementary ssDNA strands have been introduced to the surface to obtain hybridization. The gold surfaces used are not the actual gold surfaces used in the sensor, but have been fabricated by evaporating gold onto mica to meet the demands of the AFM measurements.
AFM measurements indicate that MCH can release unspecific bonds between the ssDNA molecules and the gold surface, resulting in a molecular layer where all molecules bind to the gold surface through their thiol-group. When the complementary ssDNA strand is introduced, changes in the appearance of the surface indicate that hybridization has occurred. The occurrence of hybridization is supported by an increase in the thickness of the molecular layer.

AFM measurements on polymer surfaces related to the blood-gas sensor indicate that blood proteins adsorb strongly to the polymer surfaces, and that the adsorbed layer can reduce the adsorption of blood cells and platelets to the surfaces.

During AFM measurements of gold surfaces immersed in clean water, spontaneously formed nanobubbles have been observed on both contact and tapping mode AFM images. A model of the forces between a nanobubble and an AFM tip shows that if the tip is sharp and hydrophilic, nanobubbles can be imaged as protrusions on AFM images, even if the tip has penetrated the surface of the bubbles. By combining imaging with force measurements, the real dimensions of the bubbles have been estimated.

Resumé

Biologiske og organiske molekyllag relateret til overflader af to specifikke sensorer er blevet undersøgt med *Atomic Force Microscopy* (AFM). Udover afbildning af overfladerne er der udført skrabe-eksperimenter, hvor dele af et molekylelag bliver fysisk fjernet med en AFM spids. AFM målingerne er blevet kompletteret med elektrokemiske, fluorescence- og radioaktiv-mærknings eksperimenter. De to sensorer er en fjeder-baseret sensor udviklet i BioProbe projektet på MIC og en blod-gas sensor udviklet på Radiometer Medical A/S.

I det fjeder-baserede sensorsystem bliver korte, enkeltstrengede DNA (ssDNA) molekyler immobiliseret på ultra-flade guldoverflader, hvorefter mercaptohexanol (MCH) og den komplementære ssDNA streng introduceres til overfladen for at hybridisering skal ske. De undersøgte guldoverflader er ikke de egentlige guld overflader som anvendes i sensoren, men er blevet fremstillet ved at fordampe guld på mica overflader for at imødekomme de krav, der stilles til overfladen under AFM målingerne.
AFM-målinger indikerer at MCH frigør ikke-specifikke bindninger mellem ssDNA-molekyler og guldoverfladen, og resulterer i et blandet molekyllag, hvor alle molekyler binder til overfladen gennem deres thiol-gruppe. Når den komplementære ssDNA strand introduceres, indikerer ændringer i overfladens udseende at hybridisering er sket. At hybridisering er sket styrkes af at molekylelaget bliver tykkere.

AFM målinger på polymeroverflader relateret til blod-gas sensoren indikerer at blod-proteinerne adsorberer stærkt til polymeroverfladerne, og at det adsorberede lag kan reducere adsorption af blod-celler og blodplader til overfladen.

Under AFM målinger på guldoverflader i rent vand er nanobobler, som opstår spontant på overfladen, blevet observeret på både *contact mode* og *tapping mode* AFM billeder. En model for kræfterne mellem en nanoboble og en AFM spids viser at såfremt spidsen er skarp og hydrofil, kan nanobobler afbildes som udstående strukturer på AFM billeder, selv om spidsen har penetreret boblens overflade. Ved at kombinere afbildning med kraftmålinger er boblernes rigtige dimensioner blevet estimeret.

Contents

1 Introduction **2**
- 1.1 The Project . . . 2
- 1.2 The BioProbe Project . . . 2
- 1.3 Larger Perspectives . . . 3
- 1.4 The Report . . . 4

2 Experimental **5**
- 2.1 Atomic Force Microscopy . . . 5
  - 2.1.1 AFM on Biological Samples . . . 9
- 2.2 Gold Surfaces . . . 11
  - 2.2.1 Introduction . . . 11
  - 2.2.2 Fabrication of Ultra-flat Gold Surfaces . . . 12
  - 2.2.3 Characterization of Gold Surfaces . . . 12

3 AFM Imaging in Liquid **18**
- 3.1 Surface-Structure of Gold Surfaces on AFM Images . . . 18
  - 3.1.1 Introduction . . . 19
  - 3.1.2 Edge-effect versus Hole-effect . . . 20
  - 3.1.3 Influence from the Scanning Force . . . 25
- 3.2 Regular Contamination . . . 26
- 3.3 Summary . . . 27

4 DNA on Gold Surfaces **29**
- 4.1 Background . . . 29
- 4.2 Experimental . . . 30
- 4.3 Immobilization Experiments . . . 31
  - 4.3.1 Introduction . . . 31
  - 4.3.2 Immobilization of ssDNA . . . 31
  - 4.3.3 Mercaptohexanol . . . 38
  - 4.3.4 Scratching . . . 39
  - 4.3.5 Summary . . . 41
- 4.4 Hybridization Experiments . . . 42
  - 4.4.1 Introduction . . . 42

4.4.2 Hybridization of Immobilized DNA Molecules 43
4.4.3 Scratching 45
4.4.4 Summary 47
4.5 Gold Particles 48
4.5.1 Introduction 48
4.5.2 Experimental 49
4.5.3 The Idea 49
4.5.4 AFM Measurements on Immobilized ssDNA Molecules and Gold Particles 50
4.5.5 Instability in the System 51
4.5.6 Discussion and Summary 55

5 Nanobubbles 56
5.1 Introduction 56
5.2 Contact Mode Imaging 57
5.3 Force Balance Between Tip and Bubble 59
5.4 Force Measurements 60
5.5 Tapping Mode Imaging 62
5.6 Discussion and Summary 64

6 Interaction Between Blood and Polymer Surfaces 66
6.1 Background 66
6.2 Experimental 67
6.3 Polymer Surfaces 68
6.4 Static Exposure of Blood to Polymer Surfaces 69
6.4.1 Introduction 69
6.4.2 AFM Measurements 70
6.4.3 Summary 72
6.5 Dynamic Exposure of Blood to Polymer Surfaces and Cleaning . . 73
6.5.1 Introduction 73
6.5.2 AFM Measurements 73
6.5.3 Summary 75
6.6 Dynamic Exposures of Protein Solutions to Polymer Surfaces . . . 75
6.6.1 Introduction 76
6.6.2 AFM Measurements 76
6.6.3 Summary 77
6.7 Discussion and Summary 78

7 Conclusions and Perspectives 79

A Molecules and Solutions B
A.0.1 DNA Molecules . . . . . B
A.0.2 Mercaptohexanol C

A.0.3 Phosphate Buffer C

B Langmuir Isotherms **D**

C Electrochemistry Experiments **F**

D Fluorescence- and Radioactive-labelling Experiments **H**
D.1 Sample Surfaces . . . . . H
D.2 Fluorescence-labelling Experiments . . . . . H
D.3 Radioactive-labelling Experiments I

E Blood on Polymer Surfaces - Experimental **K**
E.1 Materials . . . . . K
E.2 Static Exposure of Blood to Polymer Surfaces . . . . . K
E.3 Dynamic Exposure of Blood and Protein Solutions to Polymer Surfaces L

F AFM Images **M**

G List of Publications **P**

List of Figures

2.1 The MultiMode™ Nanoscope III used in the performed AFM measurements. . . . 6
2.2 Schematic illustration of the probe and detection system of the AFM. . . . 7
2.3 The liquid cell used in the MultiMode™ together with o-ring, plastic tubes, syringe and a hose clip. . . . 8
2.4 Force curve obtained during measurements on a gold surface immersed in water. . . . 9
2.5 AFM tapping mode image (5 μm × 5 μm) of DNA plasmid molecules on a mica surface imaged in buffer. . . . 11
2.6 AFM images (5 μm × 5 μm) of two gold surfaces with different sized plateaus. . . . 14
2.7 AFM images (10 μm × 10 μm) of gold surfaces with different amounts of holes. . . . 15
2.8 AFM images (5 μm × 5 μm) of two gold surfaces with observed Au(111) structure. . . . 16

3.1 AFM contact mode images (5 μm × 5 μm) of a gold surface immersed in phosphate buffer. . . . 19
3.2 AFM contact mode images (5 μm × 5 μm) of the same gold surface imaged in air, water, and phosphate buffer. . . . 20
3.3 AFM contact mode images (2 μm × 2 μm) of a gold surface obtained in air with two different tips. . . . 22
3.4 AFM contact mode images (5 μm × 5 μm) of a gold surfaces imaged in air and of a gold surface imaged in buffer. . . . 23
3.5 AFM contact mode images (2 μm × 2 μm) of a gold surface immersed in buffer imaged before scratching and after scratching. . . . 24
3.6 AFM contact mode image (5 μm × 5 μm) of a gold surface imaged in phosphate buffer. . . . 25
3.7 AFM contact mode image (3 μm × 3 μm) of a gold surface immersed in phosphate buffer. . . . 26
3.8 AFM contact mode image (5 μm × 5 μm) of a gold surface imaged in phosphate buffer. . . . 27

4.1 AFM contact mode images (2 μm × 2 μm) and profiles of a gold surface before and after introduction of protected ssDNA molecules. 32
4.2 Measurement of stress caused by immobilization of thiol-modified ssDNA molecules on a cantilever surface. 34
4.3 AFM contact mode images (∼1 μm × 1 μm) of a gold surface after introduction of deprotected ssDNA and MCH together with a profile. 39
4.4 Schematic illustration of a molecular layer of ssDNA molecules and a molecular layer of ssDNA and MCH molecules. 40
4.5 AFM contact mode image (1 μm ×1 μm) and profile of a gold surface to which ssDNA molecules and MCH molecules have been introduced and on which scratching has been performed. 41
4.6 Illustration of a dsDNA molecule. 42
4.7 A series of AFM contact mode images (∼1 μm × 1 μm) after introduction of different molecules. 44
4.8 Schematic figure of a mixed layer of ssDNA and MCH molecules and dsDNA and MCH molecules. 46
4.9 AFM contact mode images (∼350 nm × 350 nm) and profiles of a gold surface on which scratching has been performed. 47
4.10 Schematic figure of the different steps involved in AFM measurements on DNA molecules and gold particles. 49
4.11 AFM contact mode images (5 μm × 5 μm) of a gold surface after introduction of biotin-labelled ssDNA molecules and gold particles. 50
4.12 Schematic figure of different possible interaction between biotin-labelled ssDNA molecules, gold surface and gold particles. 51
4.13 AFM contact mode images (5 μm × 5 μm) of a gold surface before and after introduction of MCH. 52
4.14 AFM contact mode images (10 μm × 10 μm) of two different areas of a gold surface after introduction of DNA, MCH and complementary DNA molecules and gold particles. 53
4.15 AFM contact mode image with profile of a gold surface with molecules and gold particles, and on which scratching has been performed. . 54

5.1 AFM contact mode images (2 μm × 2 μm) of a gold surface immersed in clean water on which nanobubbles can be observed. . . 58
5.2 Schematic figure of a scanning AFM probe interacting with a nanobubble. 59
5.3 Force curve obtained on a gold surface with nanobubbles. 61
5.4 AFM tapping mode topographical and phase image (5 μm × 5 μm) of a gold surface with nanobubbles. 63
5.5 Profile over a nanobubble. 64

6.1 AFM tapping mode images and profiles of a clean polymer surface. 69

6.2 AFM image (100 μm × 100 μm) of Polymer 3 that has been exposed to blood for 10 minutes. 70
6.3 AFM image (10 μm × 10 μm) with profile of Polymer 2 exposed to blood for 10 minutes. 71
6.4 Experimental set-up for dynamic exposure of blood (and blood protein solutions) to a polymer surface. 74
6.5 AFM images with profiles of a surface exposed to blood and cleaned with alternately introduction of air and cleaning liquid. 75
6.6 AFM images (5 μm × 5 μm) with profiles of Polymer 1 exposed to different blood proteins solution. 77

Chapter 1

Introduction

1.1 The Project

The title of the Ph.D. project presented in this thesis is 'Organic and Biological Molecular Layers on Functionalised Sensor Surfaces Studied with Atomic Force Microscopy'. The main objective of the project has been to investigate organic and biological molecular layers related to sensor surfaces with the technique of Atomic Force Microscopy (AFM).

The system subject to the most extensive study has been a system involving the immobilization of 25 bases long, thiol-modified single stranded DNA (ssDNA) molecules on gold surfaces, and their subsequential hybridization to the complementary ssDNA strands in a solution, to form double stranded DNA (dsDNA) molecules. The system is related to the BioProbe project at MIC (Mikroelektronik Centret) at the Technical University of Denmark (DTU) (see section 1.2). The adsorption of blood-material to polymer surfaces is a second system studied during the project, and this has been done in collaboration with Radiometer Medical A/S, Denmark (see Chapter 6).

1.2 The BioProbe Project

A cantilever based sensor for label-free detection of biological reactions is developed and fabricated in the BioProbe project [1] at MIC, DTU.

The basic idea in the BioProbe sensor is to detect a change in surface stress caused by a biological reaction occurring on the surface of a cantilever with dimensions in the micrometer range. The change in surface stress causes the cantilever to bend, and this is detected by an integrated piezoresistor.

There are other groups developing cantilever-based sensors [2, 3], but in which an

optical detection system similar to the one used in an Atomic Force Microscope (see section 2.1, page 5) is used. An optical detection system gives a higher sensitivity than a piezoresistive-based detection system, but by using an integrated detection system the device can be more compact and easy to handle. Furthermore, it allows the device to be used in non-transparent liquids, for example blood.

The main application investigated for the BioProbe sensor is the detection of DNA hybridization. By immobilizing 25 bases long ssDNA molecules on one side of the cantilever and introducing the complementary strand to the system, hybridization can occur on the cantilever surface. The reaction induces a change in surface stress of the cantilever, which can be detected by the integrated piezoresistor.

The characteristics of the immobilized molecular layer is one of the most critical parameters for the function of the BioProbe sensor. Parameters such as density and conformation of the immobilized molecules, as well as their activity are important. Both density and activity of the immobilized ssDNA molecules have been studied with fluorescence- and radioactive-labelling techniques in the BioProbe project [4]. However, these techniques give little information about the conformation of the molecules, how they are distributed, and how the molecules interact with each other and the surface they are immobilized to. For this AFM is more appropriate.

1.3 Larger Perspectives

Besides from information about the specific systems studied in this project, the work has resulted in knowledge about AFM investigations in liquid on systems involving organic and/or biological material.

In addition to the interest to participate in research and development, and to promote exchange of knowledge between universities and the industry in Denmark, Danish Fundamental Metrology (DFM) has an interest in offering their customers necessary measuring methods.

The fast growing area of biotechnology is in need of measuring methods, where systems including both inorganic and organic material can be characterized, and where the quality of the devices can be measured and assessed. Most devices developed and fabricated in this area operate in a liquid environment and are minimized to reduce the cost and to make them easy to handle. Thus, the ability to investigate structures in the micrometer and nanometer range in a liquid environment is an area in demand, and can be achieved through the technique of

AFM.

1.4 The Report

In Chapter 2 the technique AFM and AFM measurements performed on biological samples are introduced. Furthermore, the gold surfaces used during investigations of the system related to the BioProbe sensor are presented and characterized.

In Chapter 3 clean gold surfaces (gold surfaces, to which no molecules have been introduced) are characterized. AFM measurements on these surfaces are used as reference to the AFM measurements performed on gold surfaces with molecules.

In Chapter 4 results from the study of immobilization and hybridization of short DNA molecules are presented and discussed. In Chapter 5 the phenomenon of nanobubbles is presented and discussed. In Chapter 6 results obtained during the study of interaction between blood-material and polymer surfaces is presented and discussed.

In Chapter 7 conclusions and perspectives are presented.

The Appendixes contains experimental details on methods used during the study, as well as some additional information about some of the subjects treated in the chapters;

• Appendix A presents the molecules used during experiments related to the BioProbe sensor.
• Appendix B contains a short presentation of Langmuir isotherms.
• Appendix C gives a short description of the electrochemistry experiments.
• Appendix D gives a short description of the fluorescence- and radioactive-labelling experiments.
• Appendix E gives some experimental details of the work related to the adsorption of blood-material to polymer surfaces.
• Appendix F contains a list of the AFM images presented in the report[1].
• Appendix G contains a list of publications.

All AFM measurements presented that are not referred to earlier published work by others are measurements performed in this study.

[1]For internal use at DFM.

Chapter 2

Experimental

2.1 Atomic Force Microscopy

Binnig et al. [5] presented the Atomic Force Microscope (AFM) in 1986, the same year as Binning and Rohrer got the Nobel prize for the invention of the Scanning Tunnelling Microscope (STM) [6]. In contrast to STM, which requires a conducting sample, AFM is a surface analyzing instrument that can be used to investigate non-conducting samples. The instrument can be used to study structures in the nanometer range and can operate in different media, such as vacuum, air and liquid.

The technique of AFM is based on a small tip that is scanned over the surface of a sample, and where the force between tip and sample surface during scanning is detected to give information about the characteristics of the surface.

The AFM used during the experiments performed is a MultiMode^{TM} NanoscopeIII AFM from Digital Instruments[1] (see Figure 2.1), and all data has been processed with the software package SPIP[2].

Hardware

In Figure 2.2 the basic components of an AFM are shown. The probe is a small tip attached to the end of a cantilever. The cantilever with its substrate is mounted in a tip holder. The tip holder is stationary during measurements. The sample is mounted on a piezoelectric tube scanner, which scans in a raster pattern in the x-y plane during imaging. It is also the piezoelectric tube scanner that provides the movements in the z-direction. The detection system is based on a laser that

[1] Now part of Vecco Instruments.
[2] Image Metrology ApS, Denmark.

Figure 2.1: The MultiMode^{TM} Nanoscope III used in the performed AFM measurements.

is focused on the backside of the cantilever and reflected back into a photodiode. The photodiode consists of four segments that are placed in pairs along the vertical and horizontal axis. By combining the signals from the segments both horizontal and vertical movements of the cantilever can be detected.

Besides from the basic hardware illustrated in Figure 2.2 the instrument includes a control mechanism that controls the x-y scanning, as well as the motion of the piezoelectric tube in the z direction. During measurements a feedback system is optimized to keep the interaction between tip and sample constant. In response to changes in the deflection or amplitude of the cantilever (dependent on the scanning mode used, see page 7) detected by the photodiode, the tube scanner moves in the z-direction to keep the interaction constant. The movements of the piezoelectric scanner are registered and can be translated to a topographical image of the sample surface.

Specific Hardware when Working in Liquid

The most 'simple' way to perform AFM investigations in liquid is to place a droplet of water or solution on the sample surface and do the measurements in an open system. However, a closed system is needed if the investigations require exchange of solution during the measurements. Furthermore, a closed system reduces the risk of contamination from the environment, as well as evaporation of liquid from the system.

Figure 2.3 shows the specific hardware used during AFM investigations in liquid, when a closed system is required.

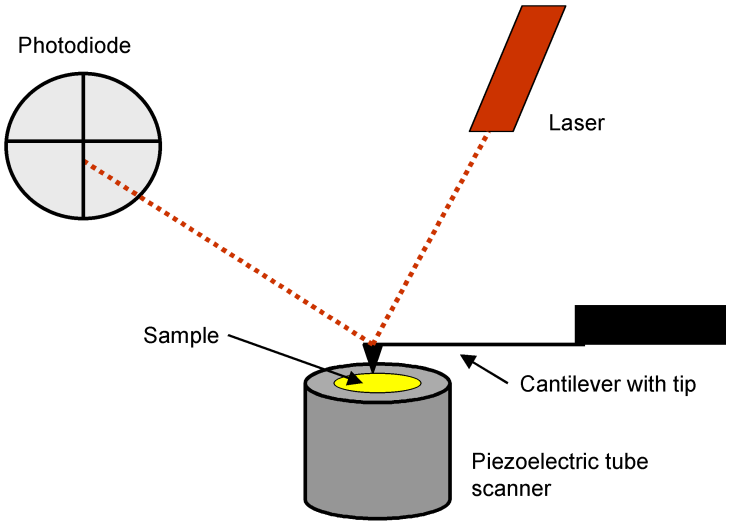

Figure 2.2: Schematic illustration of the probe and detection system of the AFM. A laser is focused on the backside of the cantilever with the tip and reflected into a photodiode. The sample is placed on a piezoelectric tube that provides motion in the x, y and z direction.

An o-ring is mounted together with the liquid cell to keep the system tight. Through a syringe and plastic tubes different solutions can be introduced into the liquid cell. The hose clips are used on the plastic tubes to minimize evaporation of liquid from the system, as well as diffusion of vapour into the system.

A different choice of probe compared to when working in air can be of advantage during AFM measurements in liquid. For example, the aluminium-coating on the backside of some probes has shown to dissolve in the phosphate buffer used during experiments with DNA molecules. Thus, non-coated probes are recommended when working in other liquids than clean water.

Contact Mode

When working in contact mode [5] the tip is kept in physical contact with the sample surface during scanning. The image parameter set-point determines the deflection of the cantilever, and thereby the scanning force applied to the sample. When the interaction between tip and sample changes during scanning, the feedback system causes the piezoelectric scanner to move in the z-direction to maintain the deflection determined by the set-point.

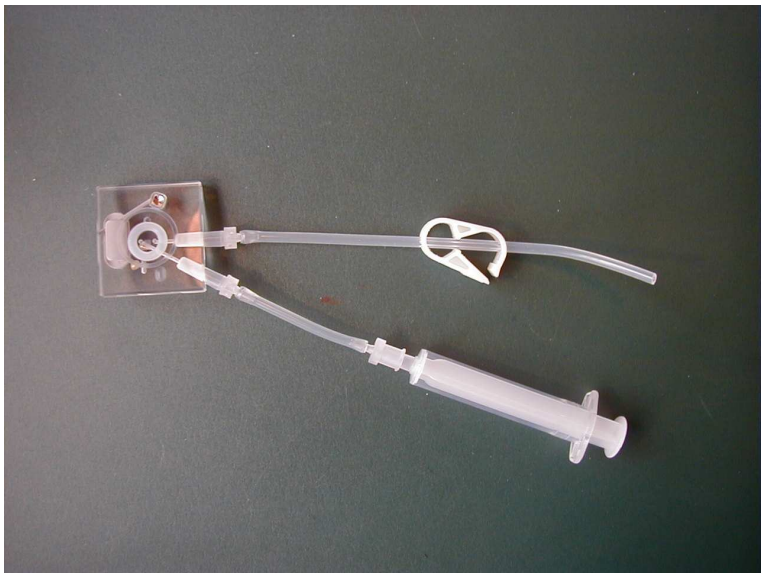

Figure 2.3: The liquid cell used in the MultiMode^{TM} together with o-ring, plastic tubes, syringe and a hose clip.

Tapping Mode

In tapping mode [7, 8] the tip is oscillated close to its resonant frequency, while it scans over the surface. The amplitude used is high enough for the tip to 'tap' the surface during the oscillation without getting trapped at the surface by attractive forces. During tapping mode the set-point determines the RMS[3] value of the amplitude of the oscillation, and it is kept constant through the feedback system after the same principle as during contact mode.
During tapping mode a so-called phase image can be obtained, where the phase lag of the oscillation of the cantilever during measurement, relative to the signal the cantilever is excited with, is registered. The phase image can give information about the elasticity of the sample surface.

Force Measurements

Information about interaction between tip and sample in a restricted area of the sample surface can be obtained by keeping the sample stationary in the x-y direction and only moving the piezoelectric tube in the z-direction [9, 10]. The measurements can give detailed information about the attractive and repulsive forces between tip and sample. During force measurements the tip is made to travel from a position, where there is no interaction between tip and sample to a position, where the tip has physical contact with the sample surface, whereafter the tip is withdrawn from the surface again. During this movement the deflection

[3]Root mean square.

of the cantilever is detected as a function of the position of the piezoelectric tube scanner. The result is a so-called force curve. In Figure 2.4 a force curve obtained during AFM measurements on gold surfaces immersed in water, where force as function of tip-sample separation is shown.

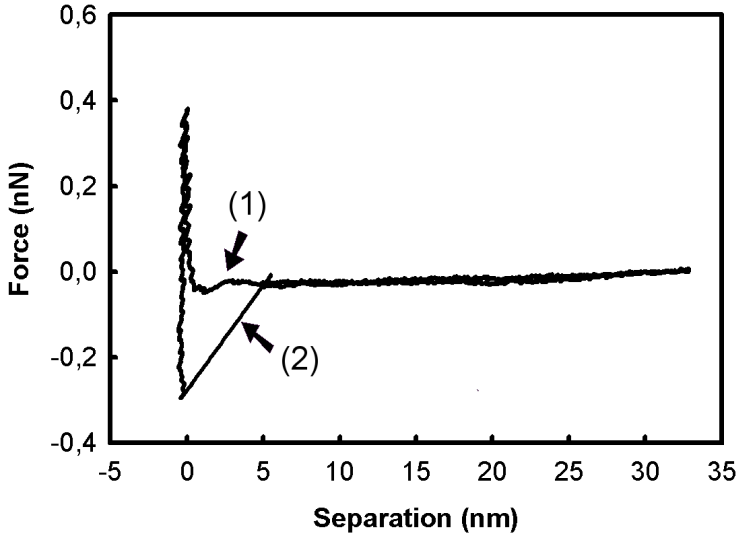

Figure 2.4: Force curve obtained during measurements on a gold surface immersed in water. The tip is approaching the surface from right to left, and the point (1) shows a small 'snap-in', where the tip comes in contact with the surface. In the retraction curve a larger 'snap-out' is observed, see point (2), where the tip looses contact with the surface.

2.1.1 AFM on Biological Samples

Characteristics such as the abillity to perform surface studies on non-conducting samples and working in both air and liquid have made AFM a popular tool for investigating biological samples. Already in 1989 (the same year as the first commercial AFM was available on the market) Drake et al. [11] showed that AFM could be used to study biological processes by monitoring the polymerization of fibrin after the enzyme thrombin was added to a sample of fibrinogen solution. Today AFM is optimized to perform faster measurements [12, 13] in order to be able to monitor biological reactions such as protein folding, which occurs at a time scale of microseconds or less.

Tapping Mode versus Contact Mode

Tapping mode is used during many AFM investigations performed on biological samples [8, 14]. By using tapping mode the friction force applied to the sample

surface is reduced compared to when contact mode is used. However, contact mode is more suitable during investigations that include scratching, where material on the surface is physically removed by using a high scanning force (see section 4.3.4, page 39). Contact mode can be used on biological samples without destroying them by working in liquid and adjusting the scanning force to be as small as possible.

Mobility of Sample

When molecules are imaged in liquid, the mobility of the molecules can cause problems. When molecules are imaged in air, they are normally 'fixed' to a surface mainly by the capillary force, and it is not necessary to use a specific immobilization technique or a forced attachment during measurements. When the sample and tip are immersed in liquid the capillary force disappears, which causes the molecules to be more loosely bound to the surface. Furthermore, most hydrated samples are more soft than dry samples, and therefore more affected by the scanning tip. Thus, it is often necessary to immobilize or use specific attachment of the molecules to the surface during AFM measurements in liquid.

Immobilization in form of chemisorption has been used during AFM investigation of the interaction between short ssDNA molecules and gold surfaces (see section 4.2, page 30). Another strategy is to use electrostatic interactions to fix a sample during measurements in liquid. Figure 2.5 shows an AFM tapping mode image (5 μm × 5 μm) of DNA plasmid molecules[4] that have been fixed to a mica surface through electrostatic interactions.

Both the mica surface and the DNA molecules have a negative charge, but by using a buffer containing divalent ions such as Mg^{+2} or Ni^{+2} a positively charged sample surface can be created [15, 16]. Thereby the negatively charged DNA molecules can be electrostatically bound to the surface.

The electrostatic interaction between the positively charged surface and the negatively charged DNA molecule has shown to be strong enough for the sample to be imaged in liquid without displacing the DNA plasmid molecules during scanning. The molecules can be observed as bright structures with a circular conformation and are not relocated by the scanning tip (see Figure 2.5).

[4] A circular DNA molecule that can exist in bacteria.

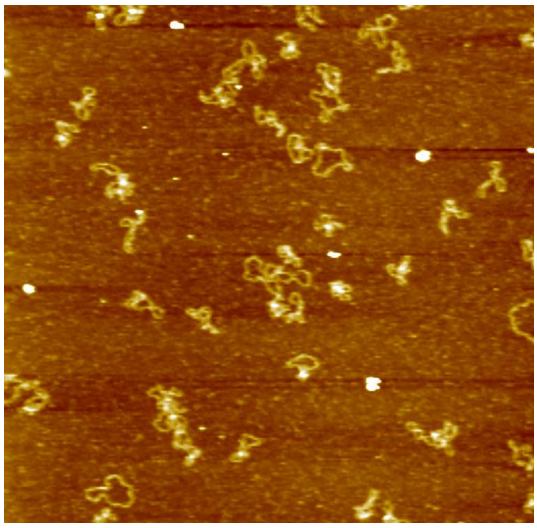

Figure 2.5: AFM tapping mode image (5 µm × 5 µm) of DNA plasmid molecules on a mica surface imaged in buffer.

2.2 Gold Surfaces

2.2.1 Introduction

Sample surfaces must fulfil some requirements when used in AFM investigations in liquid of immobilized, 25 bases long ssDNA molecules.

Short DNA molecules immobilized on surfaces have shown to have dimensions in the nanometer range, and if the surface is not ultra-flat the molecules will be hidden in the topography of the surface. Furthermore, flat plateaus with an area of at least ∼500 nm × 500 nm are of an advantage when the thickness of molecular layers is estimated though scratching experiments (see section 4.3.4, page 39).

In the BioProbe sensor (see section 1.2, page 2) the molecules are immobilized through thiol-groups that chemisorb on the gold surface, and therefore the surface used during the AFM measurements is a gold surface.

Surfaces that fulfil the mentioned requirements can be obtained by evaporating gold onto mica[5]. These fabricated gold surfaces have ultra-flat plateaus with widths of a couple of hundreds of nanometer, are inert to the phosphate buffer used during the measurements, and can be firmly attached to the sample holder during scanning.

[5]PLANO GMBH, Germany, www.planp-em.de.

2.2.2 Fabrication of Ultra-flat Gold Surfaces

The recipe after which the gold surfaces have been fabricated was initially inspired by a technique presented by Reichelt and Lutz in 1971 [17], and it has been further optimized[6] in the clean room facilities at MIC.

In Table 2.1 the fabrication of the gold surfaces is summarized.

1. Mica surfaces are cleaved and mounted in an evaporation system (Alcatel SCM600 e-gun evaporation system).
2. The mica surfaces are pre-annealed at 10^{-5}-10^{-7} mbar, $\sim$510°C for 36-60 hours.
3. 150 nm of gold is evaporated onto the mica surfaces with an deposition rate of approximately 0.3 nm/s.
4. The surfaces are post-annealed at $\sim 10^{-7}$ mbar, $\sim$510°C for at least 1 hour, and thereafter kept in the evaporation chamber without heating for approximately 1 hour.
5. The surfaces are placed in plastic boxes and put in a sealed case, in which they are stored in air until they are used in AFM experiments.

Table 2.1: Summary of the fabrication of gold surfaces.

2.2.3 Characterization of Gold Surfaces

All gold surfaces used in the AFM investigations are fabricated after the same recipe and show similar characteristics, even though there can be some minor deviations between different batches.

[6] Primarily by Karsten Waltzner and Michael Wrang Mortensen.

Contact Angle

The gold surfaces are stored in air between fabrication and usage in AFM investigations. The surfaces are put in plastic boxes and a sealed case in the clean room directly after evaporation, which minimize the adsorption of contamination in form of particles to the surfaces due to the clean environment[7]. However, during storage there can be adsorption of for example hydrocarbons on the surface, which results in an increase of the hydrophobicity of the gold surfaces.

Contact angle measurements performed on the fabricated gold surfaces with clean water[8] have shown that the surfaces have a contact angle of 95°-100°. A lower contact angle (60°) measured by others [18] on gold evaporated on mica, indicates a cleaner, and thereby a more hydrophilic surface.

A surface with a contact angle of 95°-100° can be considered to be slightly hydrophobic by defining that a pure hydrophilic surface has a contact angle of 0° and that a pure hydrophobic surface has a contact angle of 180°, and that the boundary between being mostly hydrophobic or mostly hydrophilic is considered to be at a contact angle of 90°.

Size of Plateaus

The fabricated gold surfaces consist of several ultra-flat plateaus of different sizes and shapes, where the sizes and shapes depend on fabrication parameters such as deposition rate and temperature during evaporation.

Figure 2.6 shows AFM images (5 μm × 5 μm) of two gold surfaces fabricated after the same recipe, where the surface shown in (a) has large plateaus and the surface shown in (b) has small plateaus.

The larger plateaus in Figure 2.6(a) have a width of about 1 μm and on these, smaller plateaus (a couple of hundreds of nanometers in width) are visible. Besides from having different sizes, the shape of the plateaus are quite irregular. Larger holes with a diameter of about 250 nm that form naturally during evaporation are observed on the surface.

In Figure 2.6(b) the surface is covered with relatively small plateaus with a width of about 160 nm. Essentially all plateaus have the same size and shape, and no larger holes are observed on the surface. Due to the small size of the plateaus, the gold surface shown in (b) would be rejected as a sample surface for immobilization and hybridization experiments.

[7]The clean room at MIC is of class 100.
[8]Milli-Q water from Millipore A/S.

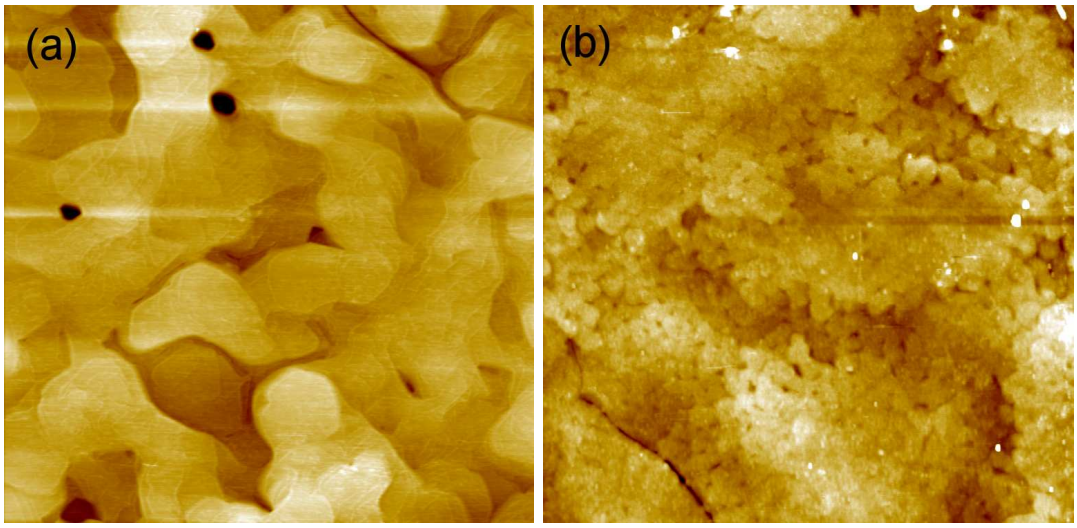

Figure 2.6: AFM images (5 µm × 5 µm) of two gold surfaces fabricated after the same recipe. Figure 2.6(a) shows a gold surface with large plateaus, while the gold surface shown in (b) has smaller plateaus.

Investigations performed by DeRose et al. [19] have showed that a high deposition temperature (400°C-550°C) results in large plateaus (a couple of hundreds of nanometer in width). The diffusion of the gold atoms increases exponentially with the temperature, and the higher the deposition temperature the larger the distance the atoms can travel before they settle down at equilibrium sites on the surface. Furthermore, a relatively long pre-annealing time (6 hours or more) at temperatures of 450°C or higher resulted in extremely flat gold surfaces, on which single-crystal structure could be observed. During the pre-annealing contamination present in the evaporation chamber is outgassed, and a long pre-annealing time is expected to result in a cleaner mica surface, which can enhance the formation of ultra-flat gold surfaces during evaporation.

In studies performed by others [20] it has been observed that a deposition rate of 0.2-0.6 nm/s at depositions temperatures over ∼300° creates gold surfaces with large plateaus (width ∼250 nm) that are more or less connected to each other in the lateral plane, while a lower deposition rate (0.02-0.1 nm/s) at the same temperature results in a gold surfaces consisting of smaller islands (diameter ∼150 nm) that have little contact to each other. The explanation was found in the competition between diffusion of gold atoms and secondary nucleation, where the diffusion process dominates at low deposition rates, and the secondary nucleation process is more distinct at high deposition rates.

The same recipe has been used during fabrication of the the two surfaces shown

in Figure 2.6, but the different sized plateaus observed on the surfaces indicate that evaporation parameters have not been identical during fabrication of the two surfaces. This in turn point towards that the evaporation system does not perform entirely reproducible, and that the adjusted parameters of the system during evaporation not always are the parameters actually performed by the system.

Roughness

In Figure 2.6 it is observed that the appearance of the fabricated gold surfaces can differ, and therefore the roughness of the surfaces can also differ. Furthermore, holes with diameters of 200-300 nm are often formed on the surface during the evaporation process, and they complicate the estimate of the roughness of the gold surfaces.

The amount of holes can alter quite much from batch to batch, and Figure 2.7 shows two extremes, where both images show a 10 µm × 10 µm scan of the gold surfaces. In (a) 64 holes are observed on the gold surface, while the gold surface in (b) only contains 4-5 holes.

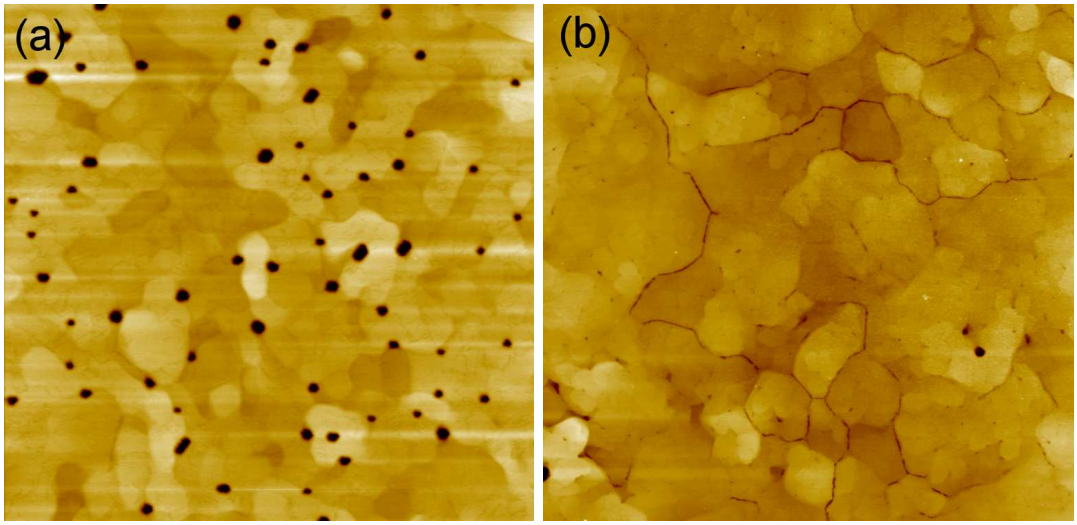

Figure 2.7: AFM images (10 µm × 10 µm) of gold surfaces, where the gold surface in (a) contains 64 holes and the surface in (b) only contains 4-5 holes.

The larger the amount of holes, the larger the roughness of the surface, but by using gold surfaces with a small amount of holes (five or less) the roughness of the surfaces can be estimated to be approximately 1.5 nm over an area of 10 µm × 10 µm. On smaller, ultra-flat areas (400 nm × 400 nm or less) a roughness

of about 0.2 nm is found, which is similar to values found in the literature [19][9].

Au(111) Structure

Figure 2.8 shows two AFM images (5 µm × 5 µm) of gold surfaces, where (a) is a tapping mode image obtained in air, and (b) is a contact mode image obtained in phosphate buffer.

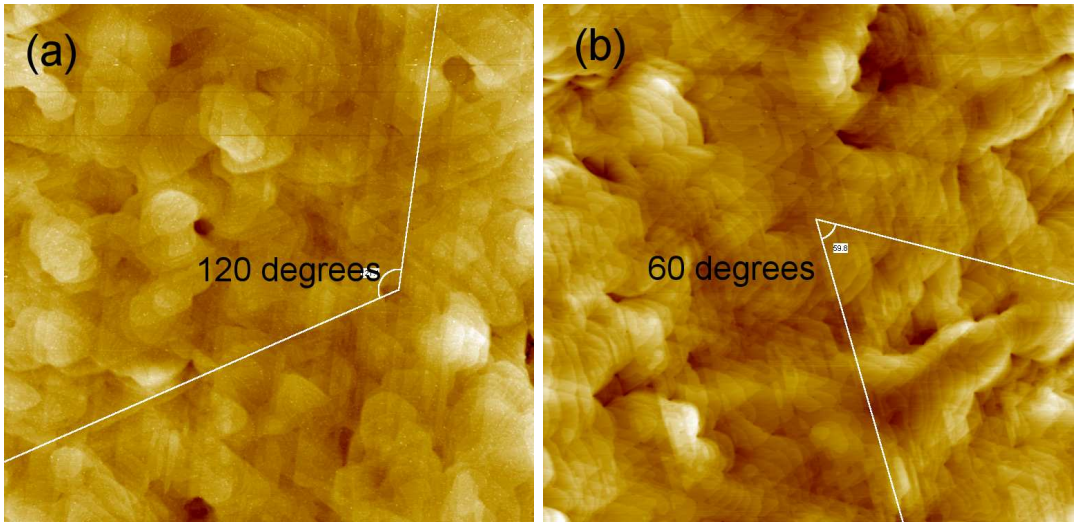

Figure 2.8: AFM images of two gold surface (5 µm × 5 µm) imaged in (a) tapping mode in air, and (b) contact mode in phosphate buffer. The angles indicated on the images corresponds to the angles observed on Au(111) crystal surfaces.

In the images shown in Figure 2.8 plateaus with different sizes and shapes are observed. However, there is also a triangular shaped surface-structure covering the gold surfaces, resembling the surface structure of Au(111) crystals [19, 21], indicating that the gold layer has been grown epitaxially in the (111) orientation. By measuring the angles between lines observed on the images, angles of 60° and 120° are found, corresponding to the angles for the Au(111) surface.

Stability of the Gold Layer

Even though the evaporated gold layer on mica has shown to adhere strong enough to the mica surface to be stable during AFM experiments in liquid, the mounting of gold surfaces together with liquid cell and o-ring in the AFM should be performed with caution. If the gold surface is squeeze too much by the o-ring, there is a risk for parts of the gold layer to fall off the mica. These parts can

[9]The images have been subject to line wise levelling of first order before the roughness are estimated.

be released into the measuring chamber and interfere with the measurements. Furthermore, the release of parts of the gold layer in the area where the gold surface and o-ring interacts can introduce leaks, which in turn result in enhanced evaporation of liquid from the system and an increased amount of air-bubbles in the measuring chamber.

Chapter 3

AFM Imaging in Liquid

When performing AFM experiments in liquid, some aspects that are not present during AFM experiments in air require attention. There are for example some additional preparation, such as cleaning of the equipment (liquid cell, o-ring etc.), protection of sensitive parts of the microscope from liquid, and assembling of liquid cell, o-ring, tubes, syringes and hose clips. Besides from the more practical aspects of working in liquid, there is also a risk of introducing features such as bubbles and contamination when liquid is introduced into the AFM set-up. The introduced liquid also has an effect on the involved forces between tip and sample, which should be taken into account during analysis of the results.

In this chapter AFM investigations of 'clean' gold surfaces are presented, where 'clean' refers to surfaces, to which no molecules have been introduced. These measurements are used as references to measurements performed with gold surfaces and molecules.

Besides from regular contaminations, 'spontaneous' changes, which are changes occurring on AFM images without any imaging parameters have been changed deliberately, are presented. Furthermore, during the study of clean gold surfaces, structures that have shown to be nanobubbles have been observed on AFM images, and this phenomenon is discussed in Chapter 5.

3.1 Surface-Structure of Gold Surfaces on AFM Images

Before gold surfaces are used in immobilization and hybridization experiments, they are imaged in buffer. To be used in experiments with molecules, the surfaces need to have plateaus that are ultra-flat on a scale of at least a couple of hundreds of nanometer in width, and they should not contain any larger grooves or other defects. Furthermore, the tip used during measurements should be sharp and has

a well-defined conic shape at the apex.

3.1.1 Introduction

During imaging of clean gold surfaces in buffer it has been observed that the appearance of the gold surfaces can change, even if no imaging parameters have been changed deliberately.

Figure 3.1 shows two AFM contact mode images (5 µm × 5 µm) of a gold surface immersed in phosphate buffer. The two images are obtained directly after each other, and the tip has not lost contact with the surface between registration of the two images. Figure 3.1(a) was obtained while the tip was scanning from the upper part to the lower part of the area, while Figure 3.1(b) was obtained during the subsequently scanning from the lower part to the upper part of the area.

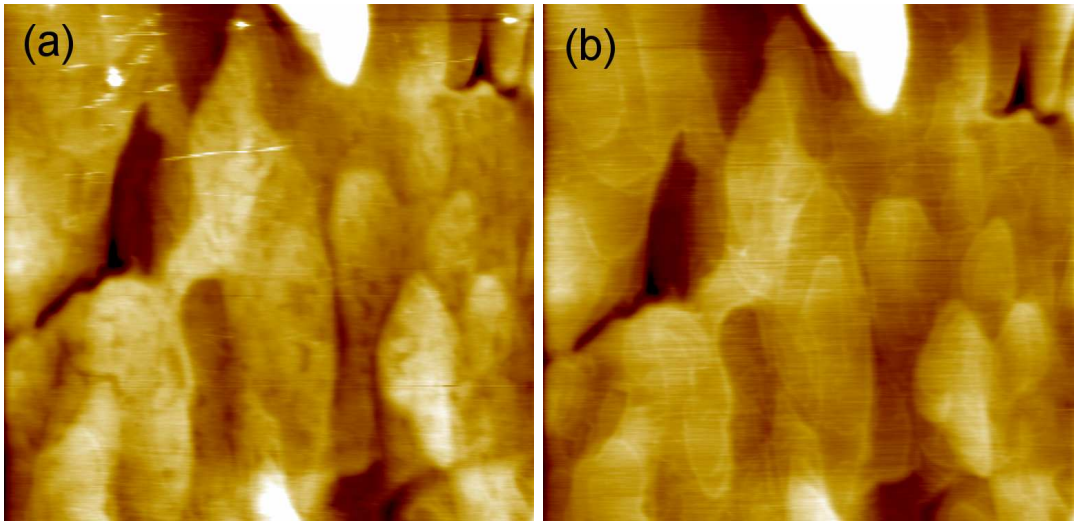

Figure 3.1: AFM contact mode images (5 µm × 5 µm) of a gold surface immersed in phosphate buffer. In (a) the tip has scanned from the upper part to the lower part of the area, and in (b) the tip has scanned from the lower part to the upper part of the area.

In Figure 3.1(a) the surface looks rather structured and one can observe darker areas with dimensions in the nanometer range on the surface. Larger plateaus are observable, but none of the smaller plateaus are visible. The somewhat blurred expression of the surface indicates that the tip is blunt and not suitable for imaging during immobilization and hybridization experiments.

In Figure 3.1(b) the appearance of the surface has altered compared to (a). There is no longer any darker areas observed on the surface, and the smaller plateaus are now visible on the AFM image. Based on the image in Figure 3.1(b) the tip

would be judged as being sharp and suitable for experiments with molecules.

The blurred look of the surface in Figure 3.1(a) indicates that something has been attached to the apex of the tip and made it blunt, while the appearance of the surface in (b) indicates that the material attached to the tip has been removed and that the tip now is sharper.

Besides from the characteristics of the tip, spontaneous changes have shown to be influenced by parameters such as medium and scanning forces used during imaging. In the following sections examples of the different surface characteristics and the influence from different parameters will be presented.

3.1.2 Edge-effect versus Hole-effect

AFM measurements in air, clean water[1], and buffer[2] on clean gold surfaces have been performed in order to analyze the origin of the observed changes on AFM images.

In Figure 3.2 AFM contact mode images (5 µm × 5 µm) are shown of a gold surface obtained in; (a) air, (b) clean water and (c) phosphate buffer. The areas shown in the three images are not exactly the same area of the surface, but their appearances are representative for the surface when imaged in the specific medium. In (b) and (c) the same structure can be observed (see arrows). The three images shown are obtained during a period of time of approximately 2 hours.

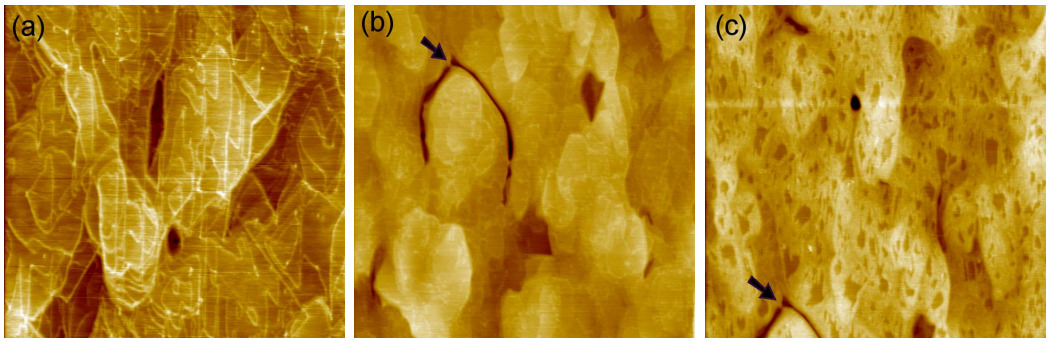

Figure 3.2: AFM contact mode images (5 µm × 5 µm) of the same gold surface imaged in; (a) air, (b) water, and (c) phosphate buffer. The images are obtained during a period of approximately 2 hours. The arrow in (b) and (c) shows a structure observable on both images.

In Figure 3.2(a) medium-sized plateaus (200-400 nm wide) and smaller plateaus

[1]Milli-Q water from Millipore A/S.
[2]The same buffer as used in immobilization and hybridization experiments.

(∼100 nm wide) can be observed. The plateaus are surrounded by a bright edge, and this kind of edge-effect has often been observed when the gold surfaces are imaged in air. From profiles the width of the edges can be estimated to be 50-80 nm and the height to be 0.5-1 nm.

The appearance of the surface changes after introduction of clean water (see Figure 3.2(b)). There is still an edge-effect, but the bright edges surrounding the plateaus are not as distinct as earlier, but more smeared out and in some places they seem to have disappeared completely from the plateaus. From profiles the widths of the edges can be estimated to be 30-40 nm and the heights to be ∼0.2 nm.

In Figure 3.2(c) the edge-effect has been replaced by what could be called a hole-effect. Darker areas with widths of 50-100 nm are now visible on the surface. The difference in brightness between the darker areas and the rest of the surface corresponds to 0.7-1 nm on the z-scale. However, the hole-effect can also be considered to be an edge-effect just presented differently. Instead of regarding the darker areas as holes, the brighter areas surrounding these holes can still be considered to be an edge, but much broader than the one observed in (a) and (b).

The bright edges observed on the images in Figure 3.2 can be due to adsorption of materials such as hydrocarbons from the environment. The gold surfaces are stored in tight-fitting boxes between fabrication and measurements, but they have been in contact with the ambient atmosphere. The steps on the surface are expected to be more active than the flat terraces [22, 23, 24] and when material is adsorbed on the surface, it is expected that it adsorbs at the steps first, and this could thereby result in the edge-effect/hole-effect observed on the images in Figure 3.2.

Influence from the Tip

In Figure 3.3 two AFM contact mode images (2 μm × 2 μm) are shown obtained in air of the same gold surface, but not of the same area of the surface. In (a) a standard silicon nitride tip[3] has been used, which has a nominal full tip cone angle of ∼70° and nominal tip curvature radius of 20-60 nm, while a standard silicon tip[4] that has a nominal full tip cone angle of ∼30° and nominal tip curvature radius of <10 nm has been used in (b).

In Figure 3.3(a) steps and terraces on the gold surface can be observed. There is no clear edge-effect, but there is a surface-structure that resembles the surface-structure mainly observed when gold surfaces are imaged in buffer.

[3]Standard Silicon Nitride Probes from Digital Instruments, now part of Veeco Instruments.
[4]ULTRASHARP Si cantilever, MikroMasch, Estonia.

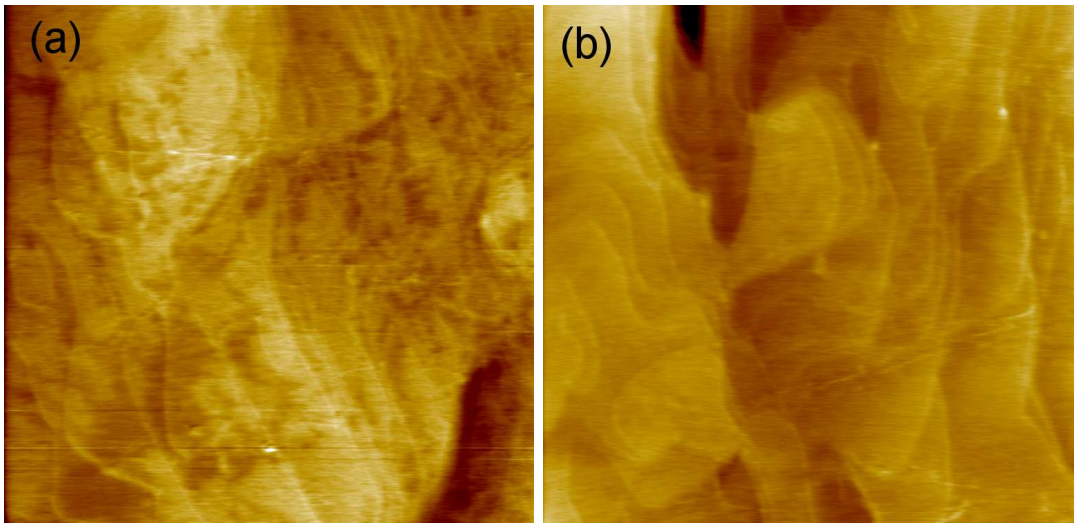

Figure 3.3: AFM contact mode images (2 µm × 2 µm) of a gold surface obtained in air with (a) a standard silicon nitride tip, and (b) a standard silicon tip. The area shown in (a) and (b) are not the same area on the gold surface.

In Figure 3.3(b) steps between terraces are quite distinct, and there is an edge-effect with bright edges surrounding the plateaus. The image in (b) resembles most other images obtained in air, and do not contain any clear surface-structure as in (a).

The difference between the images in Figure 3.3 indicates that the characteristics of the tip have a large influence on the appearance of gold surface on AFM images. A sharp tip results in a more distinct edge-effect with thin, bright edges surrounding the plateaus on the gold surface, than a blunt tip does.

Influence from the Medium

Compared to when the gold surface is imaged in air (see Figure 3.2(a)), the bright edges on the gold surface are somewhat diminished, when the surface is imaged in clean water (see Figure 3.2(b)). This could be due to the disappearance of the capillary force between tip and sample when liquid is introduced into the system, which results in a weaker interaction between tip and sample.

Some characteristics are mostly observed on the clean gold surfaces when they are imaged in a specific medium, but there are examples where of surfaces imaged in air showing a surface-structure typical for surfaces imaged in phosphate buffer, and vice versa.

Figure 3.4 shows AFM contact mode images (5 µm × 5 µm) of two different

gold surfaces, where (a) is obtained in air and (b) is obtained in buffer.

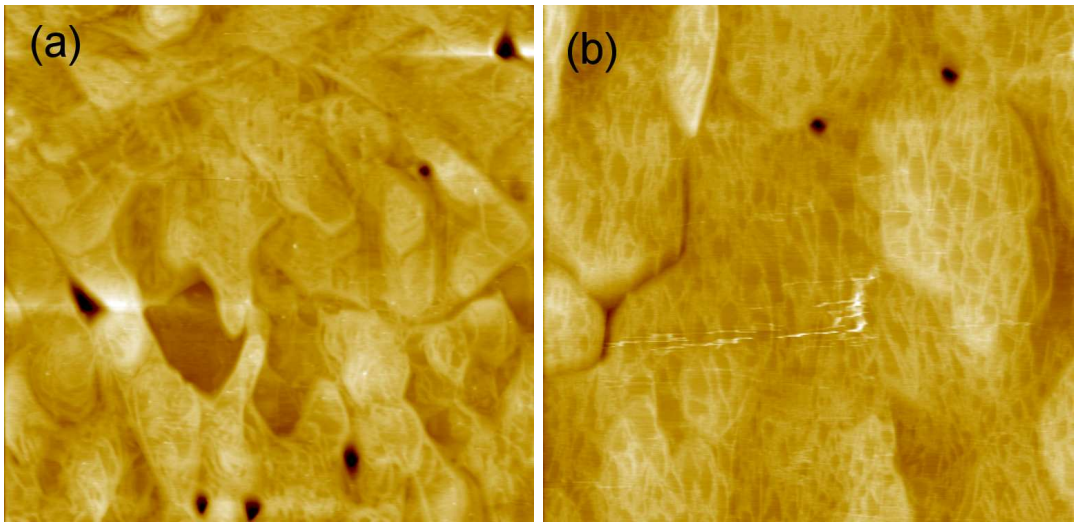

Figure 3.4: AFM contact mode images (5 µm × 5 µm) of (a) a gold surfaces imaged in air and of (b) a gold surface imaged in buffer.

In Figure 3.4(a) a kind of edge-effect can be observed, but some of the bright edges around the plateaus are rather broad. Some areas of the surface have a surface-structure that resembles the surface-structure normally observed, when images are obtained in buffer. Larger plateaus are visible on the image, but the smaller ones are not as distinct as they normally are when the gold surfaces are imaged in air.

In Figure 3.4(b) the surface shows several rather thin, bright lines, which are comparable to the bright edges most often observed on gold surfaces imaged in air. The small dimension of the lines (∼60 nm in width and ∼1 nm in height) indicates that the tip has been sufficiently sharp for being used in experiments with molecules. Even if it is not possible to identify smaller plateaus on the image, the position of the lines on the surface can be an indication of the position of smaller plateaus.

Thus, even though a clear edge-effect mostly is observed on AFM images obtained in air, and a more diffuse surface-structure is observed on AFM images obtained in buffer, the tendencies are not always unambiguous. The results indicate that the medium used during imaging has less influence on the appearance of the gold surface on AFM images, than the characteristics of the tip.

Scratching

The surface-structure observed on some of the clean gold surfaces (see for example Figure 3.1(a) and Figure 3.2(c)) shows some resemblance to the surface-structure observed on gold surfaces, to which molecules have been introduced (see Chapter 4). Darker areas observed on the surfaces, to which molecules have been introduced, are interpreted to be due to the immobilization of molecules. Since no molecules have been introduced to the clean gold surfaces, the darker areas observed on these cannot be due to immobilization of molecules.

Scratching experiments have been performed to differ between gold surfaces that resemble each other on AFM images, but that represent different situations. The scratching experiments were performed after the scheme described in section 4.3.4, page 39.

Figure 3.5 shows two AFM contact mode images (2 µm × 2 µm) of a gold surface immersed in buffer, on which a scratching experiment has been performed. Figure 3.5(a) shows the area before scratching, while (b) shows the same area after scratching. The scratching has been performed in a 500 nm × 500 nm large area in the center of the imaged area, but no signs of removed material is observed in (b).

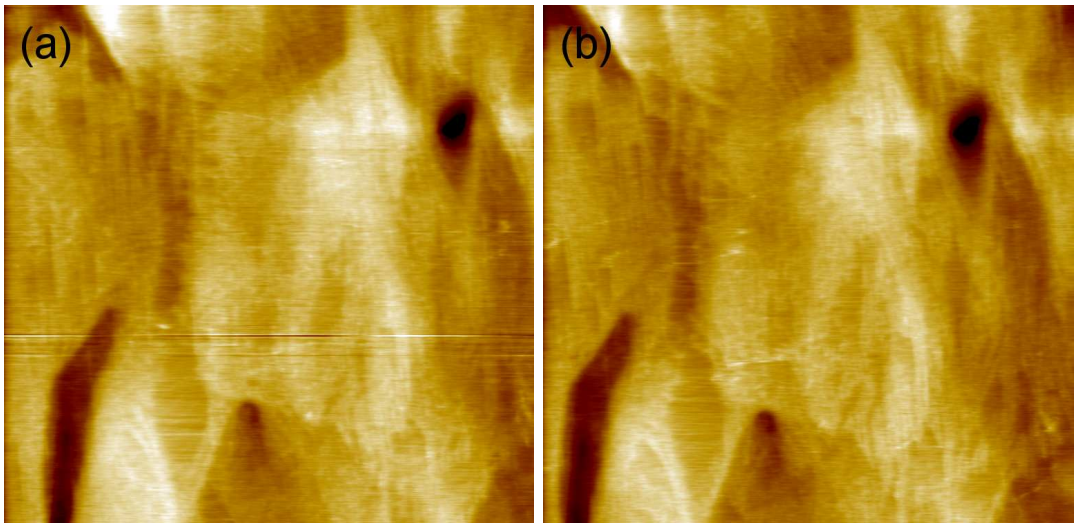

Figure 3.5: AFM contact mode images (2 µm × 2 µm) of a gold surface immersed in buffer imaged (a) before scratching and (b) after scratching.

Thus, even though gold surfaces imaged in buffer can have a surface-structure that resembles the surface-structure observed on AFM images of gold surfaces with an immobilized molecular layer, scratching experiments show prospects to be a method to differentiate between the two types of surfaces.

3.1.3 Influence from the Scanning Force

Besides from characteristics of the tip and the medium used, the scanning force used during imaging can influence the appearance of the gold surfaces on AFM images.

Figure 3.6 shows a contact mode image (5 µm × 5 µm) of a gold surface imaged in phosphate buffer. In the upper part of the image a large amount of bright structures can be observed, while the lower part of the image is depleted from these kind of bright structures. At the interface between the two areas two lines is observed (see arrow). At these lines the set-point[5] has been changed, which means that the scanning force has been altered. The scanning force used in obtaining the lower part of Figure 3.6 has been higher than the scanning force used in obtaining the upper part of the image.

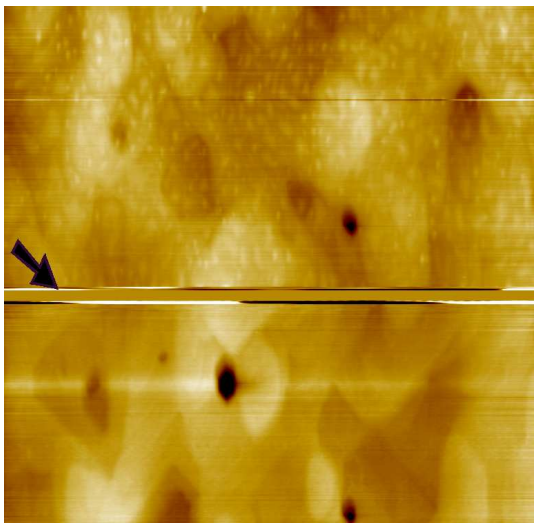

Figure 3.6: AFM contact mode image (5 µm × 5 µm) of a gold surface imaged in phosphate buffer. The arrow shows the transition from a low to a high scanning force.

Even though the upper and lower part on the gold surface in Figure 3.6 have been obtained with different scanning forces, the change in appearance of the surface can be due to a change in the characteristics of the tip. One cannot exclude that some material attached to the tip, causing the bright structures in the upper part of the image, have been removed from the tip when the scanning force was increased.

Figure 3.7 shows a contact mode image (3 µm × 3 µm) of a gold surface imaged in phosphate buffer, where the change in appearance of the surface is caused by

[5]Parameter during AFM measurements that regulate the scanning force, see section 2.1.

change in the scanning force.

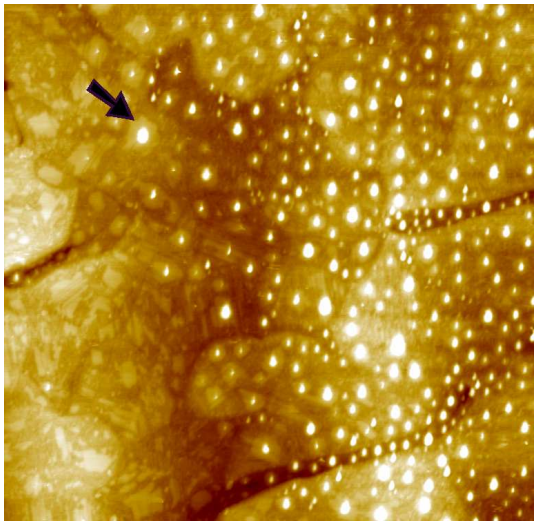

Figure 3.7: AFM contact mode image (3 µm × 3 µm) of a gold surface immersed in phosphate buffer. The bright structures in the right part of the image have measured widths of 70-100 nm and measured heights of 7-10 nm.

In the right part of Figure 3.7 round, bright objects are observed with measured widths of 70-100 nm and measured heights of 7-10 nm. In the left part of the image the bright objects have been replaced by a kind of surface-structure. However, the round, bright objects and the surface-structure could be related to each other. The arrow in Figure 3.7 shows a round object that is surrounded by a bright surface-structure, indicating that the bright objects and the surface structure are two illustrations of the same phenomenon.

The transition from surface-structure to more protruding objects on the surfaces shown in Figure 3.7 is caused by change in the scanning force during imaging, possibly due to a not firmly mounted liquid cell. The results indicate that the scanning force used during imaging can influence the appearance of the gold surface, and that the phenomenon that causes the observance of bright structures on AFM images can be concealed by using a high scanning force.

The protruding structures observed in Figure 3.7 have shown to be nanobubbles and are presented and discussed in Chapter 5.

3.2 Regular Contamination

Even though the liquid cell, o-ring and other devices used during AFM measurements in liquid are thoroughly washed before use, there is still a risk that

particles or other contaminations are introduced into the system during measurements. Furthermore, the phosphate buffer and other solutions used during the measurements can contain pollution that comes in contact with the gold surface.

Figure 3.8 shows an AFM contact mode image (5 µm × 5 µm) of a gold surface imaged in phosphate buffer, where larger plateaus on the gold surface are visible, while the smaller plateaus are more difficult to identify. Several small, bright structures are observed on the AFM image, and these are interpreted as regular contamination, probably in form of some kinds of particles.

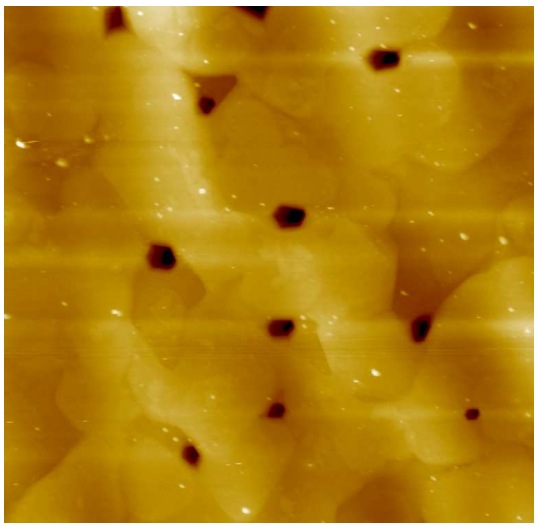

Figure 3.8: AFM contact mode image (5 µm × 5 µm) of a gold surface imaged in phosphate buffer.

Particles, or other regular contaminations present in the system during AFM experiments with molecules, can influence the experiments negatively and can for example be misinterpreted for being aggregates of molecules. Therefore, surfaces showing characteristics as observed in Figure 3.8 are rejected for use in immobilization and hybridization experiments.

3.3 Summary

Spontaneous changes, which are changes occurring even if no imaging parameters have been changed deliberately, in the appearance of the gold surfaces have been observed during AFM measurements on gold surfaces imaged in air, clean water and phosphate buffer.

Results from imaging in different media and with different tips indicate that

both medium and characteristics of the tip influence the appearance of gold surfaces on AFM images, but that the characteristics of the tip are more critical than the medium used. Furthermore, the scanning force used during imaging have an effect on the appearance of the surface.

The spontaneous changes observed on AFM images should be taken into account when results from immobilization and hybridization experiments are analyzed, and even though a tip is estimated to be suitable for experiments with molecules, the characteristics of the tip should not be considered to be constant during the AFM measurements.

Chapter 4

DNA on Gold Surfaces

The BioProbe sensor is based on immobilization of 25 bases long ssDNA molecules on a cantilever surface and their hybridization with the complementary strand present in a solution (see section 1.2, page 2). One of the most critical parameters in the sensor is the molecular layer of ssDNA molecules, and it is of great importance that the molecular layer is characterized and well-controlled. Besides from the density of immobilized ssDNA molecules and their efficiency regarding hybridization, it is of interest to study the configuration of the molecules, their distribution on the surface and how they interact with each other and the surface they are immobilized to.

In this chapter AFM investigations performed in liquid on the immobilization of 25 bases long ssDNA molecules on gold surfaces, and their hybridization to the complementary ssDNA strand are presented. Furthermore, preliminary AFM experiments with biotin-labelled ssDNA molecules and streptadivin-coated gold particles are presented and discussed.

4.1 Background

In the late 90's publications of AFM investigations of molecular layers of short DNA molecules ($\leq$50 bases) immobilized on gold surfaces started to appear in the literature [23, 24, 25, 26, 27, 28]. In 1998 Kelley et al. [25] published AFM images of molecular layers of short, thiol-modified dsDNA molecules on gold surfaces where they showed that electric fields could be used to orient the dsDNA molecules in different angles to a gold surface. In 2001 Huang et al. [24] and Satjapipat et al. [27] presented AFM images of thiol-modified ssDNA molecules on gold, where bright structures with diameters in the nanometer range were interpreted as DNA molecules. Later AFM investigations with thiol-modified ssDNA molecules with concentrations in the same range showed that the gold surface was completely covered with a molecular layer and that single ssDNA

molecules could not be identified in the molecular layer on AFM images [28]. Mourougou-Candoni et al. [23] have suggested that the brighter structures sometimes observed on AFM images of gold surfaces with introduced DNA molecules are caused by impurities or aggregation of molecules.

In 1997 Herne and Tarlov [29] proposed that dense molecular ssDNA layers accessible for hybridization on gold surface could be obtained by using a 'spacer molecule'. The spacer molecule can release unspecific interaction between gold surface and ssDNA molecules and thereby result in a molecular layer, where the ssDNA molecules only interact specifically with the gold surface, are less folded and more accessible for hybridization.

It is quite novel to use AFM as a method to investigate hybridization of short, immobilized DNA strands in a liquid environment, and the literature in this area is rather scarce [23, 24, 27, 28]. In 2002 Zhou et al. [28] presented the first AFM investigation in liquid of hybridization between short, immobilized ssDNA strands and their complementary DNA strands, where the thickness of molecular layers on gold surfaces was used to argument for the occurrence of immobilization and hybridization.

4.2 Experimental

In the AFM investigations of DNA on gold surfaces, the ssDNA molecules are attached to the gold surface through thiol-groups. When the thiol-groups come in contact with the gold, they react spontaneously with the gold, chemisorb to the surface and form bonds almost as strong as covalent bonds[1] [30]. The technique is simple and reliable, and requires a minimum of sample preparations when used during AFM measurements in liquid. Both so-called protected and deprotected ssDNA molecules (see Appendix A) have been used during the immobilization experiments.

The spacer molecule used is mercaptohexanol (MCH), which is a carbon chain of six carbon atoms that is thiol-modified in one end and has a hydroxy-group in the other end. The molecules can bind to the surface through the thiol-group, and the hydroxy-group prevents the ssDNA molecules from adsorbing to the MCH layer on the surface. Furthermore, MCH has the same number of carbon atoms in its chain as the linker molecule between the thiol-group and the ssDNA strand in the DNA molecules (see Appendix A), which minimizes the risk for MCH to interact with the hybridization reaction.

The complementary ssDNA strand used during hybridization experiments is not

[1] The bond formed between thiol and gold is approximately 40 kcal/mol.

modified in any way.

AFM imaging in both contact mode and tapping mode have been performed in a phosphate buffer with standard silicon[2] or silicon nitride[3] tips (see also section 2.1, page 5).

The substrates used are ultra-flat gold surfaces fabricated in the clean room at MIC, by evaporating gold onto mica under specific conditions (see section 2.2.2, page 12). The gold surfaces are imaged in phosphate buffer before introduction of any molecules to examine the quality of the gold surface, as well as the quality of the tip. The surface needs to have plateaus that are ultra flat on a scale of a couple of hundred nanometer in width, and the tip needs to be sharp and have a well-defined conic shape at the apex.

4.3 Immobilization Experiments

Results from AFM investigations on immobilization of ssDNA molecules on ultra-flat gold surfaces indicate that the immobilization involves several processes and that the immobilized ssDNA molecules are more or less folded on the gold surface. Furthermore, the results indicate that unspecific interactions between ssDNA molecules and the gold surface can be released by MCH and that this can be registered through AFM imaging.

4.3.1 Introduction

AFM investigations on the interaction between ssDNA molecules, MCH molecules and gold surfaces have been performed in order to obtain information about molecular layers of short, ssDNA molecules on gold surfaces, as well as about how ssDNA molecular layers can be optimized for hybridization. Information about the thickness of the molecular layers has been obtained by performing scratching experiments, where part of the immobilized layer is removed by the AFM tip.

4.3.2 Immobilization of ssDNA

Figure 4.1 shows three contact mode AFM images of the same 2 μm × 2 μm area of a gold surface immersed in phosphate buffer together with two profiles of the surface. Figure 4.1(a) shows an image of the gold surface before any molecules have been introduced, while Figure 4.1(b) shows an image obtained directly after introduction of 1 μM protected ssDNA solution and Figure 4.1(c) shows the same

[2]ULTRASHARP Si cantilever, MikroMasch, Estonia.

[3]Standard Silicon Nitride Probes from Digital Instruments, now part of Veeco Instruments.

area approximately 40-50 minutes after the introduction of the ssDNA molecules. Figure 4.1(d) is a profile of the image shown in (b), and Figure 4.1(e) is a profile over the image shown in (c).

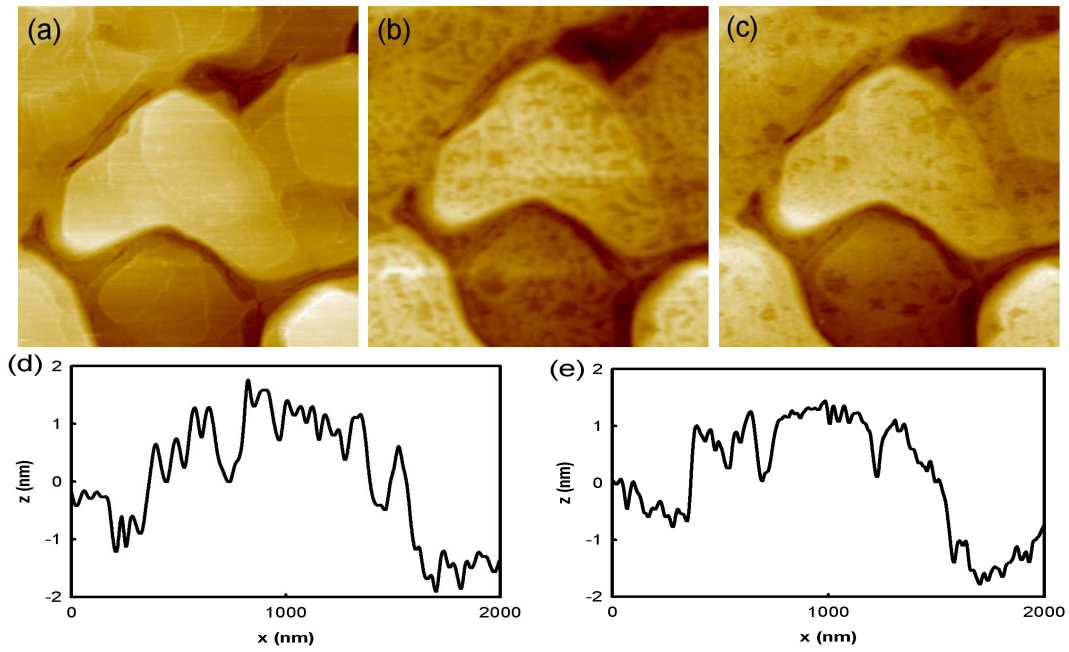

Figure 4.1: AFM contact mode images (2 µm × 2 µm) of a gold surface imaged in buffer; (a) before the introduction of 1 µM protected ssDNA molecules, (b) directly after introduction of the ssDNA molecules, and (c) approximately 40-50 minutes after introduction of the ssDNA molecules. Figure 4.1(d) is a profile of the image shown in (b), and Figure 4.1(e) is a profile of the image shown in (c).

In Figure 4.1(a) both larger and smaller plateaus on the gold surface are observed. The surface looks smooth and no surface-structure is observed on the image. In Figure 4.1(b), where the ssDNA molecules have been introduced to the surface, darker areas are observed on the surface. The difference in brightness between the darker areas and the rest of the surface corresponds to approximately 1 nm on the z-scale, and the difference in brightness does not change over time if no new molecules are introduced into the system. However, the amount of darker areas on the surface does change over time, and images obtained approximately 30-35 minutes after the image in (b) contain less amount of darker areas (see Figure 4.1(c)). There are also some changes in the shape of the darker areas between (b) and (c).

The darker areas in Figure 4.1(b) and (c) are interpreted as areas on the gold surface that are not covered with ssDNA molecules, and the change in the shapes and the amount of the darker areas over time as a sign of adsorption of ssDNA

molecules still present in the solution, and mobility of the ssDNA molecules on the surface.

Darker areas are also observed on AFM images after introduction of deprotected ssDNA molecules (see section 4.4.2, page 43). When deprotected molecules are used, the tendency of change in the amount of darker areas over time has not been as distinct as when protected ssDNA molecules are used.

Thiol versus Sulphur-bridge

From the AFM experiments performed with protected and deprotected ssDNA molecules, it has not been possible to conclude whether protected or deprotected ssDNA molecules adsorb most readily to the surface.

It has been reported in the literature [31, 32, 33, 34] that the bond between the two sulphur atoms in a sulphur-bridge is broken when introduced to a gold surface. Experiments performed and published by others [33] using alkanethiols and dialkyl disulfides have shown that molecules containing a disulfide adsorb more readily to a gold surface than molecules containing a thiol-group. This has been explained by the need of breaking the strong S-H bond in the thiol before the sulphur can react with the gold. This is not necessary when the sulphur in a sulphur-bridge reacts with the gold surface.

Thus, protected ssDNA molecules (contain a sulphur-bridge) are expected to adsorb more readily to the gold surface than deprotected ssDNA molecules (contain a thiol-group). However, the deprotected ssDNA molecules are smaller than the protected ssDNA molecules and can therefore be expected to diffuse faster to and on the surface, which can result in enhanced adsorption of the deprotected molecules relative to the protected ones.

Kinetics

Results from the performed AFM experiments point toward that the formation of molecular layers of thiol-modified ssDNA molecules on gold surfaces involves several processes. The darker areas in Figure 4.1(b) and (c) are interpreted as areas on the gold surface with no immobilized ssDNA molecules, and the change in amount and distribution of darker areas on the surface as a sign of the dynamics in the molecular layer. In Figure 4.1(b) the molecules have physisorbed to the surface, but they are still quite mobile. During the time between the recording of Figure 4.1(b) and (c) the molecules have diffused on the surface, and at the same time other molecules have desorbed from and adsorbed to the surface. The result is a change in amount and distribution of darker areas, as can be observed in Figure 4.1(c).

Studies done by others [35, 36, 37] on kinetics of immobilization of short, thiol-modified DNA molecules on gold surfaces have also shown that the formation of DNA molecular layers involves several processes, such as adsorption, desorption and diffusion. In most cases the results could be shown to follow Langmuir isotherms (see Appendix B).

A Langmuir adsorption/desorption model has been fitted to experimental data from immobilization of the short, thiol-modified ssDNA molecules on gold-coated cantilevers used in the BioProbe project (see section 1.2, page 2) with good agreement between experimental results and theoretical calculations [37]. Figure 4.2 [4] shows a measurement performed on a cantilever where thiol-modified ssDNA molecules were adsorbed to the cantilever surface. The arrow indicates flushing the system with water, which release some of the stress obtained during immobilization, and the thin line represents a Langmuir adsorption/desorption model.

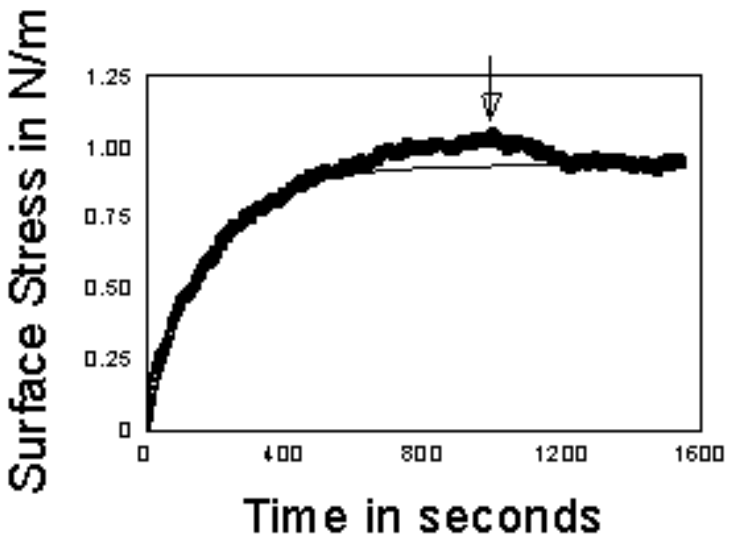

Figure 4.2: Measurement of stress caused by immobilization of thiol-modified ssDNA molecules on a cantilever surface. The arrow indicates where the system has been flushed with water, which results in release of some of the stress. The thin line represents a Langmuir adsorption/desorption model.

Influence on Immobilization from the Structure of the Gold Surface

Steps between plateaus on the gold surface are anticipated to be more active than the ultra-flat areas on the plateaus [22, 23, 24], and the molecules are therefore expected to adsorb at the steps first. Therefore, the distribution of darker areas

in Figure 4.1 could be a reflection of the distribution of steps between plateaus on the surface.

In Figure 4.1(b) and (c) steps between larger plateaus are observed on the image, and there are no darker areas positioned directly at these steps. However, the smaller steps present on the larger plateaus cannot be identified so easily on the AFM images, and it is not possible to estimate the relationship between darker areas and smaller steps from obtained the AFM images.

Conformation of ssDNA Molecules

By interpreting the darker areas observed on the AFM images in Figure 4.1(b) and (c) as holes in a molecular layer, the difference in the height between darker areas and the rest of the surface (the depth of the holes) can be used to obtain information about the conformation of the immobilized molecules.

From profiles of the AFM images shown in Figure 4.1 (see Figure 4.1(d) and (e)), the depth of the holes can be estimated to be about 1 nm, which indicates that the ssDNA molecules are folded on the surface. Theoretically, an outstretched ssDNA molecule with 25 bases should have a length of ∼16 nm [38], but since ssDNA molecules are flexible molecules with a persistence length of about 1 nm [39], they are expected to 'curl up' and be folded when immobilized on a surface. Furthermore, when imaging in contact mode in liquid there is a risk for the scanning tip to compress the molecular layer, and this can results in an even smaller depth. A folded conformation of small DNA molecules on surfaces has also been observed in AFM investigations performed by others [23, 40].

Density of Molecules

If darker areas on the gold surfaces represent areas with no immobilized molecules, this could indicate that there are not enough ssDNA molecules in the system to cover the gold surface.

The number of DNA molecules in the liquid cell (N) during immobilization experiments can be estimated from

$$N = CAV, \tag{4.3-1}$$

where C is the concentration of the ssDNA solution, A is Avogadro's constant[4], and V is the volume of the ssDNA solution in the liquid cell.

[4] 6.022×10^{23} mol^{-1}

A typical concentration of the ssDNA solutions used in the experiments is 1 μM, and the volume of the solution in the liquid cell can be estimated to be $\sim 28 \times 10^{-6}$ l, which gives

$$N \approx 1.7 \times 10^{13} \text{ molecules.}$$

One can estimate[5] the density of immobilized molecules on a gold surface to be about 10^{12} molecules/cm^2, and the area of gold surface exposed to the DNA solution in the liquid cell to be ~ 0.28 cm^2. Thus, the minimum amount of molecules needed for covering the gold surface exposed to solution in the liquid cell (M) is

$$M \approx 2.8 \times 10^{11} \text{ molecules.}$$

Thus, from these simple calculations there should be enough ssDNA molecules in the solution to cover the gold surface.

However, during immobilization the ssDNA molecules have the possibility to interact with other surfaces than the gold surface, for example the surface of the cantilever substrate and the surface of the liquid cell. Furthermore, between the ssDNA solution is made, and it is introduced into the liquid cell, it comes in contact with many different polymer surfaces. The ssDNA molecules can interact with these surfaces, resulting in a reduction of the amount of molecules available for immobilization on the gold surface.

Besides from the possibility for the ssDNA molecules to adsorb to other surfaces than the gold surface, the estimate of the density of immobilized ssDNA molecules contains some uncertainties. The density used in the presented calculation is based on fluorescence-labelling experiments done on gold surfaces with somewhat different characteristics than the gold surfaces used during AFM experiments (see Appendix D).

In AFM measurements published by others [23, 24] and done on gold surfaces comparable to the gold surfaces used in the presented AFM experiments, with ssDNA concentration in the same range, values of the density of ssDNA molecules on gold surfaces ranged from $\sim 10^{10}$ molecules/cm^2 [24] to $\sim 10^{12}$ molecules/cm^2 [23]. In these measurements the density of molecules was estimated by 'counting bright structures' on AFM images. However, the bright structures can be aggregates of molecules, or even contaminations, and the method cannot be considered to be a reliable one.

To obtain a more realistic estimate of the density of molecules on the gold surfaces,

[5] Based on fluorescence-labelling experiments performed by Rodolphe Marie, Ph.D. student in the BioProbe project.

electrochemistry experiments have been performed[6] (for experimental details, see Appendix C). From these experiments a density of about 10^{13} molecules/cm^2 was found.

During electrochemistry experiments the ssDNA molecules are immobilized on a Au(111) crystal, but even if some of the gold surfaces used in AFM experiments show characteristics similar to Au(111) surfaces (see section 2.2.3, page 16) the two surfaces cannot be considered to be identical. The gold surfaces used in the AFM experiments have a large amount of steps separating ultra-flat plateaus. The steps between the plateaus on the gold surface are expected to be more active than the ultra-flat areas on the actual plateaus [22, 23, 24], and their presence may result in a higher density of ssDNA molecules than on a Au(111) crystal surface.

Thus, electrochemistry experiments combined with characteristics of the gold surfaces used in AFM experiments indicate that the density of immobilized ssDNA molecules is closer to 10^{13} molecules/cm^2 than 10^{12} molecules/cm^2, which was used in the presented calculation. However, even if a density of 10^{13} molecules/cm^2 is used in the calculations, there should still be enough molecules to cover the surface - under assumption that all ssDNA molecules in a 1 μM solution are available for immobilization.

Independent of the amount of molecules available for immobilization, specific characteristics of molecules can result in close packaging of molecules on a surface and influence the configuration of molecular layers. However, the ssDNA molecules have a negative charge [41], which does not favor a close packaging of the molecules or a configuration with holes in a molecular layer. Furthermore, investigations performed by others [27] have suggested that there can be a tendency of steric interaction and hinderance between ssDNA molecules when they are immobilized on ultra-flat surfaces, which also would result in evenly distributed molecules on the surface, and not in the formation of a molecular layer with holes.

The presented calculations, experiments and estimations indicate that even though the solution used during the AFM experiments theoretically should contain enough molecules to cover the gold surface, other circumstances have resulted in that a reduced amount of molecules have been available during immobilization. Therefore, the darker areas observed in Figure 4.1(b) and (c) are interpreted as holes in a molecular layer on the gold surface caused by a situation, where there are

[6] In collaboration with Ph.D. Hainer Wackerbarth at the Chemistry Department at DTU and the Midterm-project students Michael Stoltenborg, Jesper Petersen and Lars von Gersdorff, see Appendix C.

not enough ssDNA molecules present in the system to cover the entire surface.

4.3.3 Mercaptohexanol

The unspecific interactions between the gold surface and the ssDNA molecules can be released by adding the small, thiol-modified molecule mercaptohexanol (MCH) to the molecular layer of ssDNA molecules. Thereby a molecular layer that consists of MCH and ssDNA, only attached through their thiol-groups can be formed.

In Figure 4.3 two AFM contact mode images are shown of the same 1 μm × 1 μm large area of a gold surface together with a profile over one of the holes observed in Figure 4.3(a). Figure 4.3(a) shows the surface after introduction of 1 μM deprotected ssDNA molecules, while (b) shows the surface approximately 50 minutes after the subsequent introduction of 1 mM MCH.

In Figure 4.3(a) several darker areas are observed on the AFM image. The darker areas have a diameter of 50-100 nm, and the difference in brightness between the darker areas and the rest of the surface corresponds to approximately 1 nm on the z-scale. After introduction of MCH the darker areas start to disappear, and after approximately 50 minutes they are essentially gone (see (b)), but the surface looks quite structured and grained compared to a clean gold surface (see for example Figure 4.1(a), page 32).

The darker areas in Figure 4.3 (a) are interpreted as holes in a molecular layer covering most of the gold surface (see also section 4.3.2, page 31). When MCH is introduced into the liquid cell, the MCH molecules can react with the gold surface, both in regions where there are no ssDNA molecules and in areas where the ssDNA molecules interact unspecifically with the gold surface. Thereby unspecific interactions between ssDNA molecules and the gold surface may be released, and a molecular layer where all molecules are attached to the surface through the thiol-group may be formed. The situation is schematically illustrated in Figure 4.4.

The more 'blurred' appearance of the surface in Figure 4.3(b) compared to (a) can be explained by a transformation from a globular conformation, (a), to a less folded conformation, (b), of the immobilized ssDNA molecules. The less folded ssDNA molecules are expected to interact more with the scanning tip than the folded molecules.

Thus, the disappearance of the darker areas on the AFM images is interpreted as the formation of a mixed layer of ssDNA and MCH covering the surface and where the ssDNA molecules are less folded than before, and thereby more available for

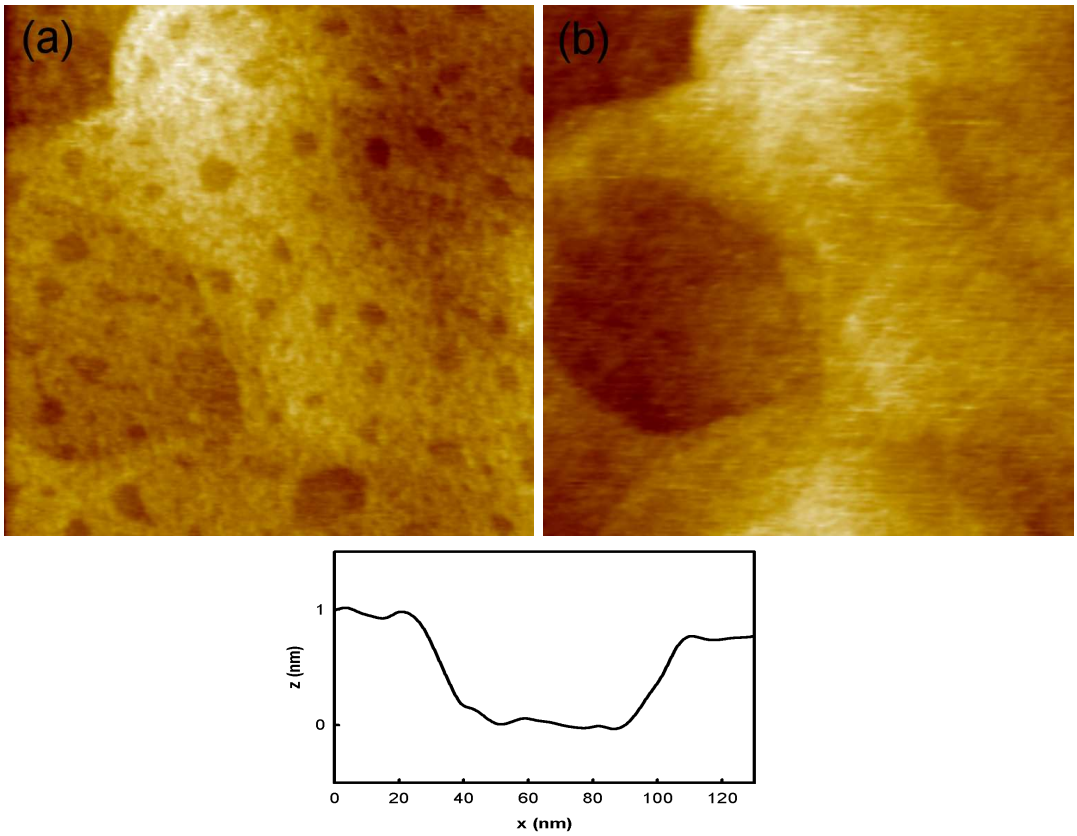

Figure 4.3: AFM contact mode images (∼1 µm × 1 µm) of a gold surface obtained (a) after introduction of 1 µM deprotected ssDNA and (b) approximately 50 minutes after the subsequently introduction of 1 mM MCH. The darker areas in (a) have a diameter of 50-100 nm and a depth of about 1 nm, which can be observed in the profile, which is a profile over one of the holes observed in (a).

hybridization.

4.3.4 Scratching

Scratching experiments have been performed to further investigate the interaction between the ssDNA and MCH molecules and the gold surface. Information about the thickness of the molecular layer, and thereby about the conformation of the molecules, can be obtained by removing parts of the immobilized layer and analyzing profiles from subsequently obtained AFM images.

In scratching experiments a limited area on the surface is scanned with a high[7] scanning force, which causes the molecules to be physically removed by the scanning AFM tip in the scratched area. During scratching the scanning motion is

[7] ∼ 10-50 nN

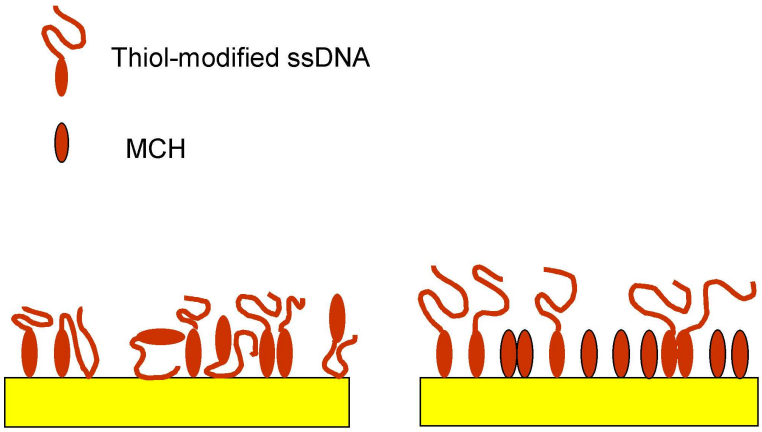

Figure 4.4: Schematic illustration of a molecular layer of ssDNA molecules (to the left) and a molecular layer of ssDNA and MCH molecules (to the right). The MCH molecules release the unspecific bonds between ssDNA molecules and the gold surface.

performed in a direction 90° to the normal scanning direction during imaging. From profiles of images obtained over a larger area with a low scanning force after scratching, one can estimate the thickness of the molecular layer that have been removed.

Figure 4.5 shows an AFM contact mode image (∼1 µm × 1 µm) and profile of a gold surface, to which ssDNA and MCH molecules have been introduced, and on which scratching has been performed. The scratched area is approximately 400 nm in width, and from the profile one can estimate the thickness of the removed layer to be about 1.3 nm.

During the performance of scratching experiments it has been found that it is easier to remove the molecules completely from the scratched area and to measure a thickness of the molecular layer, when the scratching is performed on a mixed layer of ssDNA and MCH molecules, compared to when scratching is performed on a molecular layer consisting of only ssDNA.

During scratching the scanning tip is interacting with the molecules on the surface and because of the high scanning force used, the tip can 'rip off' the molecules from the surface. For scratching to be successful the interaction between tip and molecule has to be strong enough to overcome the molecules' interaction with the gold surface. On surfaces with a mixed layer of ssDNA and MCH molecules all molecules are expected to be attached to the surface through their thiol-group, and the ssDNA molecules are less folded than they are in a layer consisting of only ssDNA molecules. Thus, stronger interaction between tip and molecules can be established during scratching in a mixed layer, and thereby it is easier to produce a clean scratch compared to when scratching is done on molecular layers

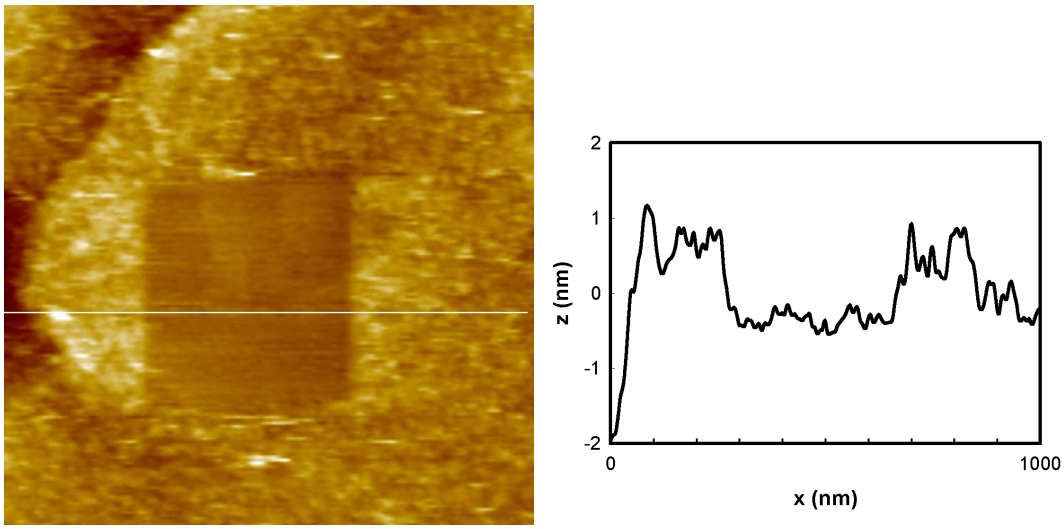

Figure 4.5: AFM contact mode image (1 µm ×1 µm) and profile of a gold surface to which ssDNA molecules and MCH molecules have been introduced, and on which scratching has been performed. The scratched area is approximately 400 nm in width and has a depth of about 1.3 nm.

consisting of only ssDNA molecules.

The estimated thickness of the removed layer in Figure 4.5 is approximately 1.3 nm, which is a small increase compared to the depth of the holes observed in a molecular layer consisting of only ssDNA (see for example Figure 4.3, page 39). MCH is a small molecule with a theoretical length of ∼1 nm and can therefore not directly result in a thicker molecular layer. However, the presence of MCH molecules results in less folded ssDNA molecules and may therefore result in observation of a somewhat thicker layer after scratching.

The small difference between the depths of the holes observed on gold surfaces with immobilized ssDNA molecules and the depth of the scratch after introduction of MCH also indicates that the observed darker areas observed on gold surfaces, to which ssDNA molecules have been introduced, are not formed because of the existence of more than one molecular layer on the gold surface.

4.3.5 Summary

Results from AFM investigations of immobilized ssDNA molecular layers on gold surfaces indicate that the ssDNA molecules are folded when immobilized on the surface.

Darker areas are observed on the gold surfaces after introduction of ssDNA molecules, and these are interpreted as areas on the gold surface without im-

mobilized ssDNA molecules. When MCH molecules are introduced to the gold surface with a ssDNA molecular layer, the darker areas disappear from AFM images, indicating that MCH binds to the gold surface and releases unspecific interactions between the ssDNA molecules and the gold surface. Thus, a mixed layer of ssDNA and MCH molecules, where all molecules are attached through their thiol-group are formed on the surface, which makes the ssDNA molecules more accessible for hybridization.

4.4 Hybridization Experiments

Changes in the molecular layer can be observed in the AFM images when the complementary ssDNA strand is introduced to the immobilized molecular layer of ssDNA and MCH, indicating that hybridization occurs between the immobilized ssDNA strands and the complementary ssDNA strands, and that the reaction can be registered through AFM imaging.

4.4.1 Introduction

DNA hybridization is the process where complementary ssDNA strands are base-paring through the bases adenine, guanine, thymine and cytosine to form the well known double helix structure of the dsDNA molecule (see Figure 4.6). The base paring in the dsDNA molecule is very specific, where adenine is pairing with thymine and guanine is paring with cytosine, and if the complementarity of the two ssDNA strands is missing a dsDNA molecule will not be formed.

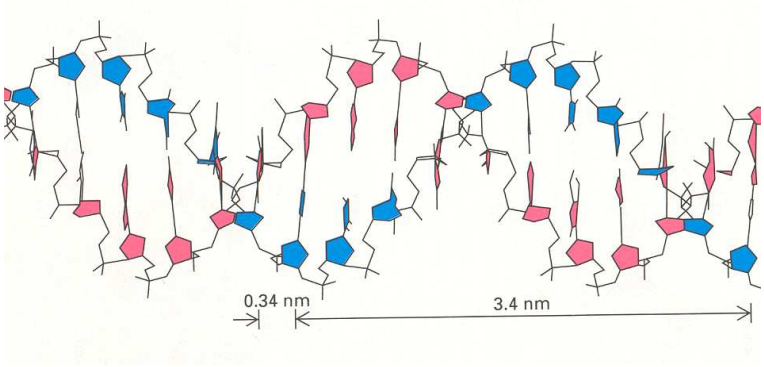

Figure 4.6: Illustration of a dsDNA molecule.

The optimal situation would be to register the hybridization through AFM imaging in real time - 'seeing the hybridization occurs'. This is experimentally quite challenging because of the time scale in which hybridization occurs[8], combined

[8]Estimated to be in the range of seconds when 25 bases long DNA strands are used.

with instability in the experimental system. The system is unstable and imaging is not possible during and in a short period of time after the introduction of solution into the liquid cell. During this period the DNA strands interact with each other, and when imaging is resumed the hybridization has already occurred. Therefore it has been chosen to obtain images before and after introduction of the complementary ssDNA strand, where the images can give information about changes in the molecular layer and thereby give information about the reactions that occur on the surface.

4.4.2 Hybridization of Immobilized DNA Molecules

Figure 4.7 shows a series of AFM contact mode images of a limited area on a gold surface ($\sim$1 μm × 1 μm) to which molecules have been introduced. There is approximately three hours between the recording of (a) and (d). The arrow in (a) shows a structure that can be identified on all images, and the scale bar in (d) is approximately 100 nm long.

Figure 4.7(a) shows the clean gold surface immersed in phosphate buffer. Figure 4.7(b) shows the gold surface directly after introduction of 1 μM deprotected ssDNA solution, and Figure 4.7(c) shows the surface approximately 15 minutes after the subsequent introduction of 1 mM MCH. Figure 4.7(d) shows the surface approximately 10 minutes after introduction of a 1 μM solution of the complementary ssDNA strand.

When the gold surface is imaged in phosphate buffer without any molecules introduced, (a), smaller steps on the flat plateaus on the gold surface can be observed. In (b), where ssDNA molecules have been introduced to the gold surface, the smaller steps are no longer visible and instead darker areas with a width of 50-100 nm are observed. These darker areas are interpreted as areas with no ssDNA molecules (described in section 4.3.2, page 31). After introduction of MCH the darker areas more or less disappears, (c), which is interpreted as adsorption of MCH to the gold surface and release of unspecific interaction between ssDNA molecules and gold surface (described in section 4.3.3, page 38).

In Figure 4.7(d), where the complementary ssDNA strand has been introduced into the system, the appearance of the surface changes once more. The surface looks more smooth and it is again possible to see the underlying structure of the gold surface on the plateaus. The change in appearance of the surface is interpreted as a situation where hybridization has occurred, and where the mixed molecular layer of ssDNA and MCH molecules has been transformed to a mixed molecular layer of dsDNA and MCH molecules.

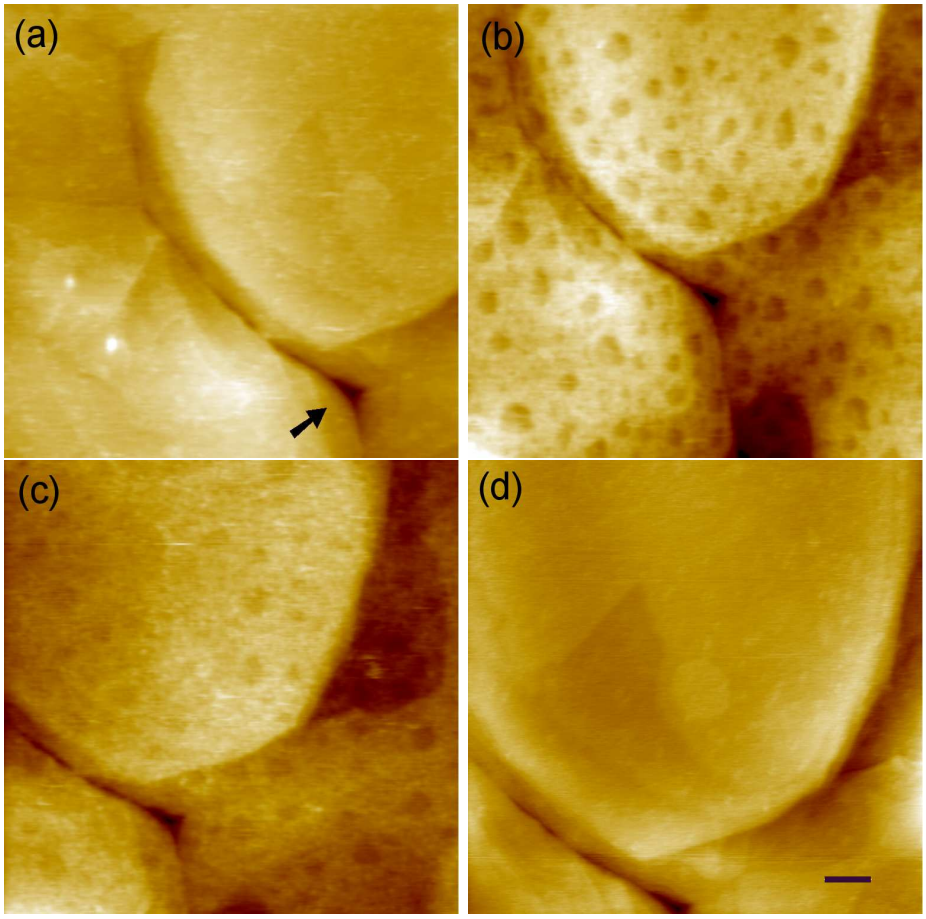

Figure 4.7: AFM contact mode images (∼1 µm × 1 µm) of; (a) the clean gold surface in buffer, (b) the gold surface directly after introduction of 1 µM deprotected ssDNA, (c) the gold surface approximately 15 minutes after introduction of 1 mM MCH, and (d) the gold surface approximately 10 minutes after introduction of the complementary ssDNA strand (1 µM). The arrow in (a) is showing a structure that can be recognized in all of the images and the scale bar in (d) is ∼100 nm long.

Fluorescence- and Radioactive-Labelling Experiments

To strengthen that hybridization can occur when the complementary ssDNA strand is introduced to a molecular layer of ssDNA and MCH immobilized on a gold surface, fluorescence- and radioactive-labelling experiments have been performed[9]. Experimental details can be found in Appendix D.

The basic idea in the fluorescence- and radioactive-labelling experiments is to introduce a complementary ssDNA strand, which is labelled with a fluorescence

[9]The experiments were performed in collaboration with Steen Guldager Petersen and Helle Kinggard Lilja-Fischer at Scandinavian Micro Biodevices A/S (SMB) and student Lars von Gersdorff.

or radioactive marker, to the immobilized layer of ssDNA and MCH molecules, and after the presumably occurred hybridization the hybridized molecules can be detected through the marker.

From the performed fluorescence- and radioactive-labelling experiments signals confirming that hybridization had occurred on the surface could be obtained, and a density of hybridized molecules of $\sim 10^{11}$ molecules/cm^2 was detected.

Since the gold surfaces used during fluorescence- and radioactive labelling experiments and the gold surfaces used in electrochemistry experiments (see Appendix C and Appendix D) are not identical, results from the different experiments cannot be compared qualitatively. In electrochemistry experiments a density of $\sim 10^{13}$ molecules/cm^2 for the immobilized ssDNA molecules was found (see also section 4.3.2, page 35). The density of immobilized ssDNA molecules is expected to be lower on the gold surfaces used during fluorescence- and radioactive-labelling experiments ($\sim 10^{12}$ molecules/cm^2), but the results indicates that the hybridization-efficiency is rather high.

Conformation of Molecules

The immobilized ssDNA molecules are more or less folded because of their short persistence length and flexibility [39] (see also section 4.3.2, page 35). When the complementary ssDNA strand is introduced into the system, hybridization is expected to occur and dsDNA molecules to be formed on the surface. The dsDNA molecules have a persistence length of about 50 nm [39] and are much more stiff and elongated than the ssDNA molecules. A mixed molecular layer of dsDNA and MCH molecules is therefore expected to be thicker and more rigid than a mixed ssDNA and MCH molecular layer. Furthermore, the dsDNA molecules have a more or less identical configuration because of their double helix structure. Thus, if a mixed layer of dsDNA and MCH molecules is formed on the surface, the underlying structure of the gold surface could be visible again, which is strongly indicated by Figure 4.7(d). The situation with the two kinds of molecular layers is schematically illustrated in Figure 4.8.

4.4.3 Scratching

The image in Figure 4.7(d) shows a surface on which it is interpreted that a mixed layer of immobilized dsDNA and MCH molecules exist. The image resembles the appearance of Figure 4.7(a), which shows a surface with no immobilized molecules. Scratching experiments have been performed to investigate if the appearance of the gold surface after introduction of the complementary ssDNA strand is caused by a reaction between molecules on the surface or by removal of

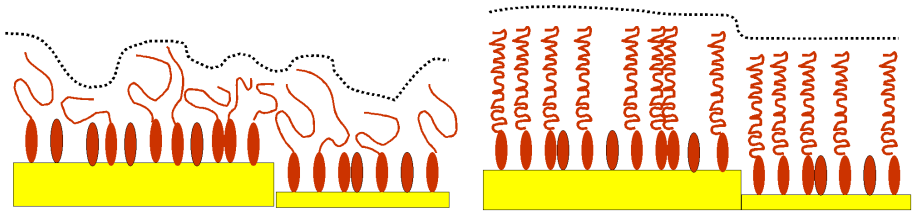

Figure 4.8: Schematic figure of a mixed layer of ssDNA and MCH molecules (to the left) and dsDNA and MCH molecules (to the right). The ssDNA molecules are flexible molecules with persistence length of about 1 nm and are in a folded state on the surface, while the dsDNA molecules are more elongated and stiff molecules with persistence length around 50 nm and can better persist the impact from the scanning AFM tip.

molecules from the surface. The scratching has been performed using the same method as described in section 4.3.4, page 39.

Figure 4.9 shows two AFM contact mode images (∼350 nm × 350 nm) and profiles of a gold surface, on which hybridization and scratching experiments have been performed. Figure 4.9(a) is an AFM image of the gold surface with immobilized ssDNA and MCH molecules. The darker area is the area where scratching has been performed, and from the profile the depth of the scratch can be estimated to approximately 0.4 nm. In Figure 4.9(b) an AFM image of the same gold surface as in (a), but after introduction of the complementary ssDNA strand with a scratched area, is shown. Here the depth of the scratch can be estimated to be approximately 1.2 nm from the profile.

Thus, the thickness of the removed molecular layer on the gold surface increases after introduction of the complementary ssDNA strand, which strengthens the assumption that hybridization has occurred between the two DNA strands. The dsDNA molecules have a more elongated configuration than the ssDNA molecules and are therefore expected to result in a thicker molecular layer.

Even though the thickness of the molecular layer increases after hybridization, the thickness is still too small compared to a theoretical value. Theoretically a dsDNA molecule of 25 bases would have a length of ∼8 nm [42], and even if the molecules are standing with an angle of ∼30° to the gold surface[10] [31, 43] the thickness found from scratching experiments is still too small.

In the AFM investigations presented the samples with immobilized molecular layers have been imaged with contact mode in liquid, and even if the scanning force is regulated to be as small as possible during imaging there is a risk for the tip to compress the molecular layer and thereby to reduced the measured thick-

[10]The tilt angle of alkanethiols is typically ∼30° on gold.

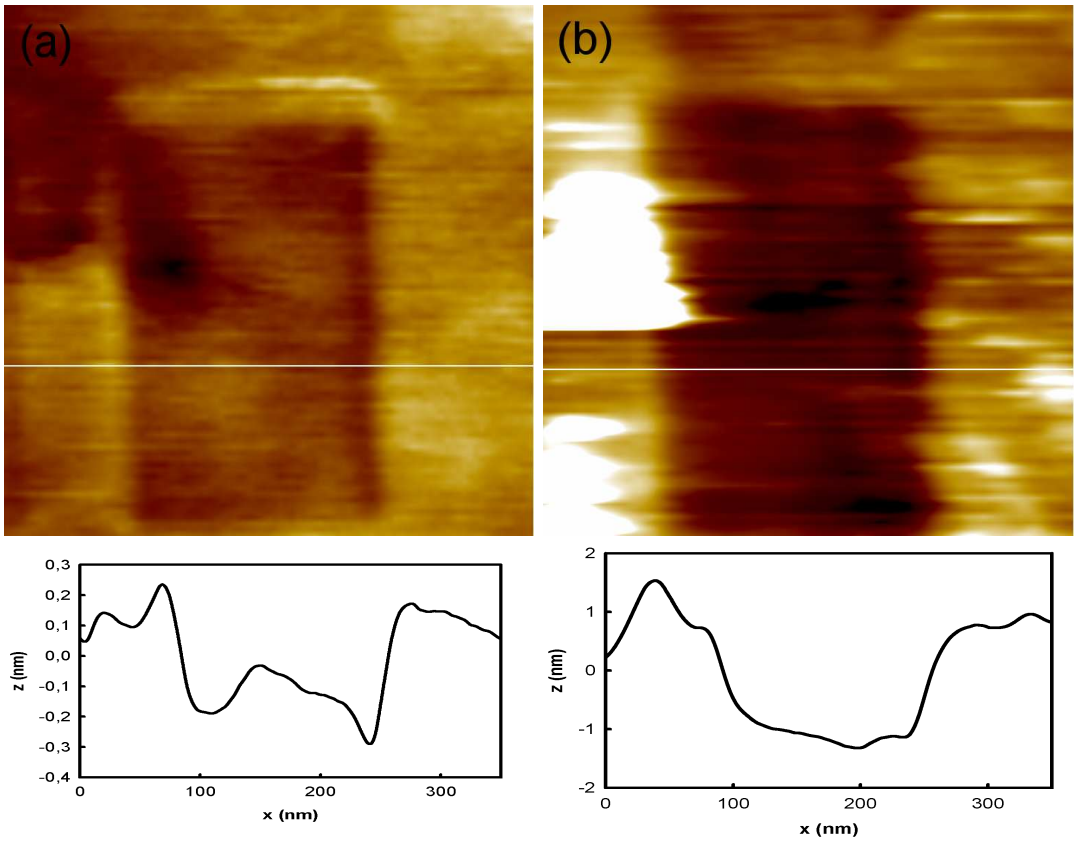

Figure 4.9: AFM contact mode images (∼350 nm × 350 nm) and profiles of a gold surface on which scratching has been performed. Figure 4.9(a) shows a scratch made on the gold surface with a layer of ssDNA and MCH molecules, while (b) shows a scratch performed on a layer of dsDNA and MCH molecules. The thickness of the removed molecular layer in (a) is approximately 0.4 nm, while it in (b) has increased to approximately 1.2 nm.

ness. Even if a molecular layer of dsDNA molecules is more rigid than a molecular layer of ssDNA molecules, the dsDNA layer cannot be assumed to react as a firm body. Instead, the molecular layers (both ssDNA and dsDNA molecular layers) can be thought of as 'seaweed on the sea floor', where the molecules are affected by the scanning tip.

4.4.4 Summary

Results from hybridization experiments on gold surfaces indicate that hybridization can occur on the surface between immobilized ssDNA molecules and introduced complementary ssDNA molecules, and that one can use AFM imaging to differentiate between mixed molecular layers of ssDNA and MCH and mixed molecular layers of dsDNA and MCH.

From scratching experiments it can be concluded that the thickness of the molecular layer on the gold surface increases after introduction of the complementary DNA strand, which support the assumption that hybridization has occurred on the surface.

4.5 Gold Particles

Preliminary AFM experiments with biotin-labelled ssDNA and straptavidin-coated gold particles with diameters in the nanometer range indicate that the gold particles are a potential marker for the existence of immobilized molecules on the gold surface.

4.5.1 Introduction

During immobilization and hybridization experiments with short DNA molecules it was concluded that it is not always straight forward to distinguish between gold surfaces with molecular layers and gold surfaces without molecular layers through AFM imaging (see section 4.4.2, page 43).

Preliminary investigations have been done to investigate the possibility of using a 'marker', something that can enhance observable changes between gold surfaces with immobilized molecular layers compared and clean gold surfaces. The marker has to be clearly recognizable on AFM images and should not interfere with the immobilization or the hybridization. One possible marker could be gold particles with diameters in the nanometer range that can bind to the molecules.

The possibility to use gold particles with diameter in the nanometer range to study DNA molecules and their interactions with other molecules and surfaces have been subject to investigation by others. In 1997 Elghanian et al. [44] showed that hybridization of short DNA strands could be detected optically by using gold particles in the nanometer range. The color of a solution with particles and molecules will change dependent on the distance between gold particles. The technique was suggested as an alternative to fluorescence- or radioactive-labelling for detecting hybridization on so-called DNA chips, and has been followed up by others [45, 46, 47]. The combination of DNA molecules and gold particles has also been suggested for use in building small structures on surfaces in a controlled manner [48, 49, 50]. AFM has been a popular method in analyzing and characterizing the systems of short DNA molecules and gold particles and all the published AFM investigations have been performed with tapping mode in air [50, 51, 52].

4.5.2 Experimental

The immobilized ssDNA molecules are the same as those used in other experiments with DNA molecules (see Appendix A), except that the molecules also are biotin-labelled in the 3' end. The complementary ssDNA strand is biotin-labelled in the 5' end. The gold particles have diameters of ∼10 nm and are coated with streptavidin. The biotin-streptavidin bond is known to be extremely specific and strong [53] and it is often used to create strong and very specific interaction between different molecules and/or objects [54].

4.5.3 The Idea

The basic idea with the experiments with DNA molecules and gold particles was to enhance changes in the obtained AFM images. By using gold particles that can bind to immobilized ssDNA molecules, or to the complementary ssDNA strand, stronger visualization of immobilization and hybridization may be obtained on AFM images.

Figure 4.10 is a schematic illustration of the different steps involved during the experiments with DNA molecules and gold particles.

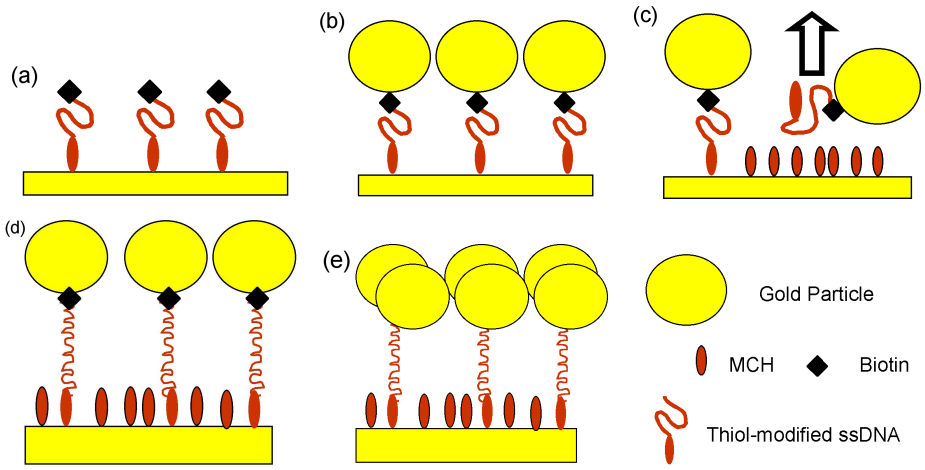

Figure 4.10: Schematic figure of the different steps involved in AFM measurements on DNA molecules and gold particles; (a) thiol-modified, biotin-labelled ssDNA molecules are introduced, (b) streptavidin-coated gold particles are added, (c) MCH molecules are introduced, (d) the biotin-labelled complementary ssDNA strand is introduced, and (e) more streptavidin-coated gold particles are added.

Thiol-modified and biotin-labelled ssDNA molecules are introduced to the gold surface and should bind to the surface through their thiol-group (Figure 4.10(a)). Streptavidin-coated gold particles with diameter of ∼10 nm are introduced and

expected to bind to the ssDNA molecules through the biotin-streptavidin interaction (Figure 4.10(b)). MCH molecules are introduced and are expected to release unspecific interactions between ssDNA molecules and gold surface (Figure 4.10(c)). The biotin-labelled complementary ssDNA strand is introduced to obtain hybridization (Figure 4.10(d)), and then more streptavidin-coated gold particles are introduced to visualize the hybridization by binding to the complementary ssDNA strand (Figure 4.10(e)).

During experiments with DNA molecules and gold particles it was indicated that the gold particles can be used to enhance changes due to immobilization of ssDNA molecules on AFM images. However, it was not possible to observe changes caused by hybridization, since no clear changes could be observed after introduction of the complementary ssDNA strand or more gold particles. Some information about the stability of the system was obtained, indicating that the introduction of MCH result in a instability in the system that is increased with increasing scanning time.

4.5.4 AFM Measurements on Immobilized ssDNA Molecules and Gold Particles

Figure 4.11 shows two contact mode AFM images (5 µm × 5 µm) of a gold surface, where (a) shows the surface after introduction of thiol-modified, biotin-labelled ssDNA molecules, and (b) shows the surface after the subsequently introduction of streptavidin-coated gold particles.

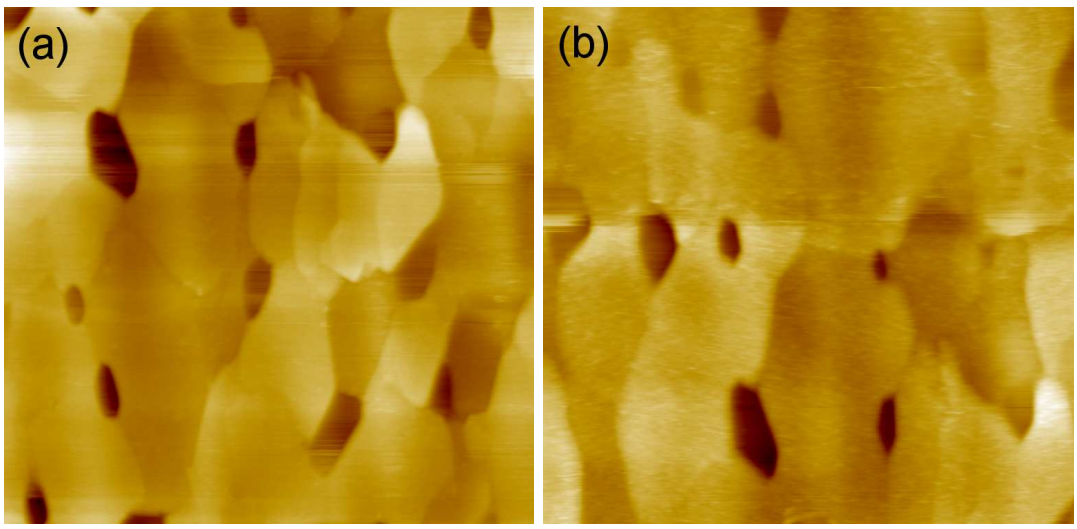

Figure 4.11: AFM contact mode images (5 µm × 5 µm) of a gold surface (a) after introduction of thiol-modified and biotin-labelled ssDNA, and (b) after introduction of streptavidin-coated gold particles.

In Figure 4.11(a) the larger plateaus on the gold surface can be observed, but the smaller plateaus are not visible. In Figure 4.11(b), the larger plateaus are still visible, but compared to (a) the surface has less defined borders between the plateaus on the gold surface and the surface looks more grained.

The grained look of the surface in (b) may be interpreted to be caused by the binding of the gold particles to the immobilized ssDNA molecules. Under this assumption, the image indicates that the gold particles are evenly distributed on the surface and that no aggregates have been formed.

Biotin contains a sulphur atom, which can interact with the gold surface when the ssDNA molecules are introduced to the gold surface. Thus, there are several ways for the ssDNA molecules to interact with the gold surface, and these are schematically shown in Figure 4.12(a) together with an illustration of possibilities of how gold particles can interact with the molecules, see Figure 4.12(b).

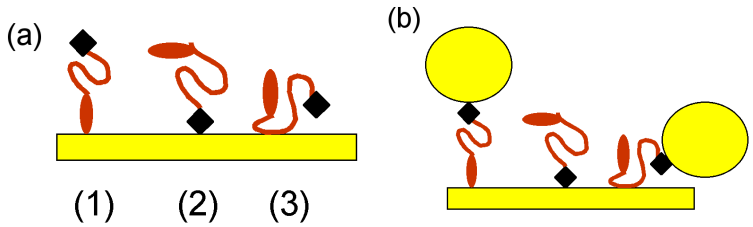

Figure 4.12: Schematic figure of (a) different possible interaction between biotin-labelled ssDNA molecules and gold surface and (b) different possible interaction between ssDNA molecules and gold particles. The ssDNA can bind specific through the thiol (1), specific through the biotin (2), and non-specific through the backbone and bases (3).

4.5.5 Instability in the System

During experiments with molecules and gold particles it has been observed that the system becomes more unstable after introduction of MCH molecules. The instability increased with increasing scanning time.

Figure 4.13 shows two contact mode AFM images (5 μm × 5 μm) of the same gold surface as showed in Figure 4.11. Figure 4.13(a) is obtained approximately 20 hours after the image in Figure 4.11(b). During these 20 hours the surface was scanned several times during a period of approximately 3 hours, where three scratching experiments were performed. During the rest of the time (∼17 hours) the sample was kept in the buffer solution in the liquid cell placed in the AFM without being scanned. Figure 4.13(b) is obtained approximately 1.5 hours after

introduction of MCH, during which scanning of the surface and one scratching experiment were performed.

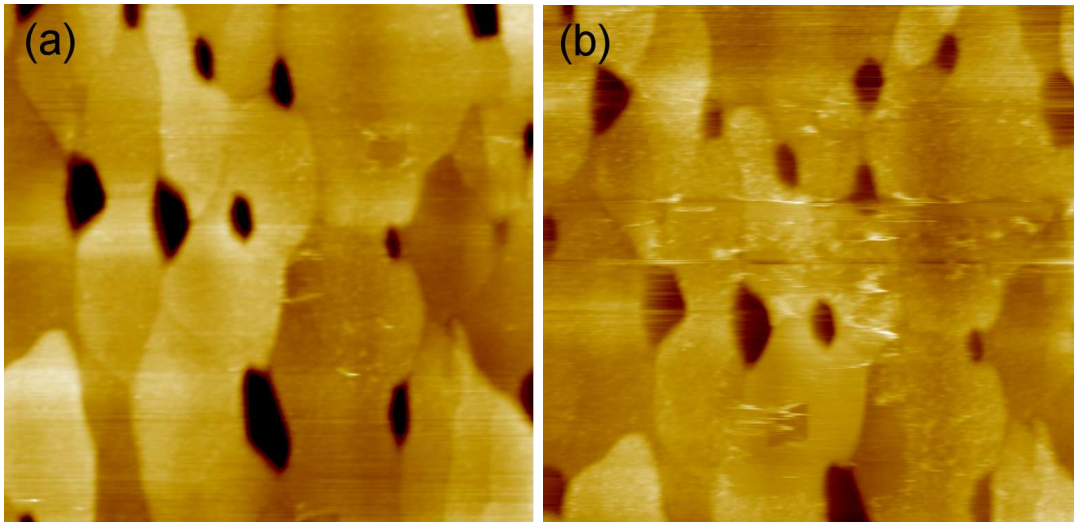

Figure 4.13: AFM contact mode images (5 µm × 5 µm) of the same area on the gold surface shown in Figure 4.11. In (a) the surface before introduction of MCH is shown, and in (b) the surface approximately 1.5 hours after introduction of MCH is shown.

Figure 4.13(a) resembles the image in Figure 4.11(b), and the sample does not seems to have been particulary affected by the scanning or the scratching experiments. In Figure 4.13(b) on the other hand, a tendency of inhomogeneity of the sample surface is observed. The surface contains both grained and smooth areas, and several bright structures can be observed on the surface, indicating formation of aggregates of molecules and/or particles.

Thus, before introduction of MCH, the sample can be subject to several scans and scratching experiments without showing tendency of instability, while the system shortly after introduction of MCH shows instability, even if only a scarce amount of scans and scratching experiments have been performed.

The objective of the introduced MCH molecules is to react with the gold surface and release unspecific interaction between the ssDNA molecules and the gold surface. However, it is possible that the gold particles hinder the MCH to come in contact with the gold surface and instead they may bind to the gold particles, or remain free in the solution. Furthermore, complexes of molecules and gold particles that are not firmly attached to the gold surface could be released to the solution and result in the formation of aggregates.

Influence on Stability from the Scanning Tip

Even though the introduction of MCH seems to be required for instability in the system, the instability is not observed if the system is not subject to scanning or scratching.

Figure 4.14 shows two AFM contact mode images (10 μm × 10 μm) of the same gold surface as the one shown in Figure 4.11 and Figure 4.13 and after introduction of biotin-labelled ssDNA, streptavidivin-coated gold particles, MCH, biotin-labelled complementary ssDNA molecules and more gold particles. In (a) an area of the gold surface that has been imaged many times is shown, while (b) shows an area of the gold surface that has not been imaged before.

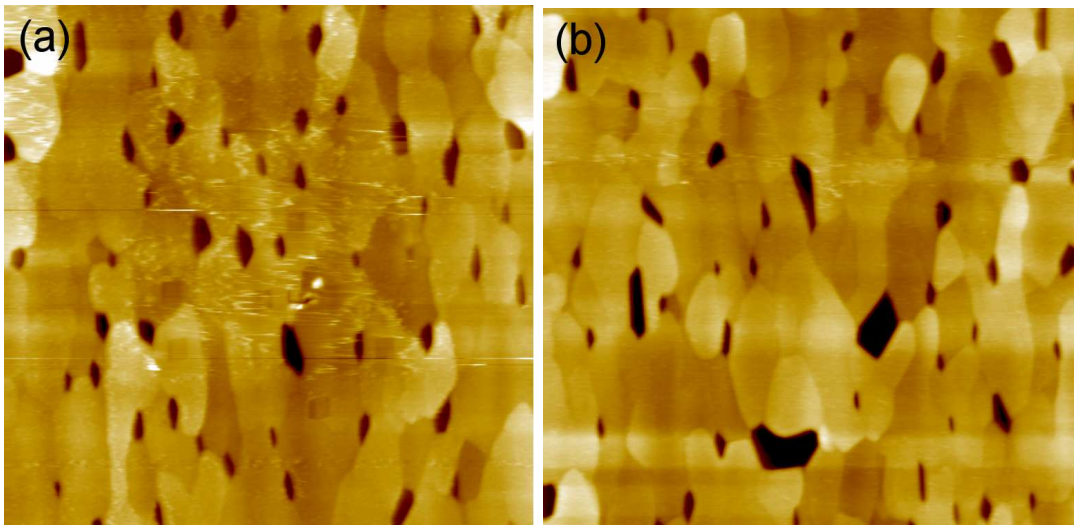

Figure 4.14: AFM contact mode images (10 μm × 10 μm) of the same gold surface as shown in Figure 4.11 and Figure 4.13 after introduction of all molecules and particles mentioned in the text. In (a) an area of the gold surface that has been imaged several times and in which scratching has been performed is shown, while (b) shows an area that is imaged for the first time.

In the central part of Figure 4.14(a), where several scanning and scratching experiments have been performed, several bright structures can be observed, indicating aggregation of molecules and/or particles. Figure 4.14(b) shows an area of the gold surface that has not been scanned before, and this area looks much more smooth than the scanned area in (a). Neither are there bright structures that indicates aggregation of material observed in (b).

The appearance of the AFM images in Figure 4.14 indicates that if the sample is not scanned it can be stable for a long period of time even after the introduction of MCH. Thus, even though the instability seems to be initiated by the intro-

duction of MCH, it is required that the surface is scanned for the instability to show.

Scratching

In Figure 4.13(b) both smooth and grained areas can be observed on the gold surface. To investigate if the smooth areas represents areas where all material has been removed from the gold surface, scratching experiments have been performed. The design and execution of the experiments are the same as described earlier (see section 4.3.4, page 39).

Figure 4.15 shows an AFM contact mode image and a profile of a gold surface after introduction of biotin-labelled ssDNA molecules, gold particles and MCH molecules, on which a 400 nm × 400 nm large scratch can be observed. The scratch is performed in an area containing both smooth and grained regions. The scratch is well defined and border to a smooth area on the right, while it on the left border to a grained area.

From the profile one can estimate the height difference between the scratched area and the smooth area on the right to be approximately 2.2 nm. The height difference between the scratched area and the more grained area is approximately 1.3 nm, but this estimate is more uncertain, since the height of the material on the surface alternates quite much in the grained region of the profile.

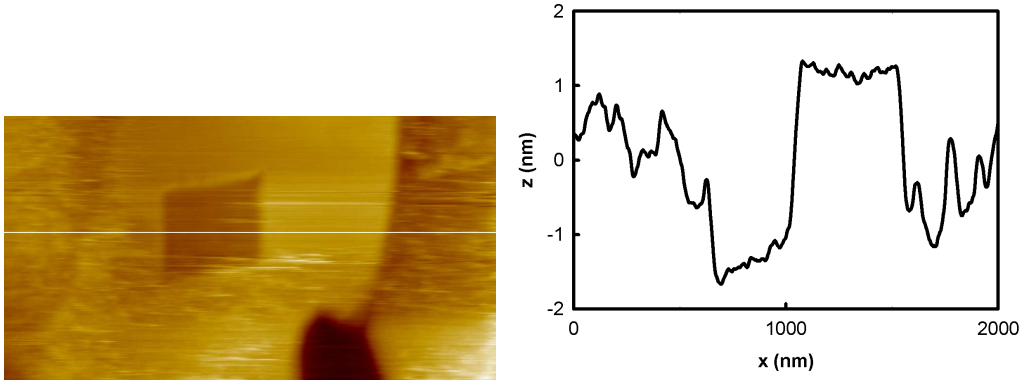

Figure 4.15: An AFM contact mode image with a 400 nm× 400 nm large scratch on a gold surface to which biotin-labelled ssDNA, gold particles and MCH have been introduced, together with a profile over the area.

Thus, material can be removed in areas where the gold surface looks smooth, indicating that these areas do not represent areas without molecules. Instead, the smooth areas can represent areas where there are immobilized molecules, but

where no gold particles are present. The more grained looking area can in return represent an area with gold particles, even if single gold particles cannot be identified.

4.5.6 Discussion and Summary

Results from preliminary experiments with molecules and gold particles indicate that one can enhance changes on AFM images during immobilization experiments by using gold particles as markers.

Immobilized ssDNA molecules and bonded gold particles show high stability over time, but after introduction of MCH the system starts to show instability, and the instability increases with increasing scanning time.

The use of gold particles as markers for enhancing the observance of reactions occurring at the surface have shown some prospects, but more investigations are needed for any clear conclusions to be made. Furthermore, it should be noted that the procedure described in this section contains some weak points. First, if would be more suitable to introduce the MCH molecules before the gold particles. There is a risk for the gold particles to hinder the interaction between the gold surface and the MCH molecules. Second, even if the gold particles have diameters in the nanometer range, they are still rather large compared to 25 bases long ssDNA molecules and can probably interfere with the hybridization process. Third, by using contact mode imaging, the tip is expected to interact and affect the molecular layer and gold particles more than if tapping mode was used.

Chapter 5

Nanobubbles

Nanobubbles, bubbles with dimension in the nanometer range, can form spontaneously on the gold surfaces when they are immersed in liquid. Results from contact mode and tapping mode imaging show that nanobubbles appears with reduced diameters and heights on AFM images. By combining imaging with local force measurements the 'real' dimensions of the nanobubbles can be estimated. A model of the forces between an AFM tip and a nanobubble shows that the bubble can be imaged as a protrusion on AFM contact mode images, even if the surface of the bubble is penetrated by the tip.

5.1 Introduction

The first publications on nanobubbles appeared in the literature in the late 1990's [55, 56], where nanobubbles were suggested to cause the so-called 'hydrophobic interaction', which is a long-range attraction between two hydrophobic surfaces in solution. The initial experimental work were force measurements performed with cantilevers onto which a sphere with diameter in the micrometer range was attached [57]. Both sample surfaces and spheres were chemically modified to become highly hydrophobic. In 2000, Ishida et al. [58] and Lou et al. [59] published the first AFM tapping mode images of what was assumed to be nanobubbles on hydrophobic surfaces, and in 2001 Tyrrell and Attard [60] presented tapping mode images of nanobubbles on hydrophobic surfaces combined with force measurements using a micrometer probe.

To investigate the phenomenon of nanobubbles both contact and tapping mode imaging, as well as force measurements have been performed on gold surfaces immersed in clean water[1] with standard silicon probes[2]. Neither probes, nor gold surfaces were chemically modified in any way. Contact angle measurements made

[1] Milli-Q water from Millipore A/S.
[2] ULTRASHARP Si cantilever, MikroMasch, Estonia.

on the gold surfaces used in the experiments have showed that the surfaces have a contact angle of 95°-100° (see section 2.2.3, page 12). In order to estimate the contact angle of the silicon probes used in the measurements, the contact angle of silicon wafers with native oxide has been measured, resulting in a contact angle of ∼4°.

5.2 Contact Mode Imaging

Figure 5.1 shows a series of AFM contact mode images (2 μm × 2 μm) of a gold surface immersed in clean water. The images have been registered with approximately five minutes interval during which only the scanning force has been changed. In (a) a scanning force as small as possible without loosing contact with the sample has been used. In (b) the scanning force has been increased with a couple of nanoNewton, and in (c) the scanning force has been reduced to be approximately the same value as when the image shown in (a) was obtained.

In Figure 5.1(a) round, bright structures can be observed on the surfaces. When the scanning force is increased essentially all the brighter structures disappears or are transformed to smaller, darker areas (see (b)). When the scanning force is decreased again, the brighter structures reappear at the same sites and with the same sizes and shapes as in (a) (see (c)). The bright structures observed in Figure 5.1 are interpreted as nanobubbles.

In Figure 5.1(c) it is observed that the bright structures reappear at the same positions on the surface after scanning with a high scanning force, which makes it unlikely that they are caused by some kind of particles in the system. Particles would typically be swept away from the scanned area and gather at the borders of the area. However, others [61] have shown that bubbles in the nanometer range can be moved and manipulated to fuse into larger bubbles by an AFM tip. Thus, the response of nanobubbles to a scanning tip depends on the characteristics of tip and surface, as well as the scanning force used.

Force curves have been recorded during the AFM investigations of nanobubbles to estimate the forces used during imaging. When forces of ∼0.5 nN or less have been used, nanobubbles appear as bright structures. When the force has been increased to ∼3 nN, or more, they have been observed as smaller, darker structures.

Figure 5.1(d) shows a profile of four nanobubbles observed on the surface in Figure 5.1(a). The diameters of the bubbles are measured to be about 100 nm, and their heights are measured to be 1-1.5 nm. The small heights compared to the diameters of the bubbles are surprisingly small, and if real, results in extremely flat, 'pancake-shaped', bubbles. However, in other AFM contact mode measure-

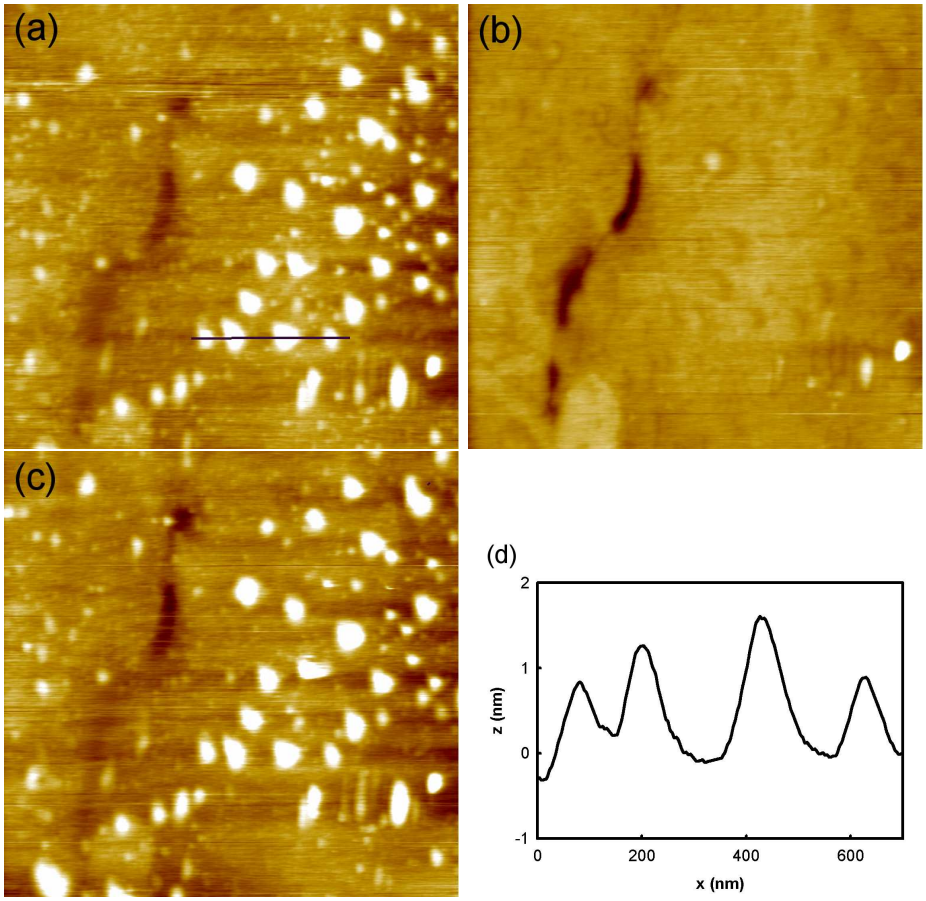

Figure 5.1: AFM contact mode image (2 µm × 2 µm) of a gold surface immersed in clean water when scanned with (a) a low scanning force, (b) a higher scanning force, and again (c) a low scanning force. In (d) a profile of four protrusions observed in (a) are shown, where the diameters of the protrusions can be measured to be about 100 nm and the heights to be 1-1.5 nm.

ments on nanobubbles with diameters in the same range as those observed in Figure 5.1, heights of about 5 nm have been measured. Furthermore, tapping mode experiments indicate that bubbles with diameters of ∼100 nm are higher than observed in Figure 5.1 (see section 5.5, page 62).

The results from contact mode imaging of nanobubbles show that the measured heights of the bubbles are influenced by the scanning force used and that the measured heights do not represent the real heights of the bubbles. In the following section a simple model of the force balance between a nanobubble and an AFM tip shows that an equilibrium between the involved forces can be obtained, and that nanobubbles can be imaged as protrusions on AFM images even though the tip has penetrated the surface of the bubble. This explains the reduced heights measured during AFM contact mode imaging.

5.3 Force Balance Between Tip and Bubble

Figure 5.2 is a schematic figure of an AFM tip interacting with a nanobubble on a gold surface[3] (not to scale).

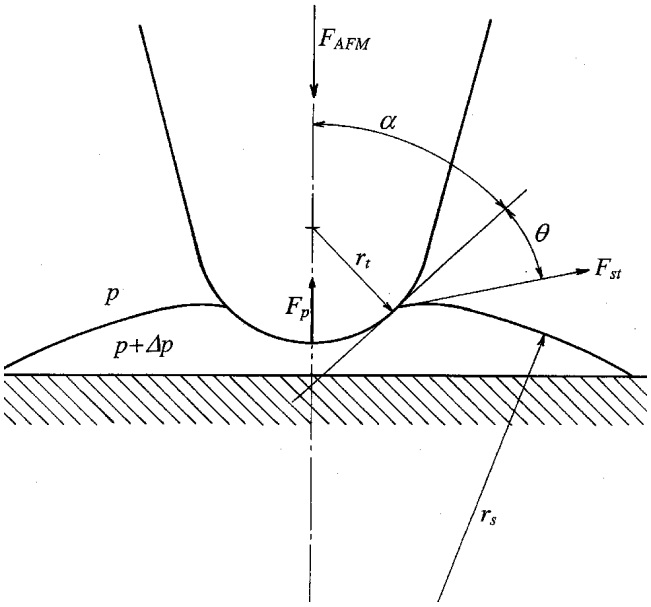

Figure 5.2: Schematic figure of a scanning AFM probe interacting with a nanobubble (not to scale).

To obtain equilibrium between forces during imaging the equation

$$F_{AFM} - F_p - F_{st} = 0 \tag{5.3-1}$$

should be fulfilled, where F_{AFM} is the vertical force applied by the AFM tip on the bubble surface, F_p is the force caused by the pressure difference across the bubble wall over the area where tip and bubble interact, and F_{st} is the vertical component of the force caused by the surface tension along the interface between tip and bubble.

Equation (5.3-1) can be written as

$$F_{AFM} - \Delta p\pi(r_t \cos\alpha)^2 - 2\pi\gamma r_t \cos(\alpha+\theta)\cos\alpha = 0, \tag{5.3-2}$$

where Δp is the pressure difference between the inside and the outside of the nanobubble, r_t is the curvature radius at the tip apex, α is the angle between

[3]Illustration made by K.A. Mörch, Department of Physics and Quantum Protein Center, Technical University of Denmark, Denmark.

the center-axis of the tip and the tangent to the circle, which approximate the tip shape at the apex, along the bubble-water interface, γ is the surface tension, and θ is the contact angle (see Figure 5.2).

Since during imaging $F_{AFM} \geq 0$,

$$\Delta p \geq -\gamma \frac{2\cos(\alpha+\theta)}{r_t \cos\alpha}. \tag{5.3-3}$$

Equation (5.3-3) can be combined with the Young-Laplace equation [62] for a bubble,

$$\Delta p = \frac{2\gamma}{r_s}, \tag{5.3-4}$$

where r_s is the radius of a sphere with the same curvature as the nanobubble.

The result is:

$$\frac{r_t}{r_s} \geq -\frac{\cos(\alpha+\theta)}{\cos\alpha}, \tag{5.3-5}$$

and since $r_t << r_s$,

$$\frac{\cos(\alpha+\theta)}{\cos\alpha} \geq 0, \tag{5.3-6}$$

which results in

$$(\alpha+\theta) \leq 90°. \tag{5.3-7}$$

Thus, the AFM tip must be sharp and hydrophilic to achieve an equilibrium, during which nanobubbles can be imaged as protrusions, even though the AFM tip has penetrated the surface of the bubble.

5.4 Force Measurements

Contact mode imaging has showed that the measured heights of the nanobubbles are not their real heights. However, the real heights can be estimated by combining AFM imaging with local force measurements. Local force curves that represent the interaction between the AFM tip and a single nanobubble can be obtained by zooming in on an area on the gold surface that contains a limited number of nanobubbles.

Figure 5.3 shows a typical force curve recorded during local force measurements, and is interpreted as the interaction between the AFM tip and a single nanobubble (diameter ~150 nm).

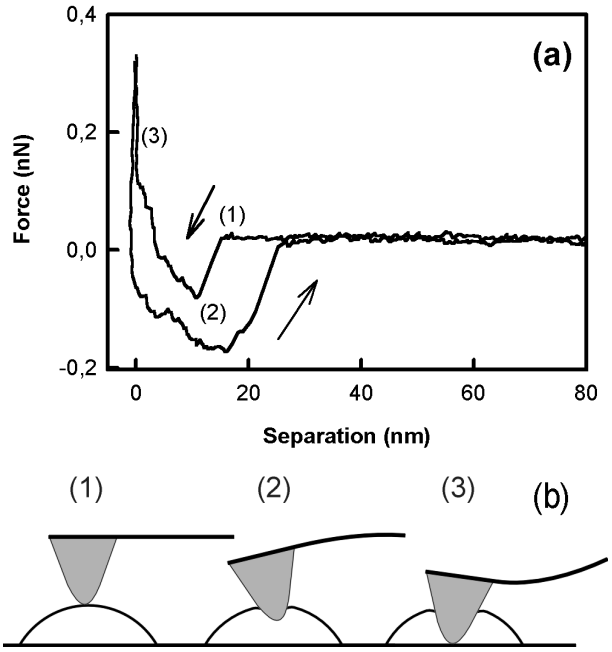

Figure 5.3: In (a) a force curve is shown, representing interaction between the AFM tip and a nanobubble with diameter ∼150 nm. There is a 'snap-in' at a tip-sample separation of 15 nm, and a 'snap-out' at a tip-sample separation of 21 nm. In (b) schematic figures are shown of the tip-bubble interaction; (1) just before 'snap-in', (2) just after 'snap-in' and (3) during hard wall contact.

In Figure 5.3 the tip is approaching the surface from right to left and at a tip-sample separation of 15 nm, the tip is 'snapped in' towards the surface, which represents the event where the tip penetrates the surface of the bubble. The position of the 'snap-in' is also a measure of the real height of the bubble (in this case 15 nm). The tip is 'snapped in' to a tip-sample separation of 11 nm, whereafter there is forced penetration of the tip through the bubble until hard-wall contact between tip and gold surface is made (see point (3) in Figure 5.3).
When the tip penetrates the surface of the bubble, α is close to 90° and Equation 5.3-7 cannot be fulfilled. Before equilibrium between forces can be obtained, the tip needs to reach the position where $(\alpha + \theta) \leq 90°$, which in this case is at tip-sample separation of 11 nm.

In the retraction curve a region of soft interaction is observed, where the tip has lost contact with the gold surface, but still has contact with the bubble. At a tip-sample separation of 21 nm the tip is 'snapped out', and there is no longer contact between tip and bubble. The tip-sample separation at 'snap-out' is larger than the tip-sample separation at 'snap-in', since the bubble can be stretched out before it looses contact with the tip during retraction.

The shown local force measurement indicates that bubbles with diameters of ∼150 nm have real heights of approximately 15 nm. Thus, measured heights of 1-1.5 nm of bubbles with diameters of about 100 nm cannot be considered to be realistic, and the real heights of bubbles with diameters of ∼100 nm are probably closer to 10 nm.

The tip used in obtaining the images in Figure 5.1 and the tip used in obtaining the force curve in Figure 5.3 are not assumed to be identical. Therefore, the forces used cannot be quantitatively compared, but it can be observed in Figure 5.3 that the forces under which nanobubbles would be imaged as protrusions have the same order of magnitude as the force estimated from imaging experiments.

5.5 Tapping Mode Imaging

Besides from contact mode imaging, tapping mode imaging of nanobubbles have been performed. The tapping mode images obtained are comparable to tapping mode images of nanobubbles published by others [58, 59].

Figure 5.4 shows a tapping mode image (5 μm × 5 μm) of a gold surface immersed in clean water, where (a) shows the topographical image and (b) shows the phase image.

In Figure 5.4(a) several bright structures, which are interpreted to be nanobubbles, are observed on the gold surface. From profiles over the surface in (a) the diameters of the medium-sized, bright structures can be measured to be approximately 200 nm, and the heights to be 10-15 nm. The phase image in (b) shows structures with positions that correspond to the positions of the bright structures in the topographical image. A change in the phase indicates a change in character of the material on the surface that the scanning tip is interacting with.

Even though there is good correspondence with change in brightness in the topographical image and change in phase in the phase image in Figure 5.4, a small deviation can be found when the profiles are analyzed. Figure 5.5 shows a profile over one of the nanobubbles observed in Figure 5.4. The upper line is the profile from the phase image, and the lower line is the profile from the topographical image.

Figure 5.5 shows that the change in phase occurs 30-50 nm before and after a change in brightness can be registered in the topographical image. In Figure 5.4(b) this is indicated as a dark edge, which more or less encircles the struc-

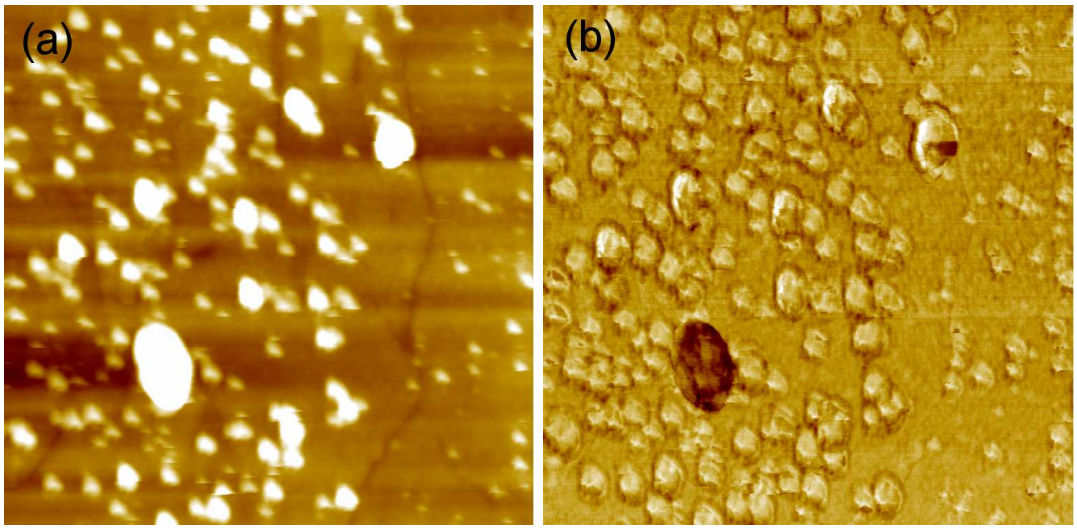

Figure 5.4: AFM tapping mode (a) topographical and (b) phase image (5 µm × 5 µm) of a gold surface showing structures interpreted as nanobubbles. The medium-sized bright structures have a measured diameter of about 200 nm and a measured height of 10-15 nm.

tures that correspond to the nanobubbles. Thus, a change in the material on the surface can be registered in the phase image a few tens of nanometer before a change in height in the topographical image is shown. This delay in registration of change in topography on tapping mode images of nanobubbles indicates that the tip penetrates the bubbles completely close to their rims, and thereby these parts of the bubbles are registered only in the phase image and not in the topographical image.

In Figure 5.4(b) the appearance of the largest structure differs from the other structures on the surface. From profiles it can be observed that change in the topographical image and change in the phase image of this structure occurs at the same position on the scanning line. Furthermore, the change in phase during interaction with the large structure does not change sign after a couple of tens of nm, as it does when the tip is interacting the the smaller structures. Instead the whole structure is observed as a dark area in the phase image. There is also a tendency for this kind of behavior in the phase image during interaction between tip and the second largest structure on the AFM image.

It is not known why the appearance of the structures differ in the phase image, but one possibility may be that the structures represent two different objects, for example nanobubbles and particles. However, the difference could also be due to the difference in size of the structures, where the interaction between a large nanobubble and the AFM tip results in a different appearance in the phase image.

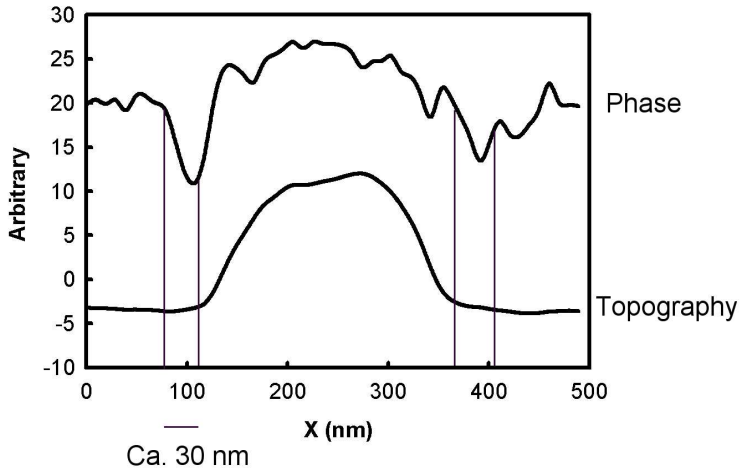

Figure 5.5: Profile over one of the nanobubbles in Figure 5.4. The upper line is the profile from the phase image and the lower line is the profile from the topographical image.

Contact mode imaging and force measurements have shown that nanobubbles can be imaged as protrusions, even if the tip has penetrated the surface of the bubble, leading to a registration of bubbles with smaller heights than their real heights on contact mode images. Tapping mode imaging indicates that the tip can penetrate the rims of the nanobubbles completely during scanning, and thereby also image them with a smaller diameter than their real diameter. Thus, measured dimensions of nanobubbles from AFM images should not be considered as the real dimensions of the nanobubbles.

5.6 Discussion and Summary

Nanobubbles can form spontaneously on gold surfaces immersed in water, and they can be imaged in both contact and tapping mode.

On AFM contact mode images, nanobubbles can be images as protrusions even though the tip has penetrated the surface of the bubble. A model of the force balance between tip and bubble shows that this requires a sharp and hydrophilic tip during imaging.

Tapping mode images show that nanobubbles can be registered in the phase image before any change in the topographical image is observed, which indicates that the tip can penetrate the rims of the nanobubbles completely during imaging.

Thus, measured dimensions of nanobubbles from AFM imaging are not the real

dimensions of the bubbles, but by combining AFM imaging and local force measurements an estimate of the real dimensions can be obtained.

In articles published by others [57, 60], AFM experiments on nanobubbles have been performed with samples made extremely hydrophobic by chemical means. The gold surfaces used in the presented AFM investigations were stored in air between fabrication and AFM measurements, and it is known from contact angle measurements that they are slightly hydrophobic. However, the surfaces were not modified to become hydrophobic and can be considered to be representative for surfaces present in many different systems. Thus, the presence of nanobubbles on these surfaces indicates that this could be a general, but overseen, phenomenon in systems involving surfaces immersed in liquid. Besides from causing problems, such as reduced wetting of surfaces in micro-fluidic systems, nanobubbles can cause image artifacts during AFM imaging, which make the images difficult to interpret.

AFM measurements with de-gased clean water have been performed, but no reduction in the amount of nanobubbles on the gold surfaces compared to when not de-gased water was used was observed. Furthermore, preliminary measurements have been performed, where the clean water were replaced by ethanol. The gold surface was mounted in the liquid cell and clean water was introduced. After registration of nanobubbles on the surface, the clean water was replaced by ethanol. It was not possible to observe any nanobubbles during imaging in ethanol, but when water was introduced into the liquid cell once more, bubbles appeared at the surface again. Thus, nanobubbles seems to be difficult to avoid without chemically modifying either surface or liquid.

Chapter 6

Interaction Between Blood and Polymer Surfaces

Radiometer Medical A/S develops and produces equipment for measuring blood gases, as well as other parameters in blood that are important when diagnosing critically ill patients.

To make devices like those Radiometer Medical A/S manufactures more flexible and easy to handle, one can make them smaller. However, when channels and chambers in the equipment become smaller, they also become more vulnerable for possible adhesion of material from the blood on their surfaces. Adsorption of blood cells and blood proteins on the surfaces in the equipment can block the blood-flow in the fluidic system, and adsorption of blood material on active sensor surfaces can cause errors when measuring, with the possible result of misjudged diagnoses.

In this chapter AFM investigations of the interaction between blood-material and polymer surfaces are presented and discussed.

6.1 Background

Others [63, 64, 65] have published Scanning Electron Microscopy (SEM) studies of blood cells[1] and platelets[2]. In these investigations it is discussed how both surface characteristics and the presence of blood proteins on surfaces influence the adsorption of platelets and blood cells on the surfaces, but it has not been possible to identify blood proteins on surfaces with SEM, since the dimensions of the proteins are in the nanometer range.

[1] Blood cells have diameters in the range of micrometers.

[2] Component in the blood that participate in blood clotting with diameters of $\sim$1 µm.

The adsorption of blood proteins on surfaces have been studied by using techniques such as ellipsometry [66, 67] and fluorescence-labelling [68, 69]. From these investigations the amount of adsorbed protein, the thickness of the adsorbed layer and to some extent the content of the layer have been estimated. However, these techniques do not give much information about the conformation of adsorbed proteins, nor do they reveal how the proteins interact with specific structures on the surface.

Most of the published AFM studies on blood proteins so far have been concentrated on force measurements, where a coated tip is interacting with a coated surface to estimate the interacting forces between the material on the two surfaces [70, 71, 72], but some imaging has also been done [73, 74], where globular structures with diameters of ∼100 nm have been interpreted as aggregates of proteins. AFM imaging of proteins with nanometer resolution is complicated by the mobility of the proteins. However, by forming two-dimensional crystals of membrane proteins high-resolution topographical AFM images have been obtained [75, 76].

The goal with the performed AFM investigations is to look for 'patterns' in the adsorption process when polymer surfaces are exposed to blood and blood protein solutions. Some of the aspects that is of interest is in what order different blood-components adsorb to the surface, if the interaction of one blood-component with the surface influence other blood-components behavior and if it does, how it does. Furthermore, to find out if specific blood proteins can be identified through AFM imaging, polymer surfaces have been exposed to 'single' blood protein solutions (solutions that contain only one blood protein).

6.2 Experimental

Three sets of investigations have been done. In the first set static exposure of blood to polymer surfaces was examined. In the second investigation the influence of several, subsequently, dynamic exposures of blood on the adsorption of blood material to a polymer surface, as well as the effectiveness of a cleaning processes, was studied. The third and last investigation was focused on the interactions between a polymer surface and single protein solutions.

Radiometer Medical A/S has chosen the three polymers used in the investigations, based on internal criteria for the specific application[3]

During static exposure experiments a drop of blood was placed on the polymer surface, while a flow-system (see Figure 6.4, page 74) was used during the

[3]The different polymer surfaces will not be specified, but be called Polymer 1, Polymer 2 and Polymer 3 due to wishes from Radiometer Medical A/S.

dynamic exposure experiments.

All measurements were made in buffer with tapping mode AFM with standard silicon probes[4].

Experimental details can be found in Appendix E.

6.3 Polymer Surfaces

Figure 6.1(a) shows an AFM image (100 μm × 100 μm) of Polymer 2 that has not been exposed to blood, and Figure 6.1(b) shows a 10 μm × 10 μm scan of the same surface. Besides from not being exposed to blood, the surface has been treated after the same scheme as the blood-exposed samples (see Appendix E). The stripes observed on the polymer surface are caused by surface structure of the mould used in the manufacturing process of the polymer samples.

The AFM images in Figure 6.1 are representative for images of the clean polymer samples investigated. The surface in Figure 6.1 has a roughness[5] of ∼16 nm over the area of 100 μm × 100 μm, and of ∼5 nm over an area of 10 μm × 10 μm.[6] The two other polymer surfaces investigated show roughness in the same range.

From contact angle measurements a contact angle of 75°-80° has been registered for the polymer surfaces, when measured in clean water[7]. A surface with a contact angle 75°-80° can be classified as 'very little' hydrophilic or 'slightly' hydrophobic (see section 2.2.3, page 13).

When adsorbed on hydrophilic surfaces, most proteins have a small contact area with the surface and there are only small changes in their configuration. When adsorbed on hydrophobic surfaces the proteins orient their hydrophobic moieties towards the surface and their hydrophilic parts towards the solution, which can cause quite large changes in the proteins configuration. Thus, proteins adsorbing to the polymer surfaces used in the presented measurements are expected to expose some of their hydrophilic moieties to the solution in channels and chambers.

[4]ULTRASHARP Si cantilever, MikroMasch, Estonia.
[5]RMS, Root Mean Square.
[6]Line-wise levelling of first order have been performed on all presented AFM images.
[7]Milli-Q water from Millipore A/S

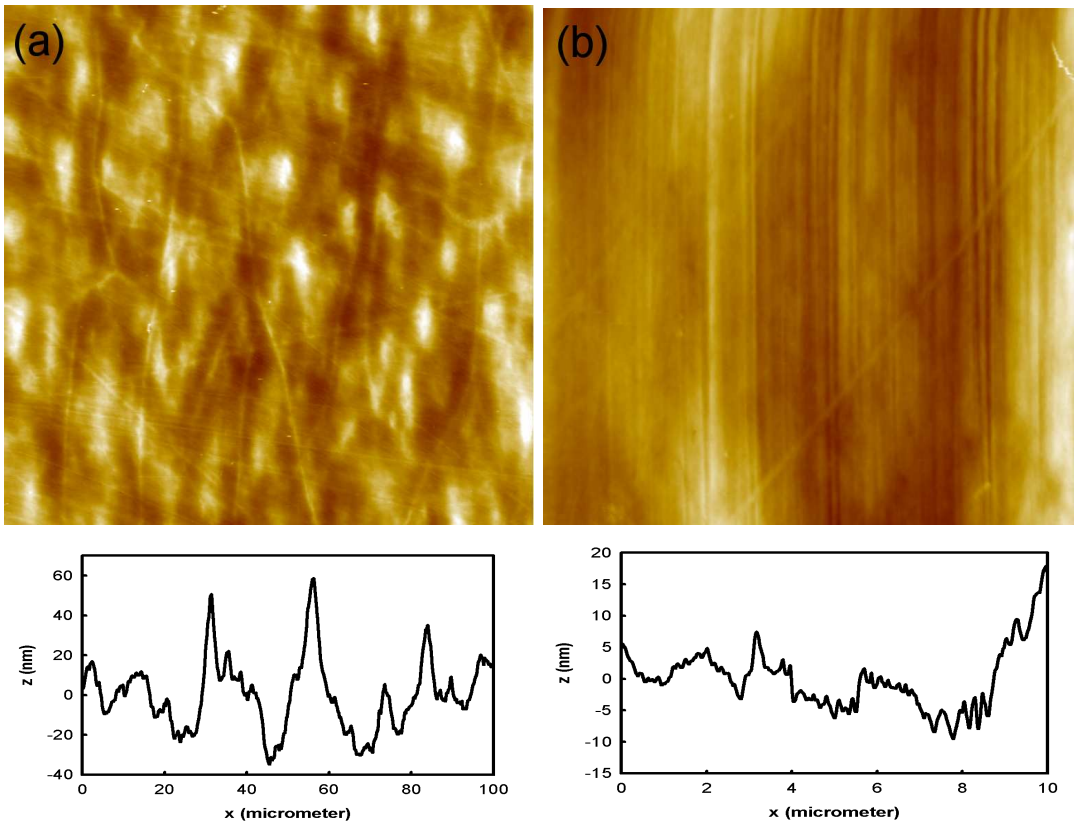

Figure 6.1: AFM tapping mode images and profiles of a clean polymer surface, where (a) shows a 100 µm × 100 µm large area and (b) shows a 10 µm × 10 µm large area. The stripes on the surface are replicated from the surface structure in the mould used in the manufacturing process.

6.4 Static Exposure of Blood to Polymer Surfaces

Results from static exposure of blood to polymer surfaces showed that it is possible to distinguish between polymer surfaces that have been exposed to blood and polymer surfaces that have not been exposed to blood on AFM images, but that it was not possible to distinguish between polymer surfaces that were exposed to blood for different amounts of time.

6.4.1 Introduction

Before AFM imaging the three polymer surfaces were statically exposed to blood, meaning that a drop of blood was placed on the polymer surface for a given period of time, i.e. 10 seconds or 10 minutes. After blood exposure the surfaces were gently rinsed with deionized water and stored in a phosphate buffer until

investigated with tapping mode AFM.

6.4.2 AFM Measurements

Figure 6.2 shows an AFM image (100 µm × 100 µm) of Polymer 3 that has been exposed to blood for 10 minutes. Figure 6.2(a) is the topographical AFM image, while (b) is the phase image. The images are representative for images of all exposed polymer surfaces, independent of the time the surface has been exposed to blood.

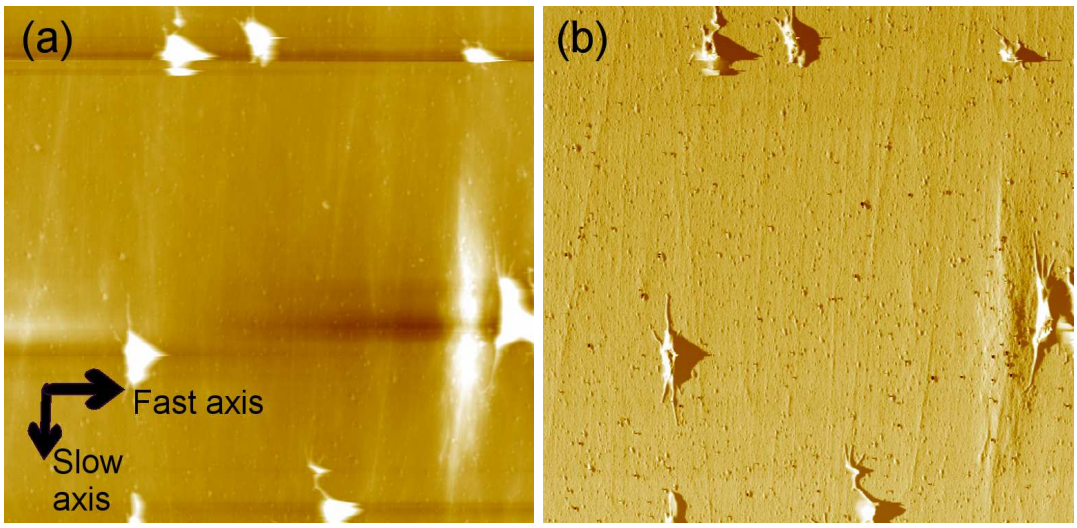

Figure 6.2: AFM image (100 µm × 100 µm) of Polymer 3 that has been exposed for blood in 10 minutes, where (a) is the topographical image and (b) is the phase image. In (a) the fast and slow scanning directions are indicated.

Several protrusions are observed on the surface in Figure 6.2(a) and these are interpreted as remains of blood cells and/or platelets adsorbed on the surface. Caused by a rather fast scanning the structures are 'smeared-out', which results in an increased width of the structures in the direction of the fast scanning axis. Taking this into account, the width of the structures (in the direction of the fast scanning axis) can be estimated to be a couple of micrometer. In the direction of the slow scanning axis the structures are more elongated and have a width of ∼10 µm. The heights of the structures are 0.5-1.0 µm.

In Figure 6.2(b) small 'arms' protruding from the adsorbed structure and stretching out on the polymer surface in the direction of the slow scanning axis can be observed. These kinds of arms (also called pseudopods) can be observed in

early stages of the activation of platelets[8] *in vivo* [77], but is also observed when platelets adsorb strongly to surfaces [64]. The direction of the pseudopods follows the direction of the stripes caused by the fabrication-mould on the surface, resulting in an asymmetrical shape of the structures. It is known from the literature [78] that the growth and motion of cells (and other structures capable of spreading and/or migration on surfaces) can be guided and controlled by the topography of the surface.

The sizes and shapes of the structures observed in Figure 6.2 indicate that they originate from platelets or white blood cells. Platelets have diameters of ∼1 μm and can form pseudopods. White blood cells, which also can show a conformation with extensions have diameters of ∼10 μm. Red blood cells have diameters of 4-5 μm, but are not capable of forming pseudopods like those observed in Figure 6.2.

Figure 6.3 shows an AFM image (10 μm × 10 μm) of Polymer 2 that has been exposed to blood for 10 minutes in an area without any larger structures adsorbed. The stripes caused by the fabrication-mould can still be observed, but compared to the not exposed surface in Figure 6.1 the surface looks more grained. The appearance of the surface in Figure 6.3 indicates that the surface is more or less covered with adsorbed material.

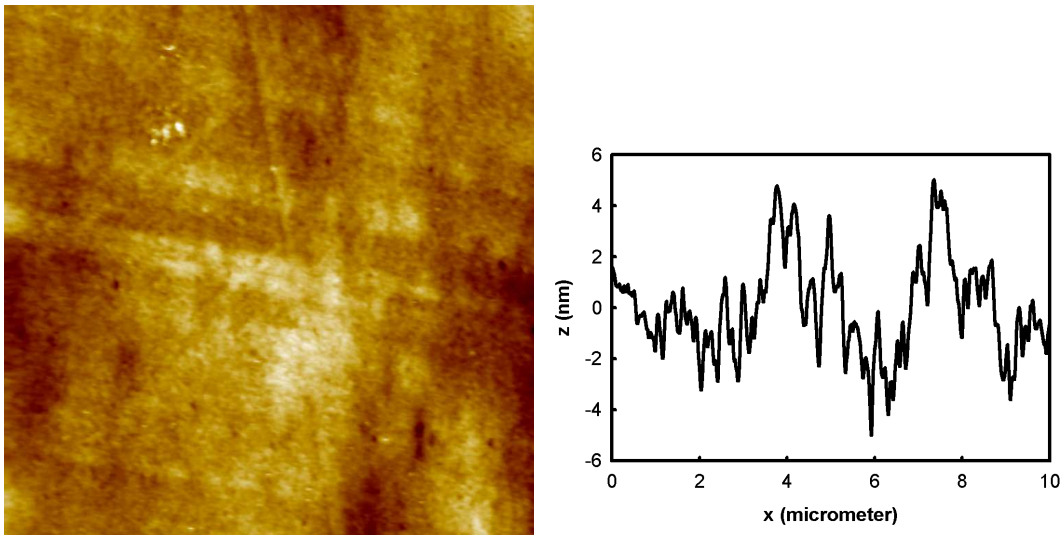

Figure 6.3: AFM image (10 μm × 10 μm) with profile of Polymer 2 exposed to blood for 10 minutes.

When surfaces are exposed to blood that contains both cells and proteins, the protein will have a tendency to adsorb before the cells because of their smaller

[8]Platelets can be activated to change shape and to become extremely 'sticky' and are thereby optimized to assist in blood clotting in damaged tissue.

size. Furthermore, the 'stickiness' of blood-components to a surface is inversely proportional to their local radius of curvature [79]. Thus, 'rough' cells are more willing to adsorb to surfaces than 'smooth' cells. Platelets and other cells capable of forming extensions will thereby adhere more strongly to the polymer surface than the smooth red blood cells, which also is indicated from the results.

Most proteins contain both hydrophobic and hydrophilic moieties and dependent on the hydrophilic/hydrophobic character of the surface they adsorb to, they will expose either their hydrophobic or hydrophilic parts to the surrounding solution. When proteins adsorb to surfaces with contact angle of 75°-80° it is reasonable to expect that the proteins will expose some of their hydrophilic moieties to the solution. Thus, when the blood cells and platelets approach a polymer surface with the adsorbed blood proteins they approach a more or less hydrophilic surface. The result is a smaller adsorption of cells and platelets than expected if they approached a clean, and more hydrophobic, polymer surface.

It was not possible to measure the thickness of the adsorbed layer by performing scratching experiments[9] since the polymer materials are rather soft. When scanning with a high scanning force in contact mode is performed on the polymer surfaces some of the polymer material is removed, and it is not possible to determine how much of the removed material during scratching that originates from an adsorbed layer of material and how much that originates from the polymer surface itself.

6.4.3 Summary

Results from AFM experiments with polymer surfaces statically exposed to blood showed that it is possible to distinguish between surfaces that have been exposed to blood and surfaces that have not been exposed to blood. However, it was not possible to observe any difference between polymer surfaces that have been exposed to blood in 10 seconds or 10 minutes.

The grained look of the surface in Figure 6.3 is interpreted to be caused by an adsorbed layer of blood proteins, and the larger structures in Figure 6.2 to be caused by adsorption of platelets and/or white blood cells to the polymer surface.

[9]Scratching experiments are described in Chapter 4 and is a technique used to remove adsorbed material on a surface with the scanning tip.

6.5 Dynamic Exposure of Blood to Polymer Surfaces and Cleaning

AFM investigations of a polymer surface subject to a cleaning procedure, where cleaning liquid and air are alternately introduced to the surface have shown that the cleaning procedure is rather effective.

6.5.1 Introduction

Polymer 1[10] have been exposed to blood, air and cleaning liquid, according to the specific scheme shown in Table 6.1.

Reference	Rinsed in DI water
Sample 1	Cleaning liquid, rinsed DI water
Sample 2	Blood, rinsed in DI water
Sample 3	Blood, cleaning liquid, rinsed in DI water
Sample 4	Blood, (air/cleaning liquid) $\times$ 10, rinsed in DI water
Sample 5	(Blood, (air/cleaning liquid) $\times$ 10) $\times$ 10, rinsed in DI water)

Table 6.1: The scheme according to which the samples are exposed to blood, air and cleaning liquid.

The exposures of blood, air and cleaning liquid were performed in a flow-cell to obtain a uniform and standardized exposure and to minimize contamination during exposure. Furthermore, to mimic the situation in the equipment developed at Radiometer Medical A/S the flow-rates of the introduced blood and cleaning liquid were adjusted to be similar to the flow-rates used in the equipment. The set-up used is schematically shown in Figure 6.4.

Blood, air and cleaning liquid are introduced to the polymer surface through syringes, mounted in pumps, and tubes with hose clips that are used to control the introduction of the different materials. The flow-cell together with a tightening o-ring are placed on a heating element to keep a constant temperature ($\sim$37°C) during exposure.

6.5.2 AFM Measurements

The reference and surfaces exposed to only cleaning liquid (Sample 1) resemble the clean surface shown in Figure 6.1, and the contact with cleaning liquid does not seem to affect the appearance of the polymer surface on AFM images.

[10]The polymer surface that was of most interest for Radiometer Medical A/S at the given time.

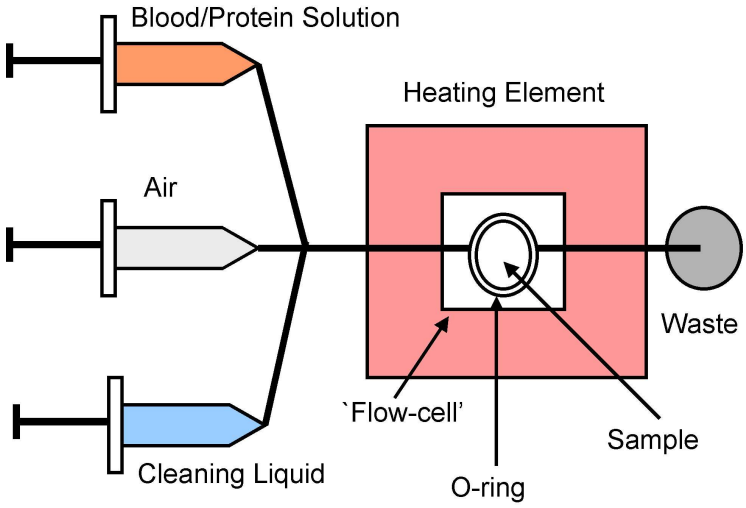

Figure 6.4: Experimental set-up for dynamic exposure of blood (and blood protein solutions) to a polymer surface.

Figure 6.5 shows two AFM images of the polymer surface exposed to blood and cleaned with an alternately introduction of air and cleaning liquid (Sample 4). In (a) a 50 µm × 50 µm large area of the surface is shown and in (b) a 10 µm × 10 µm large area of the same surface is shown.

In Figure 6.5(a) no larger structures on the polymer surface are observed. In Figure 6.5(b) a grained appearance of the surface is observed, indicating that material have adsorbed on the surface. The appearance of the surface in Figure 6.5 is representative for all surfaces exposed to blood and cleaned through alternately introduction of air and cleaning liquid into the 'flow-cell' (Sample 4 and Sample 5).

Surfaces that were not subject to alternately cleaning with air and cleaning liquid (Sample 2 and Sample 3) showed higher tendency to have larger structures (diameter >500 nm) adsorbed on the surface. These larger structures had the same characteristic as those observed during experiments with static exposure to blood (see Figure 6.2, page 70).

Experience at Radiometer Medical A/S indicates that an alternately introduction of air and cleaning liquid results in a more effective cleaning than just flushing the system with cleaning liquid. This is supported by the results from the AFM measurements, where no larger structures can be observed on the surface after use of alternately air/liquid cleaning.

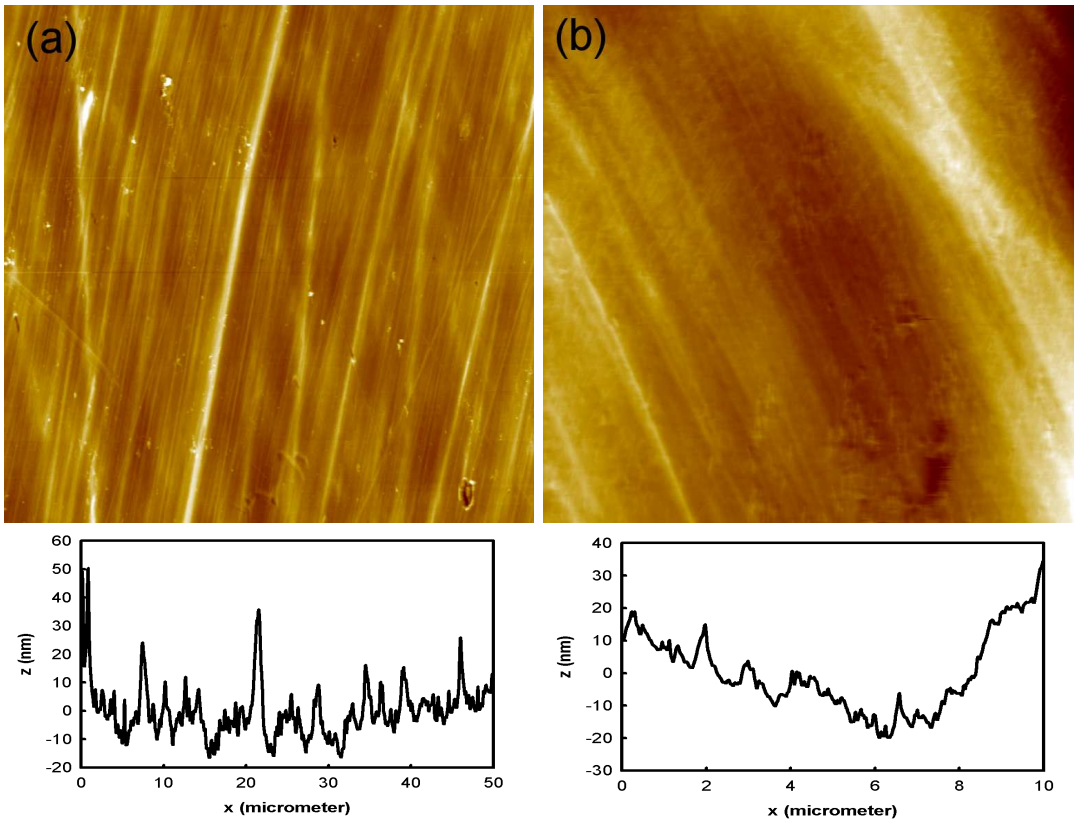

Figure 6.5: AFM images with profiles of a surface exposed to blood and cleaned with alternately introduction of air and cleaning liquid (Sample 4). In (a) a 50 µm × 50 µm large areas of the surface is shown and in (b) a 10 µm × 10 µm large area of the same surface is shown.

6.5.3 Summary

The AFM measurements show that a cleaning procedure with alternately introduction of air and cleaning liquid is rather effective in removing larger structures, such as blood-cells and platelets from polymer surfaces, but less effective in removing structures that are interpreted to be adsorbed blood proteins.

6.6 Dynamic Exposures of Protein Solutions to Polymer Surfaces

AFM images of polymer surfaces subject to dynamic exposure of protein solutions have showed characteristic of having an adsorbed layer of material on the surface. It has not been possible to distinguish between surfaces exposed to different proteins solutions, nor has it been possible to distinguish between surfaces exposed to protein solutions with different concentrations on AFM images.

6.6.1 Introduction

Indications of an adsorbed layer of material have been observed on all AFM images of polymer surfaces exposed to blood. The layer is interpreted as a blood protein layer adsorbed on the surface.

In order to investigate if specific blood proteins adsorbed on a polymer surface can be identified on AFM images, dynamic exposure experiments with single protein solutions have been performed.

The same polymer sample as the one used during experiments with dynamic exposure of blood (Polymer1) was exposed to solutions of albumin, fibrinogen and globulin. These are the most abundant proteins in blood and are expected to dominate the protein adsorption on the polymer surface during blood-exposure. Samples exposed to different concentrations of protein solutions have been examined, as shown in Table 6.2. The high protein concentrations (Sample A2, F2 and G2 in Table 6.2) correspond to the typical protein concentrations in blood.

The experiments were carried out as described in section 6.5, page 73.

Sample A1	Exposed to 0.40 mg/ml albumin
Sample F1	Exposed to 0.05 mg/ml fibrinogen
Sample G1	Exposed to 0.15 mg/ml globulin
Sample A2	Exposed to 40 mg/ml albumin
Sample F2	Exposed to 5 mg/ml fibrinogen
Sample G2	Exposed to 15 mg/ml globulin

Table 6.2: Samples exposed to single blood protein solutions of different concentrations. The higher concentrations of the proteins correspond to the typical concentration in blood.

6.6.2 AFM Measurements

Figure 6.6 shows three AFM images (5 μm × 5 μm) of Polymer 1 exposed to different protein solutions of the same concentrations as normally found in blood, and they are representative for surfaces exposed to protein solutions of both high and low concentrations.

All images in Figure 6.6 indicates that a layer of material has been adsorbed on the surface by having a grained appearance. The images in Figure 6.6 can be considered to be representative examples of images obtained on polymer surfaces

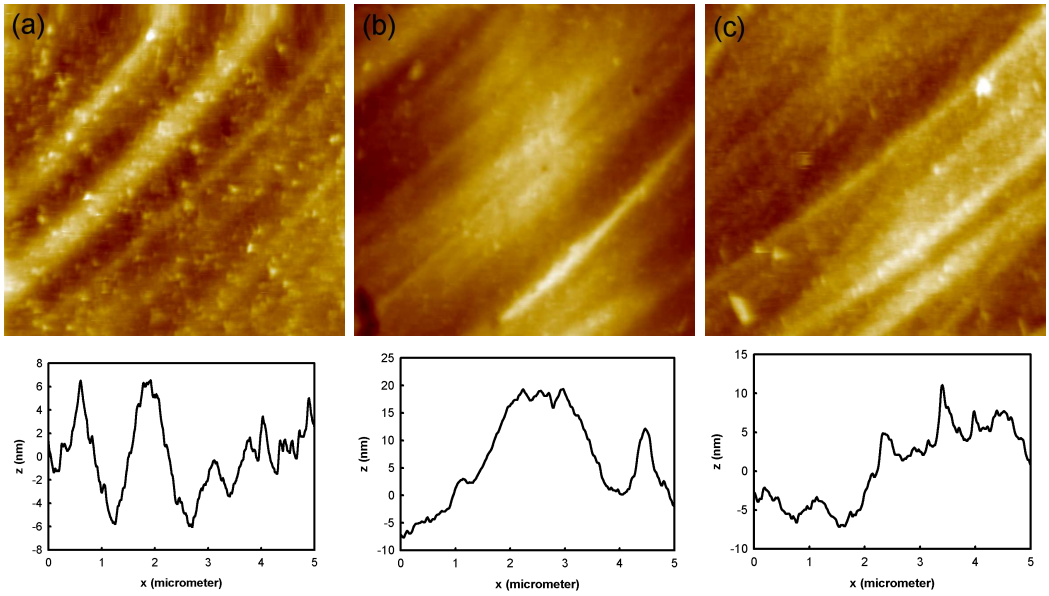

Figure 6.6: AFM images (5 µm × 5 µm) with profiles of Polymer 1 exposed to; (a) albumin solution (sample A2), (b) fibrinogen solution (sample F2), and (c) globulin solution (sample G2) with concentrations corresponding to the ones found in blood.

exposed to protein solution, independent on the concentration and the type of protein.

Both in Figure 6.6(a) and (c) one can observe small, particle-like structures. Albumin (molecular dimensions of about 4 nm×4 nm×14 nm), globulin (molecular dimensions of about 5 nm×5 nm×23 nm) and fibrinogen (molecular dimensions of about 6 nm×6 nm×45 nm) are all expected to be presented as somewhat globular structures on AFM images [66]. The small, bright structures observed on some of the AFM images of protein-exposed polymer surfaces have a round shape with a diameter of 100-300 nm and a height of 5-10 nm. The height of the observed bright structures corresponds rather well with the dimensions of blood proteins. The diameters of the structures are similar to what others have observed [73] and can represent aggregates of adsorbed proteins.

6.6.3 Summary

AFM images of all surfaces exposed to protein-solutions showed characteristic that indicates an adsorbed layer of material on the surface. However, it was not possible to distinguish between surfaces exposed to different concentrations of the protein solutions, nor was it possible to distinguish between surfaces exposed to different types of proteins. Neither was it possible to identify single proteins adsorbed on the polymer surfaces through AFM imaging.

6.7 Discussion and Summary

It has been possible to distinguish between polymer surfaces that have been exposed to blood or blood protein solutions and surfaces that have not been exposed to these solutions on the AFM images. Surfaces exposed to blood in different amount of time showed the same characteristics.

All surfaces exposed to blood or protein solutions show indications of material adsorbed on the surface by having a grained appearance on AFM images. The adsorbed material is interpreted as an adsorbed blood protein layer. Polymer surfaces exposed to blood also showed larger structures (width of a couple of micrometer), which are interpreted as remains of platelets or white blood cells.

Blood-exposed polymer surfaces that have been cleaned with alternately introduction of air and cleaning liquid have not shown any larger structures adsorbed on their surfaces on AFM images. Thus, the alternately cleaning process seems to be effective in removing platelets and blood cells, but not in removing blood proteins.

Results from AFM imaging of polymer surfaces exposed to blood indicate that when the surfaces come in contact with blood for the first time, a layer of blood proteins is formed on the surface. Larger structures, such as blood cells and platelets, are expected to be slower in the adsorption to the surface due to their larger size. An adsorbed protein layer are expected to make the surface more hydrophilic, and thereby decrease the tendency of adsorption of cells and platelets. Experience from Radiometer Medical A/S shows that surfaces exposed to blood once are more hydrophilic that surfaces not exposed to blood, which is consistent with an adsorption of proteins on the surfaces during blood exposure, and thus with the results from the AFM investigations.

Even though adsorption of material from blood on surfaces in devices like those developed at Radiometer Medical A/S is considered a problem, results from the AFM measurements indicate that adsorption of blood proteins on surfaces in the device is not entirely of negative character. Adsorption of blood proteins can decrease the adsorption of blood cells and platelets on surfaces by making them more hydrophilic. A smaller adsorption of blood cells is important since these can disturb the blood-flow. Even more important, the adsorption of blood proteins on the polymer surfaces seems to reduce the adsorption of platelets, which role *in vivo* is to create aggregates on damaged tissue and to make the blood clot. Thus, platelets have characteristics that will enhance adsorption and aggregation of blood material on surfaces and their presence on surfaces in device like those Radiometer Medical A/S develops should be avoided.

Chapter 7

Conclusions and Perspectives

The major goal of this Ph.D. project has been to study organic and biological molecular layers related to sensor surfaces with AFM. The system most extensively investigated has been the immobilization of short ssDNA molecules on gold surfaces and their hybridization with the complementary ssDNA strand in solution. This system is related to a cantilever-based sensor developed in the BioProbe project at MIC. The second system studied has been the adsorption of blood-material to polymer surfaces. This study has been performed in collaboration with Radiometer Medical A/S.

Gold surfaces have been fabricated by evaporating gold onto mica and contain ultra-flat plateaus with diameters of a couple of hundreds of nanometer. The flat character of the gold surfaces makes it possible to study the short ssDNA molecules and to perform scratching experiments.

When ssDNA molecules are introduced to the gold surface, darker areas interpreted as holes in an immobilized molecular layer appear on the images. After adding MCH molecules the holes disappear, indicating that unspecific interactions between ssDNA molecules and gold surface are released. Thus, a mixed molecular layer of ssDNA and MCH is now covering the surface, where all molecules bind to the surface through their thiol-group, and where the ssDNA molecules are more assessable for hybridization. Transformation from a grained to a more smooth look of the surfaces after introduction of the complementary ssDNA strand indicates that hybridization has occurred. This is strengthen by an observed increase in the thickness of the molecular layer. A molecular layer of dsDNA molecules is expected to be smoother and thicker than a layer of ssDNA molecules due to the more rigid and elongated conformation of the dsDNA molecules compared to the ssDNA molecules. The ssDNA molecules are flexible molecules and are expected to be folded when immobilized on the gold surface.

AFM measurements performed on polymer surfaces exposed to blood and blood

protein solutions indicate that an adsorption of blood proteins to surfaces in micro-fluidic devices is not entirely of negative character. The measurements point toward that the adsorption of blood proteins to the polymer surfaces reduces the adsorption of blood cells and platelets. Adsorption of blood cells and platelets can result in blocking of channels in the devices and should be avoided.

The presence of molecular layers on surfaces can be challenging to identify through AFM imaging. However, scratching has shown to be a method to distinguish between surfaces with an immobilized molecular layer and surfaces without these layers. Furthermore, preliminary measurements with streptavidin-coated gold particles with diameters in the nanometer range and biotin-labelled ssDNA molecules have shown some prospect to be a method to enhance observable changes on AFM images during immobilization.

When imaging molecular layers with contact mode in liquid the molecular layer can be compressed by the tip during scanning, and this could be avoided by using tapping mode. However, when scratching is performed during the measurements, contact mode is necessary. Thus, an AFM capable of switching between contact and tapping mode without changing the position of the tip relative to the sample would be an advantage when measurements involving scratching of immobilized molecular layers are performed.

Nanobubbles have been observed to form spontaneously on the gold surfaces, when these are immersed in clean water, and the bubbles have been imaged in both contact and tapping mode. A model of the forces between a nanobubble and the AFM tip shows that if the AFM tip is sharp and hydrophilic, the nanobubbles can be imaged as protrusions on AFM images, even though the tip has penetrated the surface of the bubble. The real heights of the nanobubbles have been estimated by combining AFM imaging with force measurements. Tapping mode imaging has shown that in the rim of the nanobubbles the tip can penetrate the bubbles completely, resulting in an observable change in the phase image, but not in the topographical image.

The gold surfaces used in this study have been stored in air between fabrication and use in AFM measurements, but have not been modified in any way. The existence of nanobubbles on these surfaces calls for attention and indicates that these structures can be a common, but overseen, phenomenon. If nanobubbles are present on the gold surfaces, when the ssDNA molecules are immobilized, they can influence the conformation of the molecular layer. The bubbles have shown to be firmly attached to the gold surface and could hinder the molecules to react with the surface. Thus, darker areas observed on AFM images of gold surfaces, to which ssDNA molecules have been introduced can represent areas on the surface, where nanobubbles have been present during immobilization.

To avoid nanobubbles on the gold surfaces, AFM measurements with de-gased water have been performed, but no observable change in the amount of bubbles on the gold surfaces was achieved. However, it is possible that nanobubbles can be avoided by cleaning the gold surfaces, thereby making them more hydrophilic, or by using other, more hydrophilic, surfaces.

Preliminary measurements, where the clean water in the liquid cell of the AFM was exchanged with ethanol indicate that when ethanol is used during imaging, nanobubbles are not present on the gold surfaces. Future relevant studies would include a series of measurements, where a limited area of the gold surfaces with nanobubbles is imaged in clean water, whereafter the water is exchanged with ethanol, and the same area of the surface is imaged again. Finally clean water is introduced once more, to find out if nanobubbles appear at the same sites as during the first measurements in water.

Bibliography

[1] J. Hansen O. Eriksen S.C. Rasmussen, P.A. Thaysen and A. Boisen. Optimised cantilever biosensor with piezoresistive read-out. *Ultramicroscopy*, 97:371–376, 2003.

[2] J.D. Lang H.P. Zhang J. Hunziker P. Ramseyer J.P. Meyer E. Hegner M. Arntz, Y. Seelig and Ch. Gerber. Label-free protein assay based on a nanomechanical cantilever array. *Nanotechnology*, 14:86–90, 2003.

[3] J.E. Boiadjiev V. Yi D. Pinnaduwage, L.A. Hawk and T. Thundat. Use of microcantilevers for the monitoring of molecular binding to self-assembled monolayers. *Langmuir*, 19:7841–7844, 2003.

[4] www.mic.dtu.dk/research/bioprobes/.

[5] C.F. Binnig, G. Quate and Ch. Gerber. Atomic force microscope. *Physical Review Letters*, 56:930–933, 1986.

[6] H. Gerber Ch. Binnig, G. Rohrer and E. Weibel. Surface studies by tunneling microscopy. *Physical Review Letters*, 49:57–61, 1982.

[7] D. Kjoller K. Zhong, Q. Inniss and V.B. Elings. Fractured polymer/silica fiber surface studied by tapping mode atomic force microscope. *Surface Science Letters*, 290:L688–L692, 1993.

[8] K. De Grooth B.G. Van Hulst N.F. Putman, C.A.J. Van der Werf and J. Greve. Tapping mode atomic force microscopy in liquid. *Applied Physics Letters*, 64:2454–2456, 1994.

[9] C.M. Blackman, G.S. Mate and M.R. Philpott. Interaction forces of a sharp tungsten tip with molecular films on silicon surfaces. *Physical Review Letters*, 65:2270–2273, 1990.

[10] W.F. Heinz and J.H Hoh. Spatially resolved force spectroscopy of biological surfaces using the atomic force microscope. *Nanotechnology*, 17:143–150, 1999.

[11] C.B. Weisenhorn A.L. Gould S.A.C. Albrecht T.R. Quate C.F. Cannell D.S. Hansma H.G. Drake, B. Prater and P.K. Hansma. Imaging crystals, polymers, and processes in water with the atomic force microscope. *Science*, 243:1586–1589, 1989.

[12] T.E. Paloczi G.T. Pietrasanta L.I. Smith B.L. Thompson J.B. Richter M. Rief M. Gaub H.E. Plaxco K.W. Cleland A.N. Hansma H.G. Viani, M.B. Schäffer and P.K. Hansma. Fast imaging and fast force spectroscopy of single biopolymers with a new atomic force microscope designed for small cantilevers. *Review of Scientific Instruments*, 70:4300–4303, 1999.

[13] P. Knapp H.F. Allgöwer F. Schitter, G. Menold and A. Stemmer. High performance feedback for fast scanning atomic force microscopes. *Review of Scientific Instruments*, 72:3320–3327, 2001.

[14] M.E. Wong T.M.H. O'Shea, S.J Welland. Influence of frictional forces on atomic force microscope images. *Ultramicroscopy*, 52:55–64, 1993.

[15] N.H. Smith B.L. Hansma H.G. Zhu X. Guthold M. Bustamante C. Kool E.T. Kashlev M. Kasas, S. Thomson and P.K. Hansma. *Escherichia coli* rna polymerase activity observed using atomic force microscopy. *Biochemistry*, 36:461–468, 1997.

[16] A. Soria M.R. Dunlap, D.D. Maggi and L. Monaco. Nanoscopic structure of dna condensed for gene delivery. *Nucleic Acids Research*, 25:3095–3101, 1997.

[17] K. Reichelt and H.O. Lutz. Hetero-epitaxial growth of vacuum evaporated silver and gold. *Journal of Crystal Growth*, 10:103–107, 1971.

[18] J. Zhou F. Han, S. Lin and R.L. Vellanoweth. Oligonucleotide-capped gold nanopatricles for improved atomic force microscopic imaging and enhanced selectivity in polynucleotide detection. *Biochemical and Biophysical Research Communications*, 279:265–269, 2000.

[19] T. Nagahara L.A. DeRose, J.A. Thundat and S.M. Lindsay. Gold grown epitaxially on mica: conditions for large area flat faces. *Surface Science*, 256:102–108, 1991.

[20] Z.H. Liu and N.M.D. Brown. Studies using afm and stm of the correlated effects of deposition parameters on the topography of gold on mica. *Thin Solid Films*, 300:84–94, 1997.

[21] S. Honbo, H. Sugawara and K. Itaya. Detailed in situ scanning tunneling microscopy of single crystal planes of gold(111) in aqueous solutions. *Analytical Chemistry*, 62:2424–2429, 1990.

[22] R.J. Chambliss, D.D. Wilson and S. Chiang. Ordered nucleation of ni and au islands on au(111) studied by scanning tunneling microscopy. *Journal of Vacuum Science and Technology B*, 9:933–937, 1991.

[23] C. Mourougou-Candoni, N. Naud and F. Thibaudau. Adsorption of thiolated oligonucleotides on gold surfaces: An atomic force microscopy study. *Langmuir*, 19:682–686, 2003.

[24] M. Han S. Huang, E. Satjapipat and F. Zhou. Surface structure and coverage of an oligonucleotide probe tethered onto a gold substrate and its hybridization efficiency for a polynucleotide target. *Langmuir*, 17:1215–1224, 2001.

[25] J.K. Jackson N.M. McPherson L.D. Potter A.B. Spain E.M. Allen M.J. Kelley, S.O. Barton and M.H. Hill. Orienting dna helices on gold using applied electric fields. *Langmuir*, 14:6781–6784, 1998.

[26] E.M. Barton J.K. Hill M.G. Sam, M. Boon and E.M. Spain. Morphology of 15-mer duplexes tethered to au(111) probed using scanning probe microscopy. *Langmuir*, 17:5727–5730, 2001.

[27] R. Satjapipat, M. Sanedrin and F. Zhou. Selective desorption of alkabethiols in mixed self-assembled monolayers for subsequent oligonucleotide attachment and dna hybridization. *Langmuir*, 17:7637–7644, 2001.

[28] K. Abell C. Zhou, D. Sinniah and T. Rayment. Use of atomic force microscopy for making addresses in dna coatings. *Langmuir*, 18:8278–8281, 2002.

[29] T.M. Herne and M.J. Tarlov. Characterization of dna probes immobilized on gold surfaces. *Journal of the American Chemical Society*, 119:8916–8920, 1997.

[30] A. Ulman. Formation and structure of self-assembled monolayers. *Chemical Reviews*, 96:1533–1554, 1996.

[31] S. Mizutani W. Motomatsu M. Tokumoto H. Hokari H. Azehara H. Ishida, T. Yamamoto and M. Fujihira. Evidence for cleavage of disulfides in the self-assembled monolayer on au(111). *Langmuir*, 13:3261–3265, 1997.

[32] A. Grönbeck, H. Curioni and W. Andreoni. Thiols and disulfides on the au(111) surface: The headgroup-gold interaction. *Journal of the American Chemical Society*, 122:3839–3842, 2000.

[33] B.R. Nuzzo, R.G. Zegarski and L.H. Dubois. Fundamental studies of the chemisorption of organosulfur compounds on au(111). implications for molecular self-assembly on gold surfaces. *Journal of the American Chemical Society*, 109:733–740, 1987.

[34] S.M. Bernasek S.L. Lavrich, D.J. Wetterer and G. Scoles. Physisorption and chemisorption of alkanethiols and alkyl sulfides on au(111). *The Journal of Physical Chemistry B*, 102:3456–3465, 1998.

[35] J.N. Garno J.C. Liu G.-Y. Jennings G.K. Yong T.-H. Xu, S. Cruchon-Dupeyrat and P.E. Laibinis. *In situ* studies of thiol self-assembly on gold from solution using atomic force microscopy. *Journal of Chemical Physics*, 108:5002–5012, 1998.

[36] K.P. Georgiadis, R. Peterlinz and A.W. Peterson. Quantitative measurements and modeling of kinetics in nucleic acid monolayer films using spr spectroscopy. *Journal of the American Chemical Society*, 122:3166–3173, 2000.

[37] H. Thaysen J. Christensen C.B. Marie, R. Jensenius and A. Boisen. Adsorption kinetics and mechanical properties of thiol-modified dna-oligos on gold investigated by microcentilever sensors. *Ultramicroscopy*, 91:29–36, 2002.

[38] R.M. Herne T.M. Peterlinz, K.A. Georgiadis and M.J. Tarlov. Observation of hybridization and dehybridization of thiol-tethered dna using two-color surface plasmon resonance spectroscopy. *Journal of the American Chemical Society*, 119:3401–3402, 1997.

[39] J.R. Rouzina I. Williams, M.C. Wenner and V.A. Bloomfield. Entropy and heat capacity of dna melting from temperature dependence of single molecule streching. *Biophysical Journal*, 80:1932–1939, 2001.

[40] I. Kim K. Hansma, H.G. Revenko and D.E. Laney. Atomic force microscopy of long and short double-stranded, single-stranded and triple-stranded nucleic acids. *Nucleic Acids Research*, 24:713–720, 1996.

[41] L. Stryer. *Biochemistry*. W.H. Freeman and Company, 4 edition, 1995.

[42] D. Berk A. Zipursky S.L. Matsudaira-P. Lodish, H. Baltimore and J. Darnell. *Molecular Cell Biology*. Scientific American Books, Inc., 3 edition, 1995.

[43] A. Shnidman Y. Sellers, H. Ulman and J.E. Eilers. Structure and binding of alkarethiolates on gold and silver surfaces: Implications for sel-assembled monolayers. *Journal of the American Chemical Society*, 115:9389–9401, 1993.

[44] J.J. Mucic R.C. Letsinger R.L. Elghanian, R. Storhoff and C.A. Mirkin. Selective colometric detection of polynucleotides based on the distance-dependent optical properties of gold nanoparticles. *Science*, 277:1078–1081, 1997.

[45] A. Köhler J.M. Reichert, J. Csaki and W. Fritzsche. Chip-based optical detection of dna hybridization by means of nanobead labeling. *Analytical Chemistry*, 72:6025–6029, 2000.

[46] C.A. Taton, T.A. Mirkin and R.L. Letsinger. Scanometric dna array detection with nanoparticle probes. *Science*, 289:1757–1760, 2000.

[47] A. Reichert J. Möller R. Straube-W. Köhler, J.M. Csaki and W. Fritzsche. Selevtive labeling of oligonucleotide monolayer by metallic nanobeads for fast optical readout of dna-chips. *Sensors and Actuators B*, 76:166–172, 2001.

[48] R.L. Mucic R.C. Mirkin, C.A. Letsinger and J.J. Storhoff. A dna-based method for rationally assembling nanoparticles into macroscopic materials. *Nature*, 382:607–609, 1996.

[49] A. Köhler J.M. Möller, R. Csaki and W. Fritzsche. Electrical classification of the concentration of bioconjugated metal colloids after surface adsorption and silver enhancement. *Langmuir*, 17:5426–5430, 2001.

[50] H. Maeda, Y. Tabata and T. Kawai. Two-dimensional assembly of gold nanoparticles with a dna network template. *Applied Physics Letters*, 79:1181–1183, 2001.

[51] A. Köhler J.M. Möller, R. Csaki and W. Fritzsche. Dna probes on chip surfaces studied by scanning force microscopy using specific binding of colloidal gold. *Nucleic Acids Research*, 28:e91, 2000.

[52] W. Köhler J.M. Csaki, A. Möller and W. Fritzsche. Dna monolayer on gold substrates characterized by nanoparticle labeling and scanning force microscopy. *Nucleic Acids Research*, 29:e81, 2001.

[53] D.H. Wendoloski J.J. Weber, P.C. Ohlendorf and F.R. Salemme. Structural origins of high-affinity biotin binding to streptavidin. *Science*, 243:85–88, 1989.

[54] D.G. Castner and B.D. Ratner. Biomedical surface science: Foundations to frontiers. *Surface Science*, 500:28–60, 2002.

[55] P.M. Parker, J.L. Claesson and P. Attard. Bubbles, cavities, and the long-ranged attraction between hydrophobic surfaces. *The Journal of Physical Chemistry*, 98:8468–8480, 1994.

[56] P. Attard. Bridging bubbles between hydrophobic surfaces. *Langmuir*, 12:1693–1695, 1996.

[57] L.C. Attard P. Carambassis, A. Jonker and M.W. Rutland. Forces measured between hydrophobic surfaces due to a submicroscopic bridging bubble. *Physical Review Letters*, 80:5357–5360, 1998.

[58] T. Miyahara M. Ishida, N. Inous and K. Higashitani. Nano bubbles on a hydrophobic surface in water observed by tapping-mode atomic force microscopy. *Langmuir*, 16:6377–6380, 2000.

[59] Z.-Q. Zhang Y. Li-X.-J. Hu J. Li-M.-Q. Lou, S.-T. Ouyang and F.-J. Yang. Nanobubbles on solid surface imaged by atomic force microscopy. *Journal of Vacuum Science and Technology B*, 18:2573–2575, 2000.

[60] J.W.G. Tyrrell and P. Attard. Images of nanobubbles on hydrophobic surfaces and their interactions. *Physical Review Letters*, 87:176104:1–176104:4, 2001.

[61] T. Hauss-T. Klösgen B. Krastev-R. Schemmel S. Simonsen A.C. Steitz, R. Gutberlet and G.H. Findenegg. Nanobubbles and their precursor layer at the interface of water against a hydrophobic substrate. *Langmuir*, 19:2409–2418, 2003.

[62] J. Israelachvili. *Intermolecular and Surface Forces*. Academic Press, 2 edition, 1992.

[63] N.G. Ajili, S.H. Ebrahimi and T. Khorasani. Study on thermoplastic polyurethane/polypropylene (tpu/pp) blend as a blood bag material. *Journal of Applied Polymer Science*, 89:2496–2501, 2003.

[64] H.W. Kim-Y.B. Chung, C.W. Kim and Y.H. Rhee. Poly(ethylene glycol)-grafted poly(3-hydroxyundecenoate) networks for enhanced blood compatibility. *International Journal of Biological Macromolecules*, 32:17–22, 2003.

[65] M. Mirzadeh, H. Dadsetan and N. Sharifi-Sanjani. Platelet adhesion on laser-induced acrylic acid-grafted polyethylene terephthalate. *Journal of Applied Polymer Science*, 86:3191–3196, 2002.

[66] M. Malmsten. Ellipsometry studies of the effects of surface hydrophobicity on protein adsorption. *Colloids and Surfaces B: Biointerfaces*, 3:297–308, 1995.

[67] B. Lassen and M. Malmsten. Structure of protein layers during competitive adsorption. *Journal of Colloid and Interface Science*, 180:339–349, 1996.

[68] B Lassen and M. Malmsten. Competitive protein adsorption at plasma polymer surfaces. *Journal of Colloid and Interface Science*, 186:9–16, 1997.

[69] M. Malmsten and B. Lassen. Competitive protein adsorption at phospholipid surfaces. *Colloids and Surfaces B: Biointerfaces*, 4:173–184, 1995.

[70] S.I. Schacht-E.H. Chen X. Davies-M.C. Moens M. Vansteenkiste, S.O. Corneillie and L. Van Vaeck. Direct measurements of protein adhesion at biomaterial surfaces by scanning force microscopy. *Langmuir*, 16:3330–3336, 2000.

[71] S. Kidoaki and T. Matsuda. Adhesion forces of the blood plasma proteins on self-assembled monolayer surfaces of alkanethiolates with different functional groups measured by an atomic force microscope. *Langmuir*, 15:7639–7646, 1999.

[72] Y. Kidoaki, S. Nakayama and T. Matsuda. Measurement of the interaction forces between proteins and iniferter-based graft-polymerized surfaces with an atomic force microscope in aqueous media. *Langmuir*, 17:1080–1087, 2001.

[73] Davies M.C. Roberts-C.J. Tendler S.J.B. Chen, X and P.M. Williams. Recognition of protein adsorption onto polymer surfaces by scanning force microscopy and probe-surface adhesion measurements with protein-coated probes. *Langmuir*, 13:4106–4111, 1997.

[74] Y. Kojio-K. Takahara, A. Hara and T. Kajiyama. Plasma protein adsorption behavior onto the surface of phase-separated organosilane monolayers on the basis of scanning force microscopy. *Colloids and Surfaces B: Biointerfaces*, 23:141–152, 2002.

[75] D. Scheuring-S. Rémigy H. Braun-T. Mitsuoka K. Fujiyoshi Y. Stahlberg, H. Fotiadis and A. Engel. Two-dimensional crystals: a powerful approach to assess structure, function and dynamics of membrane proteins. *FEBS Letters*, 504:166–172, 2001.

[76] A. Engel. Microscopic assessment of membrane protein structure and function. *Histochemistry and Cell Biology*, 120:93–102, 2003.

[77] P. Hunt-S. Janeway, C.A. Travers and Walport M. *Immunobiology. The immuse system in health and disease.* Garland Publishing Inc., 1997.

[78] D. Lewie-J. Raff M. Roberts-K. Alberts, B. Bray and J.D. Watson. *Molecular Biology of the Cell.* Garland Publishing Inc., 3 edition, 1994.

[79] C.J. van Oss. *Interfacial Forces in Aqueous Media.* Marcel Dekker, Inc., New York, 1994.

[80] H.C.M. Yang, M. Yau and H.L. Chan. Adsorption kinetics and ligand-binding properties of thiol-modified double-stranded dna on a gold surface. *Langmuir*, 14:6121–6129, 1998.

[81] J. Stoltenborg, M. Petersen and L. von Gersdorff. Comparison and optimisation of methods for estimating the density of dna immobilised on gold surfaces. Midterm Project, June 2002.

Appendix A

Molecules and Solutions

The molecules used during AFM investigations of the interaction between DNA molecules and gold surfaces are deoxyribonucleic acids (DNA) molecules and mercaptohexanol (MCH) molecules. The DNA molecules have been delivered by TAG Copenhagen (TAG Copenhagen A/S, Copenhagen, Denmark) and the MCH molecules, as well as chemicals used in the buffer, have been delivered by Sigma-Aldrich (Sigma-Aldrich Denmark A/S, Copenhagen, Denmark).

A.0.1 DNA Molecules

Single stranded DNA (ssDNA) molecules consist of a backbone and the bases adenine, guanine, thymine and cytosine. The backbone consist of deoxyribose molecules linked by phosphates groups. The order of the bases in the ssDNA molecules are called the sequence of the DNA molecules, and normally the bases are represented with the initial of the name of the base (A=adenine, G=guanine, T=thymine and C=cytosine).

The DNA molecules immobilized on the gold surface during the AFM investigations are 25 bases long and have the sequence:

5'-ATT AAT GCT ATG CAG AAA ATC TTA G-3'.

Protected versus Deprotected ssDNA Molecules

During immobilization experiments both so-called protected and deprotected ssDNA molecules have been used. The protected ssDNA molecules consist of the ssDNA strand, connected to a dimethoxytrityl-group through a sulphur bridge. Between the ssDNA strand and the sulphur bridge, and between the dimethoxytrityl-group and the sulphur bridge there is a linker in form of a carbon chain with six carbons.

The deprotected ssDNA molecules are thiol-modified in the 5' end and the linker between the ssDNA strand and the thiol-group is the same as the one used in the protected ssDNA molecules.

Complementary ssDNA Molecules

To form the double stranded DNA (dsDNA) molecule, two complementary ssDNA strands are needed. The expression complementary means that the ssDNA strands have bases that 'fit' to each other, where adenine is pairing with thymine and guanine is paring with cytosine. The base-pairing between two ssDNA molecules is called hybridization.

The complementary ssDNA molecules used during hybridization experiments are not modified in any way and have the sequence:

5'-C TAA GAT TTT CTG CAT AGC ATT ATT-3'.

A.0.2 Mercaptohexanol

To release unspecific interaction between ssDNA molecules and gold surface MCH is added to the immobilized layer of thiol-modified ssDNA molecules. The MCH molecule is a six carbon-atom long chain that is thiol-modified in one end and has a hydroxyl-group in the other end.

A.0.3 Phosphate Buffer

Screening of the negative charge of the DNA molecules is obtained by using a phosphate buffer during immobilization and hybridization experiments.

The phosphate buffer used during immobilization and hybridization experiments is made at the BioProbe-laboratory at MIC. By mixing 3.3 g K_2HPO_4 with 4.2 g KH_2PO_4 in 50 ml clean water[1] a ∼0.9 M phosphate buffer with ∼pH 7 is obtained.

[1] DI water from the clean room at MIC.

Appendix B

Langmuir Isotherms

The simple Langmuir isotherm is based on the assumptions:

• There is a fixed number of sites on the surface, or in other words, only one monolayer can be formed on the surface.

• The surface is uniform and all sites are equivalent.

• The adsorption of a molecule to one site is not affected by if the neighbouring sites are occupied by molecules.

The rate of adsorption to the surface depend on the concentration of molecules in solution (C_0) and the fraction of sites occupied on the surface (θ),

$$\frac{d\theta}{dt} = k_a C_0(1-\theta), \tag{2.0-1}$$

where t is the time and k_a is the rate constant for adsorption.

The rate of desorption from the surface is proportional to the number of adsorbed molecules,

$$\frac{d\theta}{dt} = -k_d\theta, \tag{2.0-2}$$

where k_d is the rate constant for desorption.

Equation 2.0-1 and Equation 2.0-2 can be combined to give

$$\frac{d\theta}{dt} = k_a C_0(1-\theta) - k_d\theta. \tag{2.0-3}$$

By integration one can find that

$$\theta \propto 1 - exp[-(k_a C_0 + k_d)t], \tag{2.0-4}$$

which can be used to 'fit' the adsorption of thiol-modified ssDNA molecules on a gold-covered cantilever surface shown in Figure 4.5.

The equilibrium constant can be expressed as,

$$K = \frac{k_a}{k_d}. \tag{2.0-5}$$

Marie et al. [37] have reported values for the different constants during immobilization of thiol-modified ssDNA molecules on a gold coated cantilever surfaces showing k_a=2.5×10^3 M^{-1} s^{-1}, k_d=4.7×10^{-3} s^{-1} and K=5.4×10^5. Similar values have been found during experiments with thiol-modified dsDNA molecules [80].

Appendix C

Electrochemistry Experiments

To investigate the density of thiol-modified, 25 bases long ssDNA molecules immobilized on a gold surface similar to the gold surface used in the AFM experiments, electrochemistry experiments have been performed.

The electrochemistry experiments have been performed as part of a Midterm-project at MIC [81] under supervision of Erik V. Thomsen and Maria Holmberg, where the students Michael Stoltenborg, Jesper Petersen and Lars von Gersdorff assisted in the experimental work mainly performed by Ph.D. Hainer Wackerbarth at the Chemistry Department at DTU.

The bond between chemisorbed thiol-modified ssDNA molecules and a gold surface can be effected by an applied electric field. Dependent on the type of bond between molecules and surface the molecules will desorb from the surface at different surface potentials. By measuring the electron transfer (the current) between molecules and surface the density of immobilized molecules on the surface can be estimated.

Besides from information about the density of molecules on the surface, the number and size of the peaks in the voltammogram (showing current as a function of reduction potential) indicates how the adsorbed molecules are organized on the surface. A voltammogram with essentially one large peak indicates that all molecules are interacting with the surface in the same way.

By performing capacitance measurements more information about the conformation of the molecular layer on the gold surface can be obtained. When the molecules are adsorbed on the gold surface they form a layer that have characteristics similar to a plate capacitor. Thus, the thicker the layer of molecules on the surface, the lower the measured capacitance.

During the electrochemistry experiments a gold wire with a Au(111) surface was

used. The reference electrode was a saturated calomel electrode, the counter electrode was a platinum electrode, and the measurements were performed in a Faradaic cage to reduce influence from external electric fields.

During the registration of the voltammograms the potential of the gold wire was varied from +100 mV to -900 mV in steps of ∼4 mV and the current was measured at each step. The procedure was repeated three times to ensure that all molecules had desorbed from the surface. During capacitance measurements the potential was varied from +600 mV to -900 mV.

Results from performed electrochemistry experiments on thiol-modified ssDNA molecules showed voltammograms dominated by a single peak, which indicates that all molecules interact with the gold surface through their thiol. The results were strengthen by the capacitance measurements where the single peak observed in the first scan was replaced by a peak at lower potential in the second and third scan, indicating reorientation of ions and reconstruction of the gold surface, which only can occur if all molecules have desorbed from the surface.

By combining the capacitance charge from capacitance measurements with the total charged found from integration of the peaks in the obtained voltammograms, the Faraday charge can be found. The Faraday charge is the charged connected to the reductive desorption of molecules from the gold surface and can be used to estimate the density of molecules on the surface by using the equation:

$$\varrho = \frac{Q_F}{AFN_A}, \tag{3.0-1}$$

where ϱ is the density of molecules on the surface, Q_F is the Faraday charge, A is the area of the electrode, F is the Faraday constant and N_A is Avogadro constant.

Appendix D

Fluorescence- and Radioactive-labelling Experiments

The basic idea in the fluorescence- and radioactive-labelling experiments is to hybridize thiol-modified ssDNA molecules with a complementary ssDNA strand that is labelled with a fluorescence or radioactive marker, which can be detected after hybridization.

D.1 Sample Surfaces

The sample surfaces in the fluorescence- and radioactive-labelling experiments are glass slides (Objektträger geschliffen, Knittel Gläser, Germany) onto which there have been evaporated[1] a layer of 0.6 nm gold on top of a 0.1 nm thick chromium layer[2].

D.2 Fluorescence-labelling Experiments

The fluorescence-labelling experiments have been performed as part of a Midterm-project at MIC [81], where the students Michael Stoltenborg, Jesper Petersen and Lars von Gersdorff under supervision of Erik V. Thomsen and Maria Holmberg, have performed the experimental work under assistant of Ph.D. student Rodolphe Marie.

During experiments using a fluorescence marker the complementary ssDNA molecules

[1]The evaporation system used is the Leybold LAB500 e-bean evaporator located in the clean room at MIC.

[2]Used to enhance the adherence of the gold to the surface.

are labelled with a Cy 5', which is a small organic molecule that emits light (fluoresce) when illuminated by light with the right wavelength.

In summary the procedure used during experiments with fluorescence markers are as follows:

• The gold covered slides are cleaned in an UV/Ozone machine.

• The gold covered slides are 'spotted' by an robot that deposit small drops of ssDNA solution on the surface.

• The gold covered slides with immobilized ssDNA molecules are rinsed.

• The gold covered slides with immobilized ssDNA molecules are immersed in a MCH solution.

• The gold covered slides with immobilized molecules are rinsed.

• The gold covered slides with immobilized molecules are immersed in a solution with fluorescence-labelled ssDNA complementary molecules.

• The gold covered slides with the molecular layer are rinsed.

After hybridization the gold slides are analyzed in a fluorescence scanner (Scanarray Lite 5000, Packard Biochip Technology, USA) where the fluorescence intensity in digital light units (DLU) per surface area can be detected.

To translate the signal from the fluorescence scanner to a density of molecules on the surface a standard curve is needed. The standard curve is a reference where the intensity in fluorescence is shown as a function of the density of Cy 5'. By assuming that all complementary ssDNA strands, which have hybridized with the immobilized ssDNA molecules are labelled with one Cy 5', the standard curve can be used to find the density of hybridized ssDNA molecules on the surface.

D.3 Radioactive-labelling Experiments

The radioactive-labelling experiments have been performed as a 'special-project' by the student Lars von Gersdorff under supervision of Anja Boisen and Maria Holmberg at MIC, DTU. The work has been done in collaboration with Steen Guldager Petersen and Helle Kinggard Lilja-Fischer at Scandinavian Micro Biodevices A/S (SMB), Farum, Denmark.

During experiments using a radioactive marker the complementary ssDNA molecules are labelled with the radioactive isotope ^{32}P in the 5' end.

In summary the procedure used during experiments with radioactive markers are as follows:

• The gold covered slides are cleaned in an UV/Ozone machine.

• The gold covered slides are 'spotted' by hand.

• The gold covered slides with immobilized ssDNA molecules are rinsed.

• The gold covered slides with immobilized ssDNA molecules are dried.

• The gold covered slides with immobilized ssDNA molecules are immersed in a MCH solution.

• The gold covered slides with immobilized molecules are rinsed.

• The gold covered slides with immobilized molecules are immersed in a solution with radioactive-labelled ssDNA complementary molecules.

• The gold covered slides with the molecular layer are rinsed.

After hybridization the gold slides are analyzed in a so-called phosphorimager (Instant Imager, Packard Bioscience Company, USA) where the density of counts per minute (CPM) is found, and just like during experiments with fluorescence-markers a calibration curve is used to convert the density of CPM to a density of marked molecules on the surface.

Appendix E

Blood on Polymer Surfaces - Experimental

During experiments of exposure of blood and blood protein solutions to polymer surfaces, experimental parts involving blood and protein solutions have been performed at Radiometer Medical A/S, while the AFM measurements have been performed at DFM.

E.1 Materials

The polymer surfaces used are polymer surfaces that have shown to be of interest for Radiometer Medical A/S in developing devices used in measurements of blood gases and other constituents in the blood. The proteins used (fibrinogen, globulin and albumin) were delivered by Sigma-Aldrich (Sigma-Aldrich Denmark A/S, Copenhagen, Denmark).

The buffer used is a phosphate buffer with ∼pH 7 made after the recipe:
0.2 g KH_2PO_4, 1.42 g $Na_2HPO_4 \times 2H_2O$, 8 g NaCl and 0.2 g KCl dissolved in 1 l of deionized (DI) water.

E.2 Static Exposure of Blood to Polymer Surfaces

• Metal 'puck' (used as sample holder in the AFM) is cleaned with ethanol and the polymer surface is rinsed in ethanol.

• Polymer surface is glued[1] to the metal 'puck' and cleaned in ultrasound bath

[1] Loctite 495 'quick-glue', 991-090.

with laboratory-soap[2] for 3 × 3 minutes.

• The samples are thoroughly rinsed in DI water and placed in phosphate buffer at room temperature for approximately 1 hour.

• The sample surfaces are covered with blood and removed after 10 seconds or 10 minutes by gently rinse with DI water.

• The samples are placed in 3% glutaraldehyde-solution for approximately 2 hours.

• The samples are placed in phosphate buffer in sealed glass-bottles, in which they are stored until used in AFM measurements.

E.3 Dynamic Exposure of Blood and Protein Solutions to Polymer Surfaces

The samples are treated after the same scheme as the one used during static exposure of blood to polymer surfaces, except that the static exposure is replaced by a dynamic one, as described in Chapter 6.

During the dynamic exposure of blood and protein solutions to the polymer surface the set-up shown in Figure 6.4, page 74, is used. The blood and protein solution is introduced into the flow-cell and kept on the surface for approximately 30 seconds, whereafter the sample either is removed from the flow-cell or subject to cleaning.

The cleaning liquid is introduced to the sample surfaces with the same rate as the blood and also kept in contact with the surface for approximately 30 seconds before the sample is removed from the set-up or exposed to air.

When the samples are alternatively exposed to cleaning liquid and air, the cleaning liquid is kept in contact with the sample surface for approximately 30 seconds before air is introduced. Air is introduced into the flow-cell until the whole sample surface are covered with air bubbles, whereafter cleaning liquid is introduced once more.

The rates with which blood, protein solutions and cleaning liquid are introduced into the flow-cell are chosen to be similar to the rates used in the devices developed by Radiometer Medical A/S.

[2]Deconex, 11 universal.

Appendix F

AFM Images

Figure 2.5 Okt2001/MIC/10241246.001 (zoom)

Figure 2.6(a) Maj2001/MIC/05171458.001

Figure 2.6(b) Jun2001/MIC/06291210.001

Figure 2.7(a) Apr2002/Huller(Las Vegas)/04230949.001

Figure 2.7(b) Jul2001/Huller(Las Vegas)/07061143.001

Figure 2.8(a) Feb2002/MIC/02271146.001

Figure 2.8(b) Mar2002/MIC/03201504.001

Figure 3.1(a) Okt2002/Huller(luft-vand-buffer)/10221621.001

Figure 3.1(b) Okt2003/Huller(luft-vand-buffer)/10221630.001

Figure 3.2(a) Sep2002/Huller/09301414.001

Figure 3.2(b) Sep2002/Huller/09301529.001

Figure 3.2(c) Sep2003/Huller/09301608.001

Figure 3.3(a) Okt2002/Huller/10171147.001

Figure 3.3(b) Okt2002/Huller/10171249.001

Figure 3.4(a) Apr2003/MIC/Koncentration/04021201.001

Figure 3.4(b) Sep2002/Huller/09271508.001

Figure 3.5(a) Okt2002/MIC/10011415.001

Figure 3.5(b) Okt2002/MIC/10011425.001

Figure 3.6 Apr2003/MIC/Koncentration/04021356.001

Figure 3.7 Aug2001/MIC/08281617.001

Figure 3.8 Aug2001/MIC/08301231.001

Figure 4.1(a) Maj2001/Huller/05171505.001

Figure 4.1(b) Maj2001/Huller/05171619.001

Figure 4.1(c) Maj2001/Huller/05171642.001

Figure 4.3(a) Apr2002/Huller(Las Vegas)/04231346.001 (zoom)

Figure 4.3(b) Apr2002/Huller(Las Vegas)/04231439.001 (zoom)

Figure 4.5 Maj2002/MIC/05032115.001 (zoom)

Figure 4.7(a) Apr2002/Huller(Las Vegas)/04231240.001 (zoom)

Figure 4.7(b) Apr2002/Huller(Las Vegas)/04231249.001 (zoom)

Figure 4.7(c) Apr2002/Huller(Las Vegas)/04231406.001 (zoom)

Figure 4.7(d) Apr2002/Huller(Las Vegas)/04231539.001 (zoom)

Figure 4.9(a) Maj2002/Skrab/05191758.001 (zoom)

Figure 4.9(b) Maj2002/Skrab/05191847.001 (zoom)

Figure 4.11(a) Apr2003/MIC/Au partikler/04271329.001

Figure 4.11(b) Apr2003/MIC/Au partikler/04271435.001

Figure 4.13(a) Apr2003/MIC/Au partikler/04281015.001

Figure 4.13(b) Apr2003/MIC/Au partikler/04281342.001

Figure 4.14(a) Apr2003/MIC/Au partikler/04281859.001

Figure 4.14(b) Apr2003/MIC/Au partikler/04281920.001

Figure 4.15 Apr2003/MIC/Au partikler/04281241.001 (zoom)

Figure 5.1(a) Nov2002/MIC/Bobler(contact mode)/11131548.001

Figure 5.1(b) Nov2002/MIC/Bobler(contact mode)/11131553.001

Figure 5.1(c) Nov2002/MIC/Bobler(contact mode)/11131559.001

Figure 5.4 Nov2002/MIC/Bobler(TM-CM-ethanol)/11281528.001

Figure 6.1(a) Aug2002/Radiometer/08281401.001

Figure 6.1(b) Sep2002/Radiometer/09101016.001

Figure 6.2 Aug2002/Radiometer/08281542.001

Figure 6.3 Sep2002/Radiometer/09161030.001

Figure 6.5(a) Apr2003/Radiometer/04111640.001

Figure 6.5(b) Apr2003/Radiometer/04101439.001

Figure 6.6(a) Jun2003/Radiometer/06061041.001 (zoom)

Figure 6.6(b) Jun2003/Radiometer/06051102.001 (zoom)

Figure 6.6(c) Jun2003/Radiometer/06051150.001 (zoom)

Appendix G

List of Publications

Referred Publications in International Journals

M. Holmberg, A. Kühle, J. Garnæs and A. Boisen, 'Hybridisation of short DNA molecules visualised with *in situ* Atomic Force Microscopy', *Ultramicroscopy*, 97:257-261, 2003

M. Holmberg, A. Kühle, J. Garnæs, K.A. Mørch and A. Boisen, 'Nanobubble Trouble on Gold Surfaces', *Langmuir*, 19:10510-10513, 2003

Contributions to Conferences

Invited Talk

M. Holmberg, A. Kühle, J. Garnæs and A. Boisen, 'Investigation of DNA Hybridisation using *in situ* Atomic Force Microscopy', *Second International Conference on Biomedical Spectroscopy*, London, UK, July 2003

Talk

M. Holmberg, A. Kühle, J. Garnæs, K.A. Mørch and A. Boisen, 'Bubble Trouble', *STM'03*, Eindhoven, Holland July 2003

Posters

M. Holmberg, A. Kühle, J. Garnæs, K.A. Mørch and A. Boisen, 'Nanobubbles on Surfaces', *Scanning Probe Microscopy, Sensors and Nanostructures 2003*, Oxford, UK, May 2003

M. Holmberg, A. Kühle, J. Garnæs and A. Boisen, 'Formation of self-assembled monolayers of short DNA molecules, investigated with *in situ* Atomic Force Microscopy', *Scanning Probe Microscopy, Sensors and Nanostructures 2002*, Las Vegas, USA, May 2002

M. Holmberg, A. Kühle, J. Garnæs and A. Boisen, 'Biosensor Surfaces Studied with Atomic Force Microscope', *Trends in Nanotechnology*, Segovia, Spain, September 2001

M. Holmberg, A. Kühle, J. Garnæs and A. Boisen, 'Biosensor surfaces studied with the Atomic Force Microscope', *Danish Physical Society Annual Meeting*, Nyborg, Denmark, May 2001